

**MEASUREMENT OF THE
TRANSVERSE DOPPLER SHIFT
USING THE MÖSSBAUER EFFECT**

By

Micah S. Coats

A thesis submitted in partial fulfillment of the
requirements for the degree of

Bachelor of Science

Houghton College

May 2020

Signature of Author.....

Department of Physics
May 19, 2003

.....

Dr. Mark Yuly
Professor of Physics
Research Supervisor

.....

Dr. Brandon Hoffman
Professor of Physics

**MEASUREMENT OF THE TRANSVERSE
DOPPLER SHIFT USING THE MÖSSBAUER
EFFECT**

By

Micah S. Coats

Submitted to the Department of Physics
on May 15, 2020 in partial fulfillment of the
requirement for the degree of
Bachelor of Science

Abstract

An undergraduate experiment to measure the transverse Doppler shift in an accelerating reference frame using the Mössbauer effect is being designed at Houghton College. Since Einstein's equivalence principle can also be applied in an accelerating reference frame the experiment will be a test of the equivalence principle and therefore general relativity. No published undergraduate experiments testing general relativity have been published so the design of this experiment would be pioneering. Recent work has focused on making weak ^{57}Co Mössbauer sources suitable for undergraduate settings and on the design of the experiment. The use of weak Mössbauer sources is made possible with a coincidence technique that reduces background.

Thesis Supervisor: Dr. Mark Yuly
Title: Professor of Physics

TABLE OF CONTENTS

Chapter 1 Introduction 5

1.1. History of Mössbauer Effect..... 5

1.2. The Mössbauer Effect in Experimentation 10

 1.2.1. Resonance and the Longitudinal Doppler Shift..... 10

 1.2.2. Mössbauer Measurements of General Relativity 14

1.3. Measuring the Transverse Doppler Shift at Houghton College..... 17

Chapter 2 Theory 22

2.1. Recoil Theory..... 22

 2.1.1. Derivation in Rest Frame 23

 2.1.2. Derivation with Temperature Considerations 26

2.2. Derivation of Doppler Shift by Special Relativity 29

 2.2.1. Derivation of the Longitudinal Doppler Shift..... 33

 2.2.2. Derivation of Transverse Doppler Shift 34

 2.2.3. Derivation of Doppler Shift in the Proposed Experiment 36

2.3. Derivation using Equivalence Principle..... 40

2.4. Implication of Uncertainty due to Longitudinal Doppler Effect 43

2.5. Derivation of Energy shift for Modified Experimental Design 48

 2.5.1. Derivation using Special Relativity 49

 2.5.2. Derivation using Equivalence Principle 57

Chapter 3 Experiment 59

3.1. Preparing the ⁵⁷Co Source 59

 3.1.1. Step 1-Foil Preparation..... 61

 3.1.2. Step 2-Preparing the ⁵⁷Co electroplating solution 61

 3.1.3. Step 3-Electroplating the ⁵⁷Co/⁵⁹Co solution onto the foil 62

 3.1.4. Step 4-Heating the foil..... 64

3.2. Experiment Description..... 67

 3.2.1. Longitudinal Doppler Shift Experiment 67

 3.2.2. Transverse Doppler Shift Experiment 71

 3.2.3. Modified Experiment to Measure Transverse Doppler Shift 72

Chapter 4 Results 76

4.1. Calibrating the Infrared Gun 76

4.2. Calibrating the NaI detector 82

Chapter 5 Conclusion..... 85

TABLE OF FIGURES

Figure 1. Diagram of emitted photon energy distributions.....	7
Figure 2. Diagram of Emitter system	8
Figure 3. Diagram of Absorber system	8
Figure 4. Diagram of Emission and Absorption energy distributions.....	9
Figure 5. Diagram of experimental setup measuring resonance emission	12
Figure 6. Diagrams of two typical setups of Mössbauer transmission experiment.....	13
Figure 7. A typical resonance spectrum for a longitudinal doppler shift experiment	14
Figure 8. Kundig’s experimental setup for the 1963 paper.....	17
Figure 9. Diagram of the experimental design to test the Transverse Doppler Shift.....	19
Figure 10. ⁵⁷ Co decay scheme	20
Figure 11. Simplified ⁵⁷ Co decay scheme.....	21
Figure 12. Diagram of transforming between inertial frames	30
Figure 13. Diagram of kx transformation between inertial frames.....	32
Figure 14. Diagram of transverse Doppler shift	35
Figure 15. Diagram of the proposed experiment with transverse velocity	37
Figure 16. Diagram of the longitudinal Doppler shift experiment	39
Figure 17. Side Diagram of collimated source and angled disc.....	45
Figure 18. Diagram of Modified experiment for transverse Doppler shift.....	47
Figure 19. Diagram of photon traversing rotating disc.....	49
Figure 20. Diagram of L frame and S' frame aligned along emitter velocity v'	51
Figure 21. Diagram of kz and $k \perp$ components of photon wave vector k	52
Figure 22. Rotating the L frame.....	53
Figure 23. Diagram of L_{rot} frame and S'' frame aligned along absorber velocity v'	54
Figure 24. Diagram of the photon path geometry	55
Figure 25. Electroplating setup	62
Figure 26. Exponential fit to an electroplating run.....	63
Figure 27. Diagram of chamber apparatus to heat foil.....	65
Figure 28. Vacuum chamber setup	66
Figure 29. Diagram of experiment for longitudinal Doppler shift.....	68
Figure 30. Apparatus for longitudinal Doppler shift experiment	69
Figure 31. Circuit diagram of Longitudinal Doppler shift experiment.....	70
Figure 32. Diagram of originally proposed transverse Doppler shift experiment.....	72
Figure 33. Schematic of Modified experiment for transverse Doppler shift.....	74
Figure 34. External view of the IR gun used to measure foil temperature.....	77
Figure 35. Calibration setup to heat and record foil temperature.....	78
Figure 36. Plot of IR calibration of foil at emissivity setting 0.3.....	79
Figure 37. Plots of IR calibration curve at emissivity setting 0.95	80
Figure 38. Comparison of calibration curves taken outside and inside the chamber	82
Figure 39. Plot of NaI detector calibration peaks.....	83

Chapter 1

INTRODUCTION

1.1. *History of Mössbauer Effect*

The Mössbauer effect is based in the phenomena of resonance fluorescence. In resonance fluorescence, electromagnetic radiation incident onto a material results in the absorption of the radiation which is then reemitted with the same frequency at some later time. It was first experimentally confirmed by R.W. Wood in 1903 when sodium vapor fluoresced under incident light from a sodium lamp at the same wavelength as the incident light [1]. The Bohr model developed in 1913 explained many of the features of resonance fluorescence such as the same wavelength reemission. Atoms in the irradiated material had quantized energy states with energy differences between states that were therefore also quantized. These energy differences corresponded to the energies of photons that the atoms could either absorb or emit. An atom could absorb a photon and jump to an excited state. The excited state could decay at some later time and reemit the photon in an arbitrary direction. Unfortunately, the description was too simplistic and aspects of fluorescence resonance such as the linewidth of resonance spectra could not be explained by the model [2].

Of particular importance for this paper, it was realized that the energy of the emitted photons had a narrow distribution of energies instead of one discrete value, an effect that is referred to as the linewidth of the emitted radiation. There were two main reasons for this. First, almost every system will have some thermal energy associated with it. This corresponds to individual atoms of the emitter system having a range of kinetic energies. By conservation of momentum, an emitted photon must cause the emitter atom to recoil in the opposite direction. This results in an energy loss of the outgoing photon if the emitter atom was initially at rest. However, if the emitter atom has some initial momenta component in the direction of the emitted photon, the emitted photon will impart less energy to the recoiling atom than if it were stationary. The emitted photon will therefore have an increased energy as compared to the situation where the emitter atom is at rest. On the other hand, if the emitter atom has some initial momenta component in the opposite direction of the outgoing

photon, the recoil effect will result in even more energy imparted to the atom compared to when the atom is at rest. Hence less energy will be given to the photon compared to the case of the stationary atom. Therefore, a system of emitter atoms with thermal energy will have a distribution of emitted photon energies corresponding to the distribution of momenta in the emitter system. This thermal broadening increases with increasing temperature (and therefore thermal energy) of the system.

Second, and perhaps more fundamentally, the Heisenberg uncertainty principle requires an inherent uncertainty δE in the energy of a photon emitted by an excited state. The uncertainty in the excited state decay time δt is related to δE by Heisenberg's uncertainty principle which gives that $\delta E \delta t \approx \hbar$, where $\hbar = h/2\pi$ with h being Planck's constant. Thus, the energy E of the emitted photon will have uncertainty $\delta E \approx \hbar/\delta t > 0$ and so the emitted photons from the decay process will have some energy distribution rather than a single discrete energy. The full width of the distribution at half the maximum height (FWHM), typically used to parameterize the spread of the energy distribution, is called the linewidth Γ of the photon emission. A plot of the probability distribution of the photon energy is shown in Figure 1. Neglecting thermal broadening and Heisenberg's uncertainty principle gives a single line for the photon energy. With their inclusion, the line is stretched out into a narrow distribution.

Both effects are also at play in the absorption of the photon by an absorber system. The momentum of the absorber atom relative to that of the incoming photon affects the energy available to excite a state if the atom were to absorb the photon. Furthermore, the uncertainty principle means that the absorber system has a probability distribution of photon energies that could be absorbed by the system.

To address these issues the Dirac theory of radiation was applied by Weisskopf [2] to explain what the Bohr model could not. Because the nucleus has energy levels analogous to atomic energy levels it was expected that resonance fluorescence should also be observed in atomic nuclei. However, experiments to demonstrate resonance fluorescence in atomic nuclei were relatively more difficult than previous experiments with atomic systems and it was not until 1950 that Moon was able to demonstrate resonance fluorescence with ^{198}Au [3]. The

difficulty lay in the increased recoil energy of systems that underwent radiative emission. Since momentum must be conserved in a photon-emitter system, it can be shown (see Section 2.1.1) that the emitter system will recoil with energy R that is approximately proportional to the square of the transition energy E_r when the system de-excites. Since energy is conserved, the emitted photon has a somewhat reduced energy relative to the transition energy between the two energy states. As seen in Figure 2, this reduced energy is given by $E_r - R$.

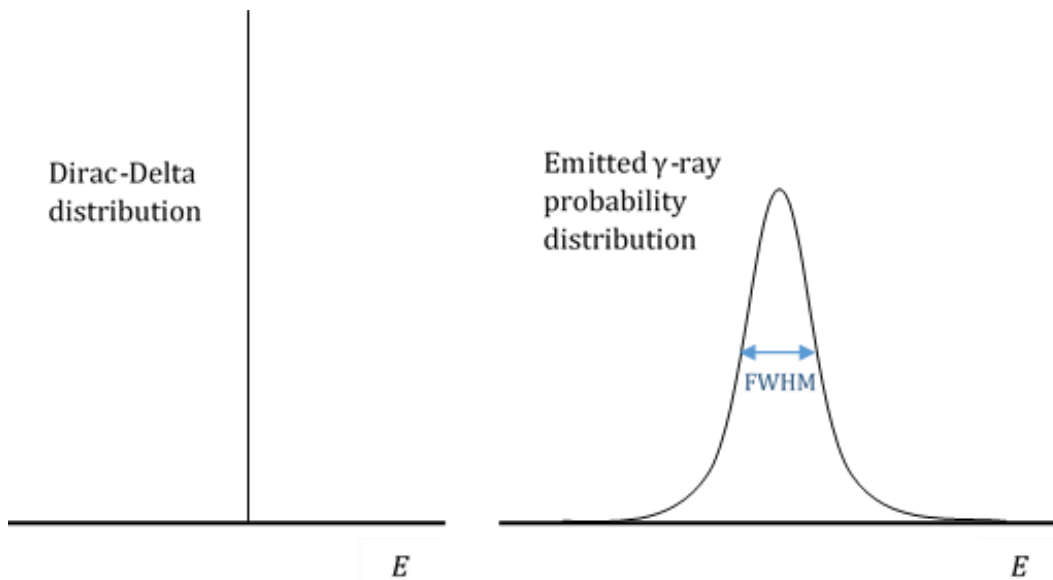


Figure 1. Diagram of emitted photon energy distributions. The left plot incorrectly gives the photon energy distribution of emitted γ -rays neglecting Heisenberg's uncertainty principle and thermal broadening. The right plot illustrates that inclusion of both stretch out the distribution into a narrow Lorentzian distribution with the linewidth given by the Full Width at Half the Maximum (FWHM).

On the other hand, for a photon to be absorbed by the system the photon must deliver the transition energy E_r to the system plus the required recoil energy (the assumption here is that the absorbing system was stationary). Thus, the absorption process forces the absorbed photon to have an increased energy relative to the transition energy equal to $E_r + R$. Figure 3 illustrates this. The result, which is illustrated in Figure 4, is that the energy distribution for emission spectrum will be shifted down by an energy R and the energy distribution for absorption spectrum will be shifted up by an energy R .

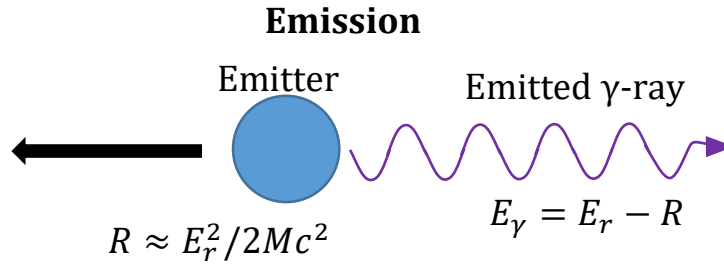


Figure 2. Diagram of Emitter system. The emitter system, initially at rest, de-excites with a transition energy of E_r . The recoil energy R delivered to the system is given by $R \approx E_r^2 / 2Mc^2$ and to conserve energy the photon is given an energy of $E_\gamma = E_r - R$.

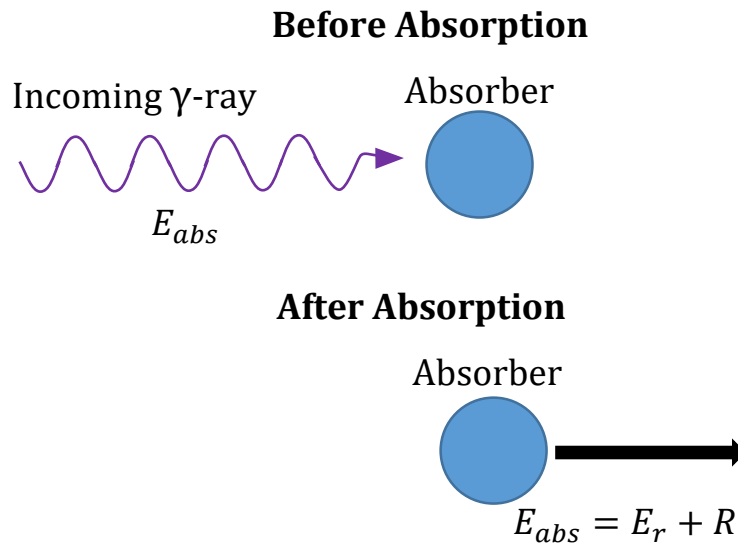


Figure 3. Diagram of Absorber system. The absorber system recoils with energy $R \approx E_r^2 / 2Mc^2$ (the same as the emission recoil energy) upon absorption of gamma ray of energy E_{abs} . The total increase of the energy of the absorber system is given by $E_r + R$ where E_r is the transition energy needed to excite the system.

Where overlap of the emission and absorption distributions occurs resonance fluorescence is allowed to take place. As shown in Figure 4, the extent to which these linewidths overlap describe the portion of the emissions which can be absorbed. Since $R \propto E_r^2$, low energy emissions, such as those found in atomic processes, have a line shift $2R$ comparable to or smaller than the linewidth itself. Considerable overlap of the two distributions will therefore occur and resonance becomes possible. For higher energy transitions, such as those found in

atomic nuclei, the line shift $2R$ becomes much larger than the linewidth due to the much greater E_γ so the overlap is radically reduced. Here, fluorescence resonance is unlikely to occur at all unless the linewidth is increased by some other factor or the value for R is artificially reduced. For Moon [3], the resonance was achieved by moving the ^{198}Au source very rapidly toward the ^{198}Hg absorber giving the emitted photons an additional Doppler boost in energy. The emitter distribution was shifted up in energy and so a small overlap of the absorber and emitter distributions was achieved.

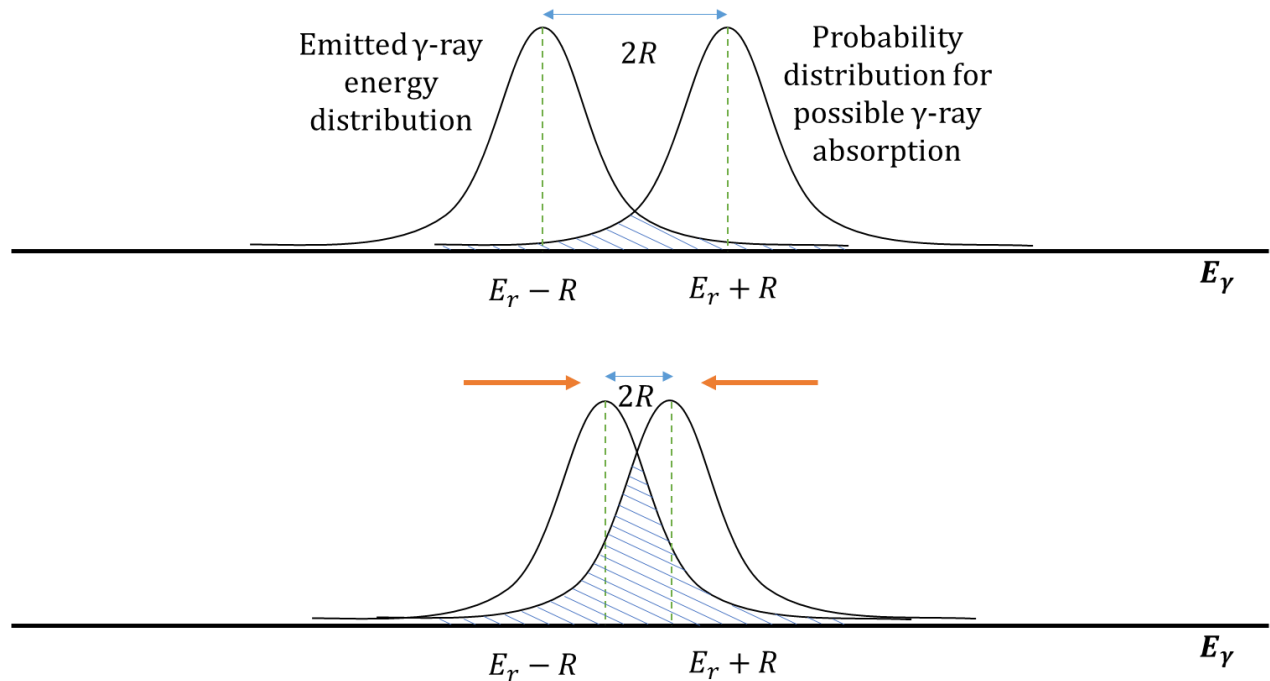


Figure 4. Diagram of Emission and Absorption energy distributions. The distributions are Lorentzian in shape. The shaded overlap region represents the portion of emissions that can also be absorbed by an emitter system. The top diagram is a more nuclear type transition with large R relative to linewidth. A decreased R relative to linewidth (bottom diagram) can make for a very significant increase in the fraction of photons that can be absorbed and is more typical of atomic transitions.

In some cases however, the fluorescence resonance of high energy emissions can still be fairly significant depending on the mean decay time for the emission and thermal broadening. This is the case for ^{191}Ir which has a 129-keV gamma emission. In 1957 R. L. Mössbauer constructed an experiment [4,5] in which he hoped to reduce this effect by narrowing the linewidth of the emitter and absorber through cooling of the source and

absorber. Instead, he discovered that the resonance actually increased. At low temperatures, Mössbauer realized some fraction of the emissions and absorptions were recoilless and so significant linewidth overlap could be achieved. This recoilless nuclear resonance fluorescence was called the Mössbauer effect.

Mössbauer used solid ^{191}Ir as an absorber and emitter. The previous discussion on recoil had assumed that the emitter and absorber systems were individual atoms or nuclei which is valid for a gas. For source atoms or nuclei imbedded in a solid crystal structure the entire crystal becomes the emitter system. Momentum imparted to the emitter system can be distributed across the entire crystal instead of a single atom. Since kinetic energy of a moving body is given by $E = p^2/2M$ where p is the momentum of the body and M is the mass of the body, the kinetic energy of the recoiling crystal is almost negligible compared to the energy of a recoiling atom. However, recoil energy can also be expended in the form of lattice vibrations. The lattice vibration then become the primary mode by which recoil energy is expended when the source is imbedded in a lattice structure. The overall effect on the distribution of energies of the emitted and absorbed photons was assumed to remain fairly similar to that describing individual atoms and nuclei. It was therefore surprising to find that some of the emissions from ^{191}Ir were without any associated recoil energy. To answer why these emissions were recoilless, Mössbauer postulated that in some fraction of the emissions/absorptions the photons were emitted/absorbed without any corresponding lattice vibrations [4].

1.2. The Mössbauer Effect in Experimentation

1.2.1. Resonance and the Longitudinal Doppler Shift

When harnessed the Mössbauer effect was particularly significant because it offered a very precise method for observing small frequency shifts of emitted photons. A Mössbauer source and absorber in resonance have their unshifted lines, which is the energy distribution of the recoilless photons, superimposed on each other. A small shift in frequency (and therefore a shift in energy) of the emitted photons relative to the absorber will cause the distributions to move off of each other resulting in a greatly changed overlap region and a corresponding change in resonance absorptions. This method became even more powerful as new

Mössbauer sources were discovered that had even narrower linewidths than ^{191}Ir , allowing for even more accurate measurements. Not long after Mössbauer's discovery of the effect in ^{191}Ir , it was discovered that ^{57}Fe displayed a very large Mössbauer effect [6] with a linewidth of $4.6 \times 10^{-9}\text{eV}$, (a linewidth about 1000 times smaller than that observed in ^{191}Ir) [7,8] and a relative linewidth on the order of 10^{-13} compared to only 10^{-11} for ^{191}Ir . Additionally, the Mössbauer effect in ^{57}Fe was retained at even high temperatures (over 1300 K)[6] making possible Mössbauer experiments at room temperature. The combination of these factors made the Mössbauer effect in ^{57}Fe particularly precise and useful as a measurement technique.

One common use for the Mössbauer Effect is using the longitudinal Doppler shift to measure some other parameter. In such an experiment, a Mössbauer source and absorber are moved longitudinally relative to each other. If the source and absorber are moving towards each other then an emitted photon will be Doppler shifted to a higher frequency in the frame of reference of the absorber. If the absorber and source move away from each other then the photon will be Doppler shifted to a lower frequency in the frame of reference of the absorber. This technique can be used to find the probability distribution for absorption and emission by varying the relative velocities of absorber and emitter. The experimenter can scan over the relative overlap of emitter and absorber spectra by shifting the respective lines across each other. Because the sources and absorbers are Mössbauer ones (i.e. they utilize a lattice structure to dissipate recoil momentum over the whole system) and therefore have unshifted lines, the relative velocity corresponding to the line shift necessary to measurably decrease resonance may be extremely small, perhaps on the order of cm per second or smaller.

A typical experimental setup for a longitudinal Doppler shift experiment uses a thin absorber and thin source moving toward one another at speed v . A detector either is set obliquely to the source-absorber axis and measures the count rate of resonance emissions from the absorber as seen in Figure 5, or the detector is positioned behind the thin absorber and measures the transmission of the photons through the absorber sheet as seen in Figure 6. In the case of the setup measuring resonance emission a low resonance emission count

corresponds to a low absorption rate by the absorber while a high resonance emission count corresponds to a high absorption rate by the absorber. However, the large majority of Mössbauer experiments do not measure scattering from resonance absorption and instead measure the transmission rate through the absorber sheet [9]. Measuring the transmission rate generally offers more “favorable geometry” and higher intensities while scattering experiments typically suffer from smaller intensities due to the small fraction of absorptions that result in reemitted gamma rays instead of internal conversions [9].

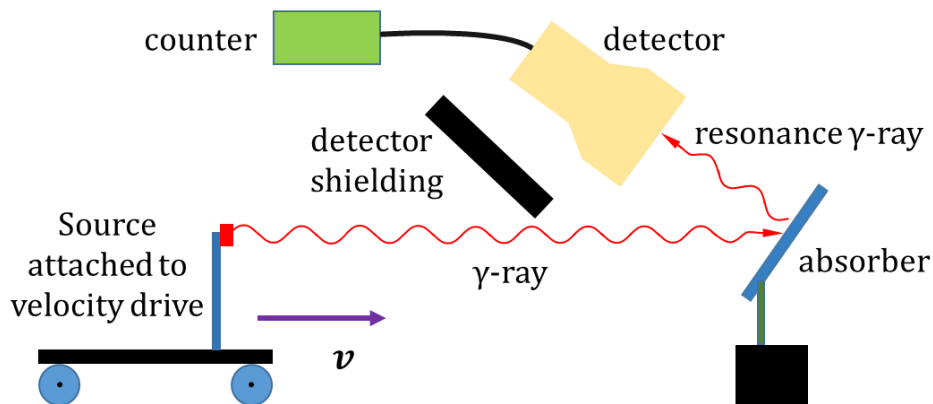


Figure 5. Diagram of experimental setup measuring resonance emission. In this setup the resonance emission count rate from the absorber is measured as a function of the speed v of the velocity drive. The speed v can be ranged from a negative value to a positive value to scan over the entire emission and absorption spectrum. This method for measuring the longitudinal Doppler shift is not typically employed since it is usually more advantageous to measure the transmission rate through the absorber.

Measuring a high transmission rate corresponds to a low fraction of absorbance by the absorber sheet while a low transmission rate indicates a higher fraction of absorbance by the absorber sheet. Figure 7 displays a typical absorption spectrum over a range of different velocities for a transmission longitudinal Doppler shift experiment. If the absorption and emission lines are truly unshifted when emitter and absorber are in the same inertial frame then a plot of the detector count rate as a function of the relative velocity v will show that the peak is centered at $v = 0$. Otherwise, the peak of the curve will be centered at some non-zero relative velocity corresponding to the Doppler shift needed to have the two distributions achieve maximum overlap.

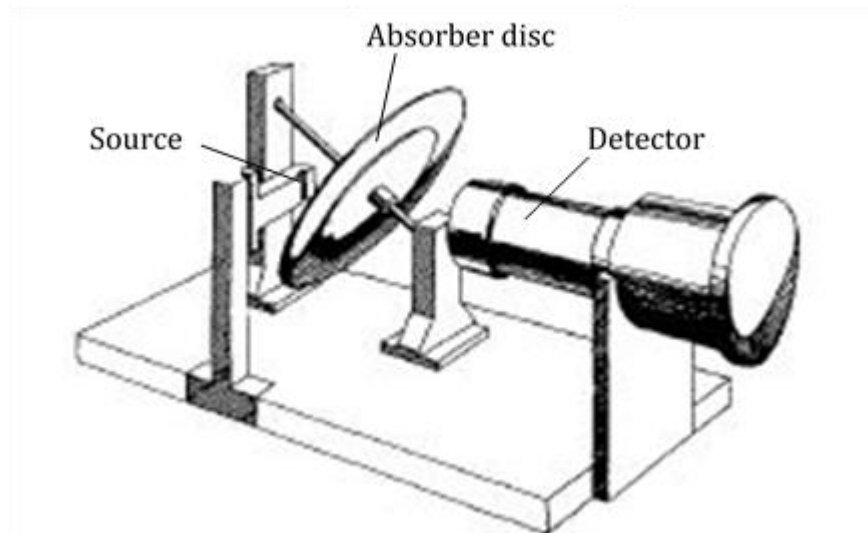
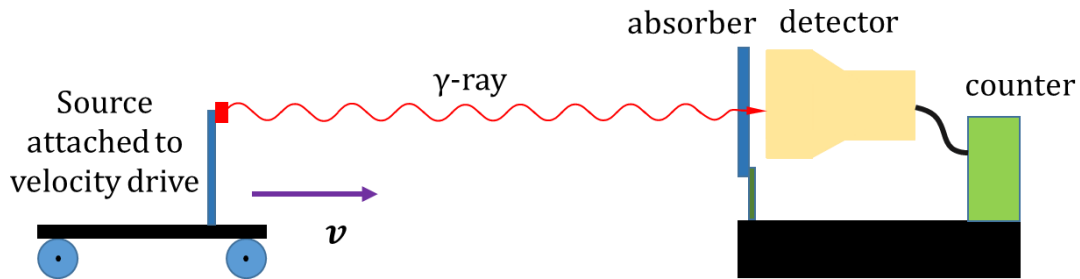


Figure 6. Diagrams of two typical setups of Mössbauer transmission experiment. The top diagram shows the source attached to the velocity drive with the transmission count rate through the absorber being measured. The bottom diagram shows a setup where the emitter is fixed and the absorber moves in the lab frame. The absorber disc is spun at low speeds and tilted such that there exists a longitudinal velocity component of the absorber along the source-detector axis. The angular speed or tilt of the disc can be varied to allow the experimenter to measure the transmission rate as a function of velocity. Bottom diagram taken from Ref. [11].

Once this absorption spectrum is known for a given source and absorber then the data can be applied to a wide range of uses. In the case of spectroscopy, the microscopic structure of the absorber material in question is often unknown but a given resonance spectrum (analyzed using the longitudinal Doppler shift) can give significant insight into the structure of the material when compared against known resonance spectrums [10]. Mössbauer spectroscopy can measure the effects of hyperfine interactions such as isomer shifts and electric quadrupole splitting, often enabling determination of the crystal or atomic structure around Mössbauer atoms [10].

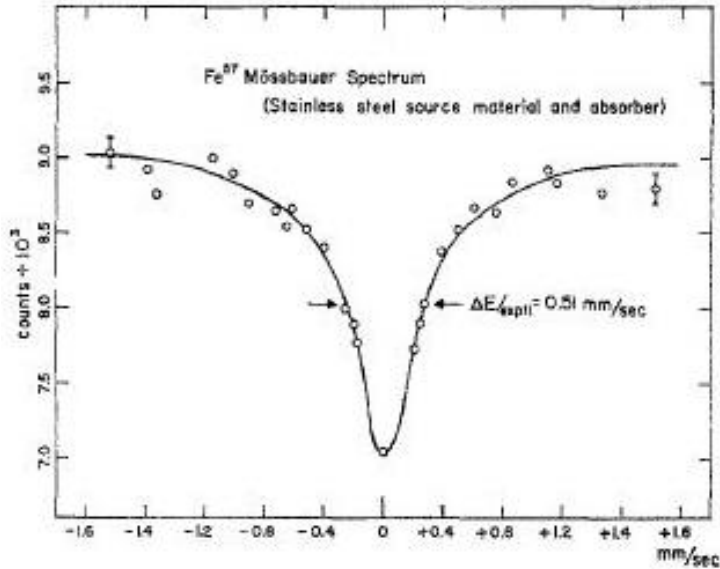


Figure 7. A typical resonance spectrum for a longitudinal doppler shift experiment. The transmission count rate through the absorber is measured as a function of the linear relative velocity of source and absorber. This experiment uses ⁵⁷Co as the source and ⁵⁷Fe as the absorber, both at a temperature of 300 K. Figure taken from Ref. [11].

1.2.2. Mössbauer Measurements of General Relativity

Of particular interest for this paper is the use of the transverse Doppler shift to test general relativity effects. In this experiment the longitudinal Doppler shift can be used to make the experiment considerably more accurate and to calibrate the system since most experiments of this type require that the resonance spectra be known.

In 1959 Pound and Rebka published a paper [12] describing a theoretical test of the gravitational Doppler shift predicted by general relativity when a photon moves in a gravitational field. It was rapidly followed by their landmark paper in 1960 [13] where they successfully performed the experiment. A Mössbauer source and emitter were placed 22.5 m apart in height and the absorption of the emitted photons was measured. By general relativity, the photons experienced a frequency shift proportional to the change in gravitational potential energy between source and emitter. Since this shift was small, the Mössbauer effect proved to be highly effective in measuring the correspondingly small line shift. A velocity drive that moved the source toward and away from the absorber at constant speed allowed Pound and Rebka to use the longitudinal Doppler shift to scan over the

resonance spectrum and determine the gravitational frequency shift of the photon when it traveled between source and absorber. Using this method they were able to obtain an experimental value, to which the theoretical value predicted by general relativity agreed within the measurement uncertainty of 10%. In a later experiment this uncertainty was later reduced to less than 1% with corresponding agreement [14]. Their 1960 experiment would be a verification of the last of the three classical tests of general relativity which were set forth by Einstein [15].

In 1960 and in the subsequent years several experiments [16,17] were also performed to test the equivalence principle of general relativity which states that the relativistic effects in an accelerating reference frame are the same as those due to a gravitational field. Therefore, if a source and absorber were to be placed in an accelerating reference frame, for a given photon emitted by the source one could expect to measure a Doppler shift at the absorber equal to the gravitational shift that would have resulted from the equivalent gravitational field.

Actually, the derivation for the gravitational shift resulted from the Doppler shift expected for a photon moving in an accelerating reference frame. The experiments paid little heed to the order of derivation however. Pound and Rebka [13] performed their famous experiment in 1960 and continued to improve on the procedure over the coming years. The first published results for an experiment of the Doppler shift due to an accelerating reference frame was in 1960 by Hay et al. [16] and gave a description of their method for accelerating the emitter-absorber system. Their results were in agreement with the expected theoretical redshift in frequency for the emitted photons [16]. In 1963 Champeney and Moon [17] measured the shift in frequency of a gamma ray moving from an emitter to an absorber that were both attached to the ends of a spinning rotor. Both absorber and emitter were at the same distance from the center of the rotor and therefore at the same potential in the frame of the rotor. By the equivalence principle this corresponded to an overall zero change in the frequency of the gamma ray between emitter and absorber, which Champeney and Moon subsequently found in their measurements.

In 1963 Kundig [18] performed another experiment testing the equivalence principle of general relativity. In this experiment, he set up a rotating system where a source and emitter were placed in a channel that ran through the center of the rotating system (Figure 8). As the system was rotated the absorber experienced a centripetal acceleration towards the center of the rotating system. By the equivalence principle this could be considered a gravitational potential well. In the frame of the disc photons moving between source and absorber would pass through the gravitational field, moving from higher potential to lower potential, and would be shifted up in energy. However, when considered from the reference frame of the laboratory, the energy shift results from the transverse Doppler shift of the photon. Whereas the longitudinal Doppler shift results from a source and absorber moving toward or away from each other, the frequency shift of the photon due to the transverse Doppler effect is a result of special relativity when the absorber and source move perpendicularly relative to each other. Since this effect is much smaller than the longitudinal Doppler shift, the velocities needed to observe it must be considerably larger. For his experiment Kundig spun his absorber at speeds of up to 300 m/s relative to the source, a factor of about 10^6 greater than the speed necessary to observe a similar longitudinal Doppler shift.

Unlike Hay et al. or Champeney and Moon, Kundig's experiment incorporated the use of a linear velocity drive into the experimental setup [18,19]. The emitter was attached to a transducer that was driven by a triangularly varying voltage. Thus, while the system was being rotated at a given speed the source was being moved linearly toward and away from the source with the transmission count rate through the absorber being measured. This incorporation of a linear velocity drive meant that the measurement of the transverse Doppler shift was independent of line shape. As Kholmetski et al. pointed out [19], earlier experimenters had not incorporated such a drive into their setups and had simply been measuring the absorption as a function of rotational frequency. This required fairly precise knowledge of the resonance spectrum and Kundig's experiment revealed that, in fact, the resonance shape broadened with increased frequency [18]. Kundig reported an agreement with theory with measurement uncertainty about 1% [18].

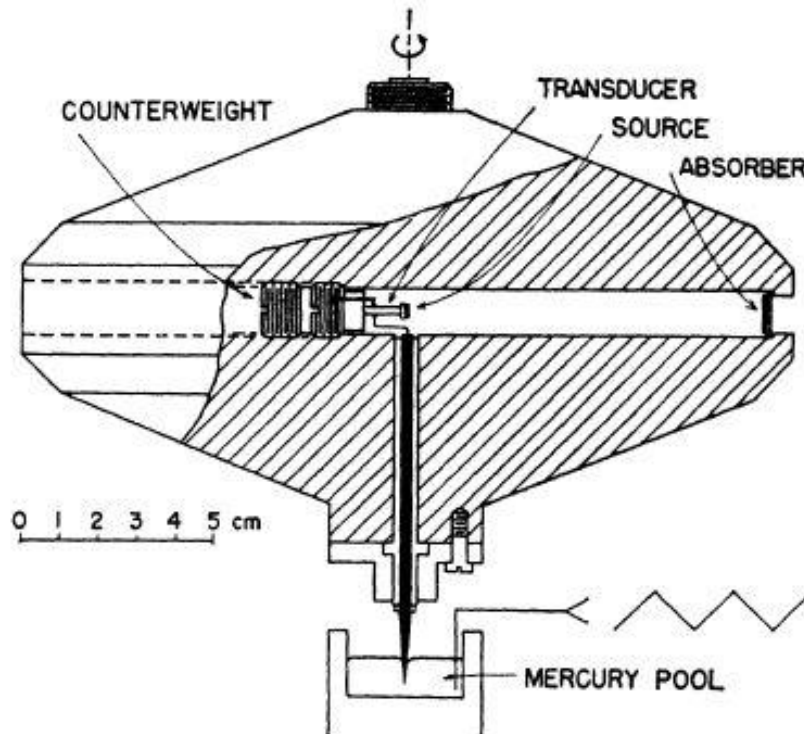


Figure 8. Kundig's experimental setup for the 1963 paper. The rotor was rotated at angular frequencies up to 35,000 RPM. Figure taken from Ref. [18].

As Kholmetski et al. pointed out in 2008 [19], the experimental accuracy and success of these experiments with testing the transverse Doppler effect, particularly by Kundig, “deprived physicists in further repeating similar experiments”. Kundig’s experiment, along with its predecessors, became one of the “remarkable confirmations of the relativity theory” [19]. Interestingly, Kholmetski et al. found what appeared to be a misprint in Kundig’s data giving the theory a significant deviation from the experimental value. Kholmetski’s group has since repeated the experiment using a different methodology to find that the theoretical value also deviated from their experimental value [20]. The explanation for the deviation still remains an open question.

1.3. Measuring the Transverse Doppler Shift at Houghton College

At Houghton College an undergraduate experiment to measure the transverse Doppler shift using the Mössbauer effect is being developed. Part of the motivation for such an experiment is to design an undergraduate experiment testing general relativity that could be performed

in most undergraduate facilities. This would be particularly notable because while there are a few undergraduate experiments on special relativity [21,22] there are no published undergraduate experiments using general relativity. When Pound and Rebka performed their famous experiment on the gravitational redshift of photons they used 15 GBq (0.4 Ci) of ^{57}Co [13]. Kundig's experiment used 370 MBq (10 mCi) of ^{57}Co [18]. Radioactive sources of this size are unsuitable for undergraduate labs, especially those without a license allowing the university or college to own highly active sources. As such it seems desirable to design an experiment that uses an exempt source on the order of 37 kBq (1 μCi) or less. This has been a major goal for the design of the experiment set to be performed here at Houghton College.

Additionally, such an experiment would offer additional and independent data to the ongoing discussion over the transverse Doppler shift. Kundig's experiment reanalyzed showed deviation between the theoretical and his experimental value [19]. Kholmetski et. al.'s new measurement of the transverse Doppler shift showed an even greater deviation between the experimental and theoretical value [19]. This gives a powerful motive for independently redoing the experiment under different conditions in order to investigate the existence and possible source of the deviation.

The current design of the experiment uses less than 37 kBq (1 μCi) of ^{57}Co that is electroplated onto a thin steel foil sufficiently thin to reduce self-absorption of the emitted gamma rays from the decaying ^{57}Co . The absorber is a steel coated disc that can be rotated along its principal axis up to 20,000 rpm. As seen in Figure 9, a coincidence detector system using CdTe and NaI detectors is situated so that the 14.4 keV emitted gamma rays from the ^{57}Co source can be measured in coincidence with the 122 keV gamma ray also emitted by the source. The CdTe detector will measure the rate of 14.4 keV gamma rays transmitted through the absorber in coincidence with a 122 keV gamma ray detected by the NaI detector. As the disc is rotated at high velocities the absorber ^{57}Fe nuclei on the disc will be placed in an accelerating reference frame. Gamma rays passing through the disc become blue shifted in the frame of reference of the disc due to Einstein's equivalence principle. The derivation for this is discussed in Section 2.3. The emission spectrum of the 14.4 keV gamma rays will

therefore be shifted up in energy in the reference frame of the disc. Alternatively, this energy shift can be explained by use of the transverse Doppler shift. The section of the disc between the source and detector will be moving transversely to the 14.4 keV gamma rays in the laboratory frame of reference. In Section 2.3 it is shown that, due to the transverse Doppler shift, these gamma rays are shifted up in energy in the frame of the disc section.

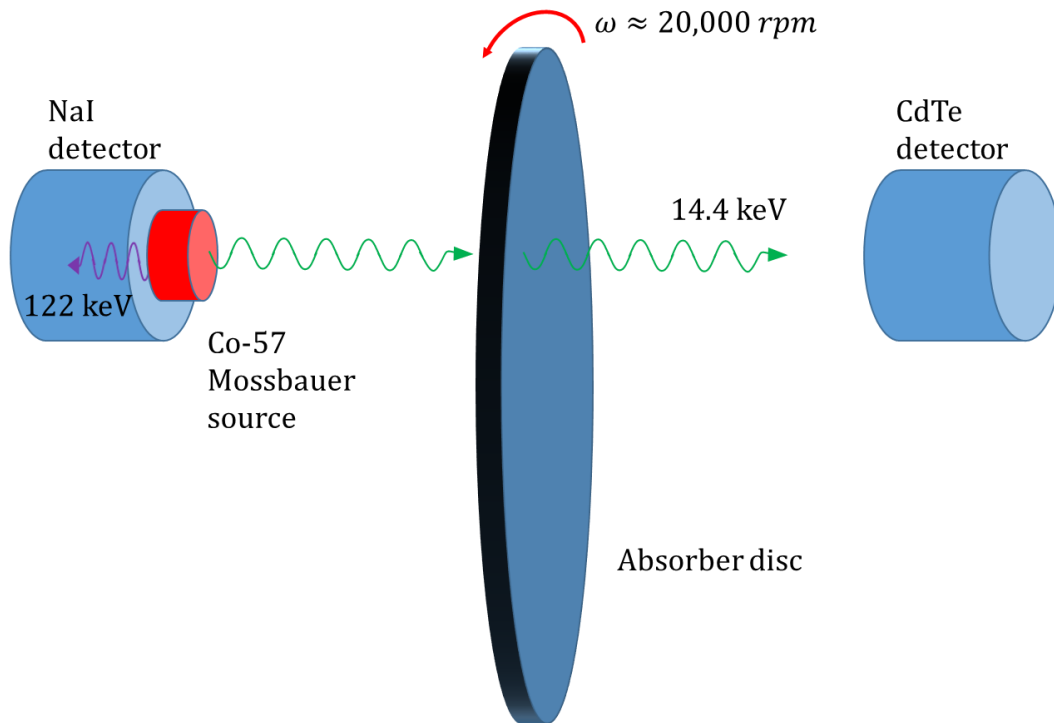


Figure 9. Diagram of the experimental design to test the Transverse Doppler Shift. The NaI and CdTe are set up to measure in coincidence the 14.4 keV gamma ray and 122 keV gamma ray (respectively) that are emitted simultaneously when ^{57}Fe de-excites to the ground state.

A full decay scheme for ^{57}Co is shown in Figure 10. A ^{57}Co nucleus decays to the 136.5 keV excited state of ^{57}Fe 99.8% of the time and it is this decay chain that is of interest in the Mössbauer effect for ^{57}Fe . A simplified scheme of this decay path is shown in Figure 11. About 85% of the time the 136.5 keV excited level of ^{57}Fe de-excites to the 14.4 keV excited state by emitting a 122.1 keV gamma ray. The 14.4 keV excited state then decays to the ground state by either internal conversion or by a 14.4 keV gamma emission. Since the half-life of the 14.4 keV excited state is 98.3 ns the 122 keV and 14.4 keV gamma rays are coincident with each other. This offers a measuring technique by which most of the background radiation entering

the CdTe detector can be eliminated. Pulses from the CdTe detector will be counted only if they are in coincidence with a 122 keV pulse from the NaI detector. The increase in signal to noise ratio this coincidence technique offers for the experiment (a 10,000 fold increase) allows for a small source to be used. This is a particularly important consideration since it enables the experiment to be performed by even modestly equipped undergraduate departments. Should this experiment be successfully performed it would be an undergraduate experiment testing Einstein's equivalence principle (and therefore also general relativity), something which appears to have never been done before.

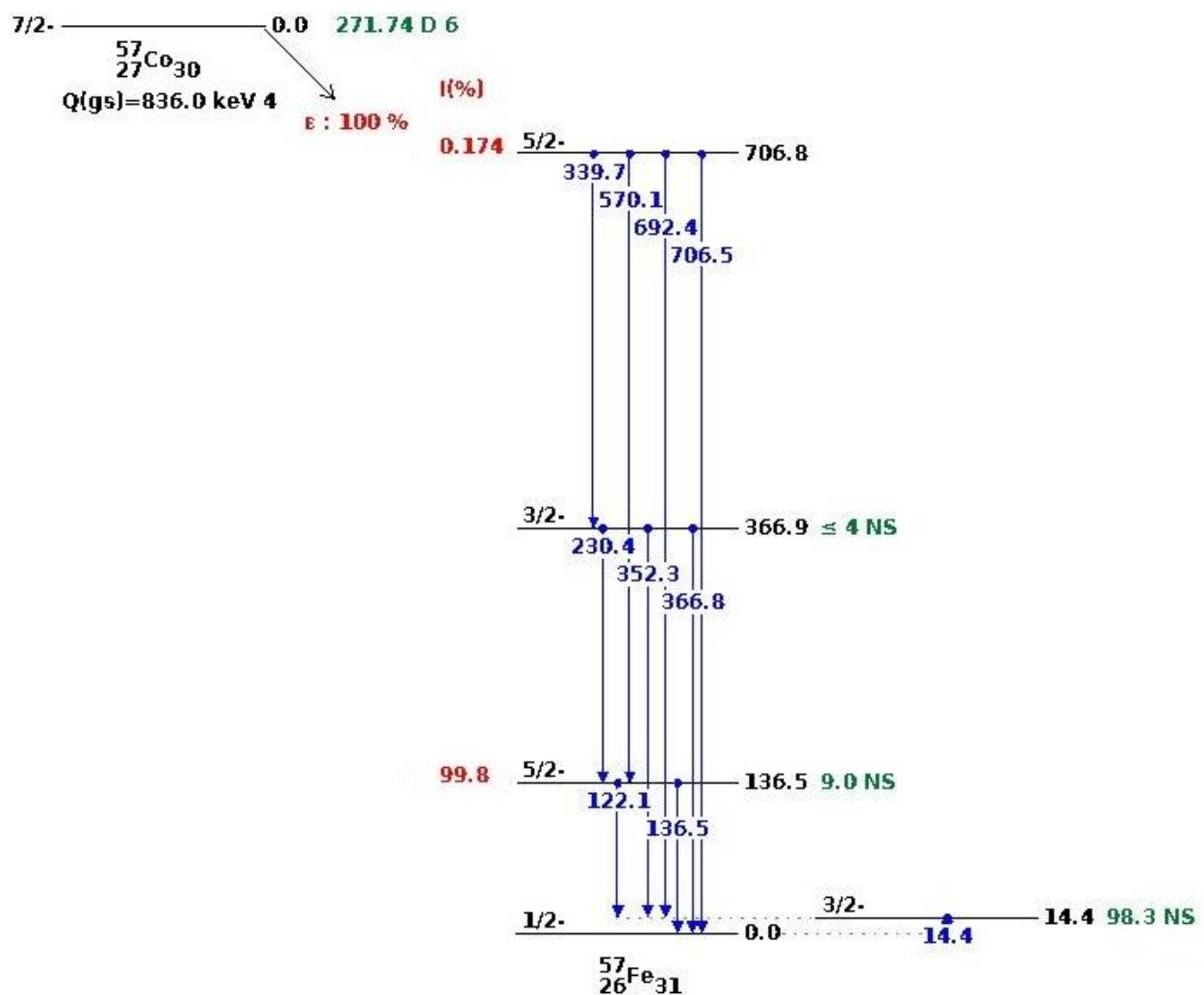


Figure 10. ^{57}Co decay scheme. ^{57}Co decays to ^{57}Fe either by electron capture or by positron emission. The primary path of interest to the experiment is the decay to the 136.5 keV energy level of ^{57}Fe followed by the decay to 14.4 keV energy level via the 122.1 keV gamma emission and then finally by the decay to the ground state by the 14.4 keV gamma emission [7].

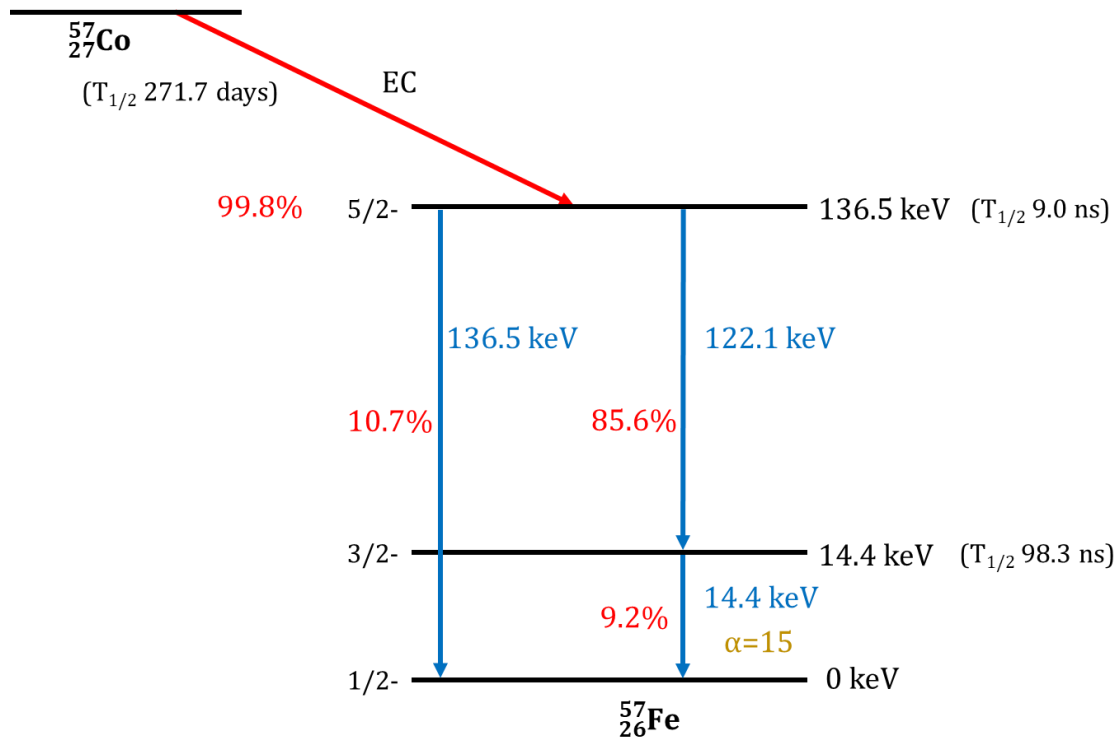


Figure 11. Simplified ^{57}Co decay scheme. ^{57}Co decays to the 136.5 keV energy level of ^{57}Fe 99.8% of the time. It then proceeds to the ground state either by emitting a single 136.5 keV gamma ray or by a two step process which occurs 85.6% of the time. In the two step process the ^{57}Fe decays to the 14.4 keV level by emitting a 122.1 keV gamma ray. This is followed by either a 14.4 keV gamma ray emission or by an internal conversion step. The ratio α of internal conversions to gamma emissions for the 14.4 keV level is about 15. Information taken from [7].

Chapter 2

THEORY

This section derives a number of the fundamental results that describe the Mössbauer effect, focusing on the results important for the transverse Doppler. A simplified derivation of recoil and related temperature effects will be followed by the derivation of the longitudinal and transverse Doppler shifts, since these are of particular significance to the proposed experiment at Houghton. A derivation of the experimental energy shift predicted by general relativity is also included here to demonstrate that it is consistent with that predicted by the transverse Doppler shift.

2.1. Recoil Theory

Recoilless nuclear resonance (the Mössbauer effect) is what allows nuclear resonance to even be achievable. As will be shown in Section 2.1.1 the recoil energy R of free emitter and absorber systems is related to the transition level energy E_r and mass M of the system by the approximation

$$R \approx \frac{E_r^2}{2Mc^2}. \quad (2.1)$$

Since the energy separation of the peaks in the emitter and absorption energy spectra is $2R$, Eq. (2.1) indicates that the necessary overlap for resonant absorption in free systems is negligibly small for the large transition level energies E_r typical in nuclear processes, which are frequently on the order of 10-100 keV. This decrease in emitter and absorption spectra overlap is depicted in Figure 4. Atomic processes involve much smaller transition level energies, typically less than 10 eV, greatly reducing R . Resonance can therefore occur in atomic free systems because of the considerable overlap of emission and absorption spectra. As an example, the 14.4 keV transition of ^{57}Fe has a calculated free recoil energy of 1.95×10^{-3} eV with a linewidth $\Gamma = 4.64 \times 10^{-9}$ eV if temperature effects are neglected. The separation $2R$ is therefore 10^6 larger than the linewidth of the emitter and absorption spectra so resonance will never occur. By comparison, the associated free recoil energy for

the atomic sodium doublet, which have wavelengths 589.0 nm and 589.6 nm respectively [23], is averaged to be 103×10^{-12} eV. This about 10^7 smaller than for the recoil energy of the 14.4 keV transition of ^{57}Fe . When temperature is neglected the averaged linewidth of the sodium doublet lines is 4.05×10^{-8} eV [23]. In this case the linewidth is 10^2 larger than the separation energy $2R$ for the sodium doublet absorber and emitter peaks meaning that resonant absorption always occurs.

In actuality, the recoil energy R_a of an absorber system due to absorption of a photon is in general different than the recoil energy R_e of an emitter system due to emission of a photon, even if the two systems are identical. The emitter recoil energy $R_e(E_{re}, M_e)$ is a function of the emitter transition level energy E_{re} and the mass M_e of the emitter system. Similarly, the absorber recoil energy $R_a(E_{ra}, M_a)$ is a function of the absorber transition level energy E_{ra} and the mass M_a of the absorber system. However, when absorber and emitter systems are identical (represented from now on as $M_a = M_e = M$ and $E_{re} = E_{ra} = E_r$) and their masses are large (i.e. on the order of an atomic nucleus mass) the recoil energy of both systems can be shown to be the same to 2nd order in terms of E_r . The approximation in Eq. (2.1) (which is to 2nd order in terms of E_r) will therefore hold for both emitter and absorber systems and so allows for the two recoil energies to be treated as the same value.

2.1.1. Derivation in Rest Frame

The derivation of the emitter system recoil energy is now examined in the rest frame. The physical situation is depicted in Figure 2. The emitter system under consideration is originally at rest with a transition energy E_r between an excited state and a less excited state. When the system decays from the excited state, it simultaneously emits a photon of energy E_γ and recoils with energy R_e . By conservation of energy,

$$E_r = E_\gamma + R_e. \quad (2.2)$$

Similarly, by conservation of momentum

$$\vec{P}_\gamma = -\vec{P}_R \quad (2.3)$$

in the rest frame of the emitter body before emission where \vec{P}_γ is the momentum of the photon and \vec{P}_R is the momentum of the recoiling body. Assuming that the recoiling emitter body is moving non-relativistically then

$$R_e = \frac{P_R^2}{2M}. \quad (2.4)$$

The recoil energy is always less than the nuclear transition energy which is usually less than one MeV. For the recoiling body to be moving relativistically it would need an energy at least a hundredth of the recoil body mass-energy. Since a nucleus has mass-energy on the scale of GeVs the recoil energy can be treated non-relativistically.

The energy E of a photon is given by

$$E = pc \quad (2.5)$$

where p is the momentum of the photon and c is the speed of light. Substituting Eq. (2.3) into Eq. (2.4) and then substituting into Eq. (2.2) gives

$$E_r = E_\gamma + \frac{P_\gamma^2}{2M}. \quad (2.6)$$

Rearranging Eq. (2.5) and then substituting into Eq. (2.6) gives

$$E_r = E_\gamma + \frac{E_\gamma^2}{2Mc^2} \quad (2.7)$$

which is a quadratic equation and can be solved to obtain the double solution

$$\begin{aligned} E_\gamma &= \frac{-2Mc^2 \pm \sqrt{(2Mc^2)^2 + 8Mc^2E_r}}{2} \quad (2.8) \\ &= -Mc^2 \pm Mc^2 \left(1 + \frac{2E_r}{Mc^2}\right)^{\frac{1}{2}}. \end{aligned}$$

As $E_r \ll Mc^2$ the binomial expansion can be applied to give the first order solutions

$$E_\gamma \approx -Mc^2 \pm Mc^2 \left(1 + \frac{E_r}{Mc^2}\right), \quad (2.9)$$

for $E_r \ll Mc^2$. This reduces to

$$E_\gamma \approx E_r, \quad E_\gamma \approx -2Mc^2 - E_r. \quad (2.10)$$

Clearly, the second solution is impossible since $E_\gamma > 0$ so $E_\gamma \approx E_r$. To obtain the recoil energy, the first solution is substituted back into Eq (2.2) to give

$$R_e = E_r - E_\gamma = E_r - \left[-Mc^2 + Mc^2 \left(1 + \frac{2E_r}{Mc^2}\right)^{\frac{1}{2}}\right]. \quad (2.11)$$

A binomial expansion then gives

$$\begin{aligned} R_e &\approx E_r - \left[-Mc^2 + Mc^2 \left(1 + \frac{E_r}{Mc^2} - \frac{E_r^2}{2(Mc^2)^2}\right)\right] \\ &= \frac{E_r^2}{2Mc^2} \end{aligned} \quad (2.12)$$

for $E_r \ll Mc^2$.

For the absorber system a similar calculation is employed. With the absorber system an incoming photon of energy E_γ is absorbed by the system in a lower energy state exciting it to a higher energy state. If the absorber system is identical to the emitter system then this transition energy will also identically be E_r (there are of course multiple possible transition energies corresponding to the multiple energy levels in a nucleus but the one of interest is that matching the emitter system). The absorber system will also recoil with energy R_a to conserve momentum. By conservation of energy,

$$E_r + R_a = E_\gamma. \quad (2.13)$$

Letting \vec{P}_γ be the momentum of the gamma ray and \vec{P}_r be the momentum of the recoiling absorber system, then conservation of momentum requires that

$$\vec{P}_\gamma = \vec{P}_r. \quad (2.14)$$

Since the same assumptions for non-relativistic motion used for the emitter system apply to the absorber system

$$R_a = \frac{P_r^2}{2M}. \quad (2.15)$$

Using the same argument to that used for the emitter system, the recoil energy R_a can be shown to be

$$R_a \approx \frac{E_r^2}{2Mc^2}. \quad (2.16)$$

As was the case with the derivation for the recoil energy of the emitter system, a second solution was also obtained but is physically irrelevant and so discarded. Comparing Eq. (2.16) with Eq. (2.12) shows

$$R_e \approx R_a \approx \frac{E_r^2}{2Mc^2} \equiv R \quad (2.17)$$

to second order. This is a somewhat simplified derivation since it neglects any initial kinetic energy of emitter or absorber systems. The approximation given here for the recoil energy would also imply that the photon energy necessary for emission and absorption of a gamma ray by emitter and absorber systems is a single discrete value for each. Thermal energy of both emitter and absorber systems as well as the Heisenberg uncertainty principle act to broaden this single energy value into a distribution of energies, as shown in the next section.

2.1.2. Derivation with Temperature Considerations

Supposing an emitter system has initial momentum \vec{P}_i before emitting a photon, its final momentum \vec{P}_f after emitting a photon is given by

$$\vec{P}_i = \vec{P}_\gamma + \vec{P}_f \quad (2.18)$$

where \vec{P}_γ is the momentum of emitted photon. By conservation of energy the recoil energy R' imparted to the emitter system of mass M is

$$R' = \frac{P_f^2}{2M} - \frac{P_i^2}{2M}. \quad (2.19)$$

Rearranging Eq. (2.18) and substituting into Eq. (2.19) gives

$$\begin{aligned} R' &= \frac{(\vec{P}_i - \vec{P}_\gamma)^2}{2M} - \frac{P_i^2}{2M} = \frac{P_\gamma^2}{2M} - \frac{\vec{P}_i \cdot \vec{P}_\gamma}{M} \\ &= \frac{P_\gamma^2}{2M} - \frac{P_i P_\gamma}{M} \cos\theta \end{aligned} \quad (2.20)$$

where θ is the angle between \vec{P}_i and \vec{P}_γ . By recalling Eq. (2.5) the recoil energy R' can then be rewritten as

$$R' = \frac{E_\gamma^2}{2Mc^2} - \frac{P_i E_\gamma}{Mc} \cos\theta. \quad (2.21)$$

To a first order approximation Eq. (2.21) will be conveniently simplified to look like R plus an additional term. Conservation of energy requires that

$$E_r = E_\gamma + R' \quad (2.22)$$

for the emission of a photon by a system with initial momentum. Substituting Eq. (2.21) into Eq. (2.22) gives

$$E_r = E_\gamma + \frac{E_\gamma^2}{2Mc^2} - \frac{P_i E_\gamma}{Mc} \cos\theta \quad (2.23)$$

which is identical to Eq. (2.7) except for the final term that can be simplified to

$$\frac{v_i}{c} E_\gamma \cos\theta \quad (2.24)$$

where v_i is the initial speed of the emitter system. Since $\frac{v_i}{c} \ll 1$ for typical temperatures the expression (2.24) is very small compared to E_γ and has little contribution to Eq. (2.23). The solution to Eq. (2.23) can therefore be approximated with the solution to Eq. (2.7). The

energy E_γ can then be approximated as $E_\gamma \approx E_r$ as in Eq. (2.10). The expression for R' then becomes

$$R' \approx \frac{E_r^2}{2Mc^2} - \frac{v_i E_r}{c} \cos\theta. \quad (2.25)$$

Since the first term is just R by Eq. (2.17), R' can be finally simplified to

$$R' \approx R - \frac{v_i}{c} E_r \cos\theta \quad (2.26)$$

which, when substituted back into Eq. (2.22), gives the expression

$$\begin{aligned} E_\gamma &= E_r - R' \\ &\approx E_r - R + \frac{v_i}{c} E_r \cos\theta. \end{aligned} \quad (2.27)$$

For a collection of emitter systems in thermal motion, θ takes on a distribution resulting in E_γ becoming a distribution of energies centered at $E_r - R$. A similar derivation can be done for absorber systems to show that

$$E_\gamma \approx E_r + R - \frac{v_i}{c} E_r \cos\theta \quad (2.28)$$

meaning that the probability distribution for gamma absorption by absorber systems with thermal energy will be a probability distribution centered around $E_r + R$.

The previous discussion is primarily valid only when the emitter and absorber systems are essentially free bodies (such as a gas of radioactive nuclei) which explains why fluorescence resonance for nuclear gamma ray emissions is essentially impossible. The centers of the probability distributions for the absorber and emitter are separated by a value of $2R$ with $R \propto E_r^2$. Overlap of the distributions therefore becomes negligible for high energy emissions which typically have recoil energies on the order of 10^{-2} eV with linewidths on the order of 10^{-6} [6], a factor of 10,000 smaller than the peak separation. Even temperature broadening of the distributions is not sufficient to overcome the large distribution separation for nuclear like emissions.

However, the situation is different in solids. In this case recoil energy may be minimal since the whole structure (typically a crystal lattice) may recoil. The recoil energy R from Eq. (2.17) of the system becomes negligible as the mass of the emitter or absorber system goes from that of a single nucleus to that of an entire crystal. Instead, the recoil energy from an emission or absorption is typically expended in the form of lattice vibrations. It is here that the significance of Mössbauer's discovery becomes evident. A small but significant number of emissions and absorptions involve no corresponding expenditure of energy in the form of lattice vibrations and so these emissions and absorptions are recoilless. This allows for significant overlap of the unshifted lines for identical Mössbauer source and absorber since both unshifted lines will be centered at E_γ . Significant resonance can therefore occur.

2.2. Derivation of Doppler Shift by Special Relativity

Historically, there have been two main methods used to analyze the expected frequency shift of a photon between different locations in an accelerating reference frame. The first method is to analyze the frequency shift of the photon by considering the Doppler shift between two locations in the accelerating reference frame. This is typically done by transforming the photon from the inertial reference frame of the first location to the inertial frame of the second location. This method relies heavily on special relativity and is particularly important to the experiment because it not only explains the frequency shift in an accelerating reference frame through the application of the transverse Doppler shift but also offers a calibration technique through the use of the longitudinal Doppler shift. The current section is devoted to the general derivation of the Doppler shift, which is then applied to the experimental situation in Section 2.2.3. The second method to analyze the frequency shift is to use Einstein's equivalence principle to view the accelerating reference frame as an equivalent gravitational field that will result in the photon being blueshifted or redshifted as it moves through the field from the first location to the second location. It is because this method can be applied to the experiment that enables it to be used as a test for Einstein's equivalence principle. The derivation of the frequency shift by using the equivalence principle is discussed in Section 2.3.

The Doppler shift of photons between an emitter and absorber moving at some constant relative velocity to each other is obtained through the application of special relativity. One consequence of special relativity is that not only are the position and time coordinates of objects dependent on the inertial reference frame but the frequency and wave vector of electromagnetic radiation are also dependent on the inertial frame. The longitudinal and transverse Doppler shifts of a photon are therefore the relativistic changes in the photon's observed frequency when it is observed from a different inertial frame. Deriving this shift is elegantly done with the use of 4-vectors. Consider Figure 12, which shows two inertial frames A and A' with frame A' moving at velocity $v\hat{i}$ relative to frame A . An arbitrary point in frame A is given the 4-position $X^\mu = (ct, \vec{r})$ where \vec{r} and t are the space and time coordinates respectively of the point in Figure 12. The covariant representation of the 4-position is denoted $X_\mu = (ct, -\vec{r})$. A photon in the same frame is assigned the 4-wavevector $K^\mu = \left(\frac{\omega}{c}, \vec{k}\right)$ where \vec{k} is wave vector, and ω is the angular frequency of the photon.

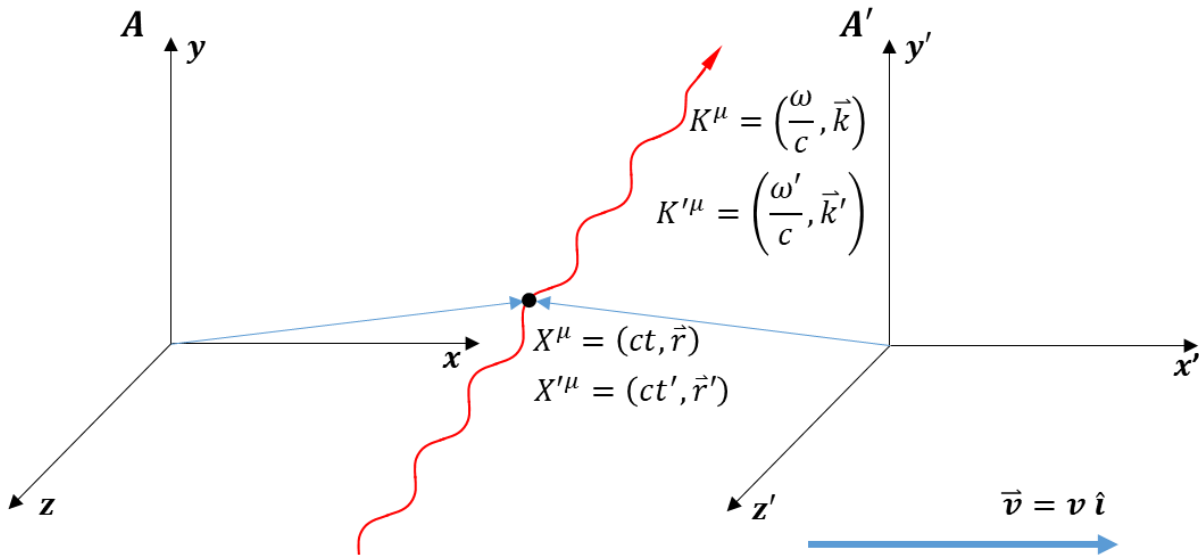


Figure 12. Diagram of transforming between inertial frames. Inertial frame A' moves at velocity $\vec{v} = v\hat{i}$ relative to inertial frame A . An arbitrary 4-vector point/coordinate in the inertial frame A is labeled X^μ and the red electromagnetic wave has 4-wave vector K^μ . In the A' inertial frame these 4-vectors are denoted as X'^μ and K'^μ respectively.

The 4-vector product $K^\mu X_\mu$ is invariant under a transformation to a different inertial frame.

Therefore,

$$K^\mu X_\mu = K'^\mu X'_\mu \quad (2.29)$$

where K'^μ and X'_μ are respectively the 4-wavevector of the photon in the A' frame and the covariant 4-position of the point in the A' frame. This can be rewritten as

$$\frac{\omega}{c}(ct) - \vec{k} \cdot \vec{r} = \frac{\omega'}{c}(ct') - \vec{k} \cdot \vec{r}' \quad (2.30)$$

where the unprimed coordinates are in the A frame and the primed coordinates are in the A' frame.

The boost in the \hat{i} direction of frame A' has no effect on the y and z coordinate of the point when transforming from A to A' (i.e. $y = y'$, $z = z'$). Denoting $\beta = v/c$, and $\gamma = (1 - \beta^2)^{-\frac{1}{2}}$, the Lorentz transforms

$$ct = \gamma(ct' + \beta x'), \quad (2.31)$$

$$x = \gamma(x' + \beta ct') \quad (2.32)$$

transform the other two coordinates (x and t) from the A' frame to the A frame. These transformations now allow for Eq. (2.30) to be rewritten such that the space and time coordinates of the point are expressed entirely in terms of the primed coordinate system. Substituting Eqs. (2.31) and (2.32) along with the equalities $z = z'$ and $y = y'$ into Eq. (2.30) and gathering like terms gives

$$\begin{aligned} ct' \gamma \left(\frac{\omega}{c} - \beta k_x \right) - x' \gamma \left(k_x - \beta \frac{\omega}{c} \right) - y' k_y - z' k_z \\ = ct' \frac{\omega'}{c} - x' k_x' - y' k_y' - z' k_z'. \end{aligned} \quad (2.33)$$

Comparing like primed space-time coordinates conveniently shows that $k_z = k_z'$ and $k_y = k_y'$, which is to be expected since a boost in the \hat{i} direction does not affect the y or z coordinates. For ω' and k_x' , a comparison of the coefficients of t' and x' gives

$$\frac{\omega'}{c} = \gamma \left(\frac{\omega}{c} - \beta k_x \right), \quad (2.34)$$

$$k'_x = \gamma \left(k_x - \beta \frac{\omega}{c} \right), \quad (2.35)$$

which are the Lorentz transforms for the photon frequency and wave vector. Eq. (2.34) is of particular interest since additional manipulation can turn the equation into an expression relating ω' to ω and the angle the photon makes with the x -axis in the A frame. Figure 13 depicts how k_x and k'_x are respectively related to the angle the photon makes with x -axis in the A frame and A' frame.

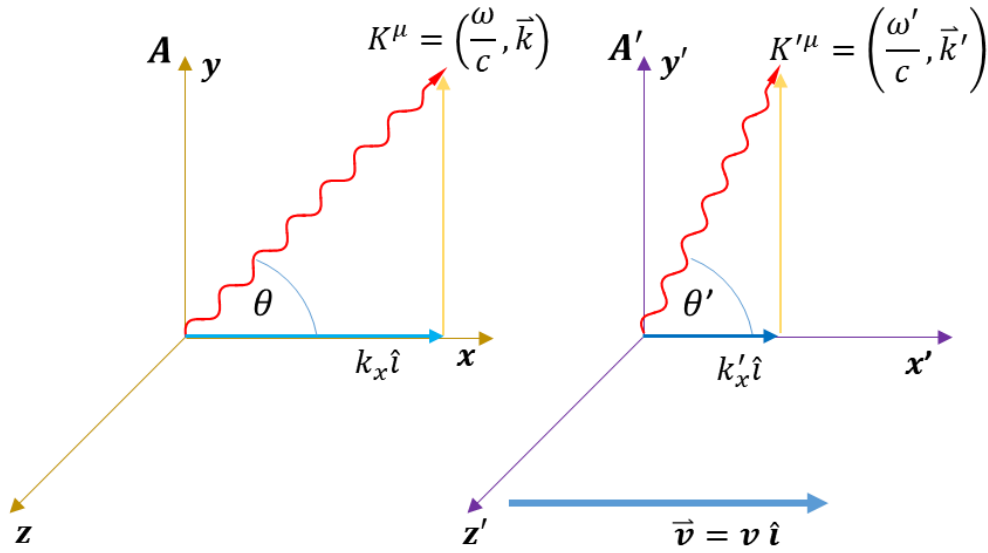


Figure 13. Diagram of k_x transformation between inertial frames. Inertial frame A' moves at velocity $\vec{v} = v\hat{i}$ relative to inertial frame A . A photon with 4-wave vector K^μ in the A frame (K'^μ in the A' frame) is depicted in each of the inertial frames. The k_y and k_z components are unchanged between the two frames but the K^μ components ω and k_x undergo transformation with $k'_x < k_x$ and $\omega' < \omega$. The angles θ and θ' are respectively the angles the photon path makes with the x -axis in the A and A' frame. Since $k'_x < k_x$ and k_y and k_z are unaffected by the transformation, it holds true that $\theta < \theta'$.

Letting the magnitude of the photon wave vector \vec{k} be given as k , an examination of Figure 13 shows that the value k_x in the A frame, which is the component of \vec{k} in the \hat{i} direction, can be written as

$$k_x = k \cos(\theta) \quad (2.36)$$

where k is the magnitude of the photon wave vector in frame A and θ is the angle \vec{k} makes with the x -axis in the A frame. Noting that

$$\frac{\omega}{c} = k, \quad (2.37)$$

Eq. (2.37) can be substituted into Eq. (2.36) and the resulting expression for k_x can be substituted into Eq. (2.34) to yield

$$\begin{aligned} \omega' &= \gamma(\omega - \beta\omega \cos(\theta)) \\ &= \gamma\omega(1 - \beta \cos(\theta)). \end{aligned} \quad (2.38)$$

This is the most general equation relating frequency shifts between two different inertial frames. From Eq. (2.38) immediately follow the equations for the longitudinal Doppler shift and the transverse Doppler shift.

2.2.1. Derivation of the Longitudinal Doppler Shift

The longitudinal Doppler shift is the frequency shift when the source and absorber move towards or away from each other longitudinally. For the longitudinal Doppler shift the absorber frame can be considered to be the A' frame and the emitter frame to be the A frame. Then, the photon will move between them along the source-absorber axis which is the x -axis. The angle θ will therefore be zero and Eq. (2.38) will reduce to the longitudinal Doppler shift equation

$$\omega' = \gamma\omega(1 - \beta). \quad (2.39)$$

For $v \ll c$, Eq. (2.39) can be approximated with a binomial expansion by noting that

$$\gamma = (1 - \beta^2)^{-\frac{1}{2}} \approx 1 + \frac{\beta^2}{2} \quad (2.40)$$

since $\beta \ll 1$. Substituting Eq. (2.40) into Eq. (2.39) gives the first order approximation in powers of β

$$\omega' \approx \omega(1 - \beta). \quad (2.41)$$

The relative longitudinal Doppler shift is the shift in the photon energy between source and absorber relative to its original energy in the emitter frame. This is denoted $\Delta E/E$ where E is the energy of the photon in the emitter frame. Since the energy of a photon is given by

$$E = \hbar\omega, \quad (2.42)$$

Eq. (2.41) can be rearranged to give the relative longitudinal Doppler shift

$$\frac{\Delta E}{E} = \frac{\hbar\omega' - \hbar\omega}{\hbar\omega} \approx -\beta \quad (2.43)$$

between the absorber and emitter. The notation in Eq. (2.43) is equivalent to the convention that defines positive v of the absorber to be moving away from emitter. Adopting the more standard convention for measuring frequency shift of waves where v is defined as positive when source and absorber are moving toward each other, Eq. (2.43) becomes

$$v = c \frac{\Delta E}{E}. \quad (2.44)$$

For an ^{57}Fe Mössbauer emitter and absorber the relative velocity necessary to move the unshifted lines off each other by a linewidth Γ is given by $v = c\Gamma/E$. Given that $\Gamma/E = 3.2 \times 10^{-13}$ for ^{57}Fe , the velocity necessary to shift the absorber and emitter lines by a linewidth is found to be about 0.1 mm/s.

2.2.2. Derivation of Transverse Doppler Shift

The transverse Doppler shift is the frequency shift the photon undergoes between emitter and absorber when the emitter and absorber move only transversely to each other. The transverse Doppler shift can be found by letting frame A be the emitter frame and frame A' be the absorber frame which moves at velocity $\vec{v} = v\hat{i}$ relative to frame A . In the transverse Doppler shift the absorber absorbs a photon at the precise moment that it is only moving perpendicularly to the emitter as seen in Figure 14. In order for the displacement vector between the absorber and emitter at moment of absorption to be perpendicular to $\vec{v} = v\hat{i}$, it must have no x -component. The photon wave vector travels along this displacement vector

in the A frame and therefore is emitted at angle $\theta = \pi/2$ relative to the x -axis in reference frame A .

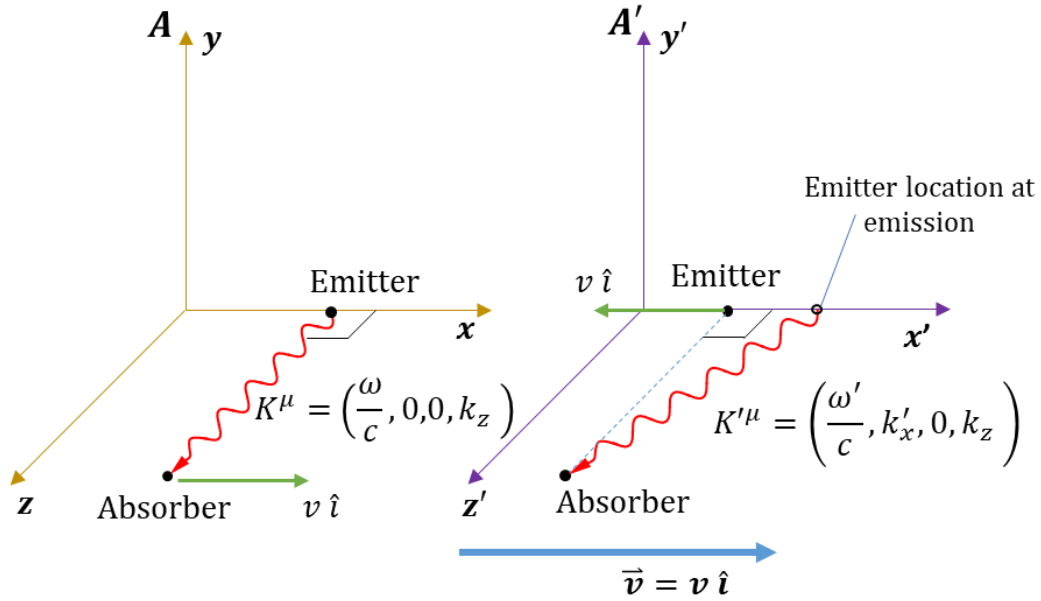


Figure 14. Diagram of transverse Doppler shift. The absorber inertial frame A' moves at velocity $\vec{v} = v\hat{i}$ relative to the emitter inertial frame A . The wave vector of a photon moving between emitter and absorber is shown in both the A and A' frames. The emitter and absorber have the same x -coordinate at the moment of photon absorption. Therefore, in frame A the photon wave vector component $k_x = 0$. Since absorber velocity $\vec{v} = v\hat{i}$, the wave vector \vec{k} is perpendicular to \vec{v} in reference frame A . However, the absorber observes the photon as having originated from the emitter location at the time of emission, which does not have the same x -coordinate as absorber location at absorption in the A' frame. Therefore, in the A' frame $k'_x \neq 0$.

Since $\cos\left(\frac{\pi}{2}\right) = 0$, Eq. (2.38) simplifies to the transverse Doppler shift equation

$$\omega' = \gamma\omega. \quad (2.45)$$

For $\beta \ll 1$, the approximation for γ in Eq. (2.40) can be substituted into Eq. (2.45) to give

$$\omega' \approx \omega \left(1 + \frac{\beta^2}{2}\right). \quad (2.46)$$

The relative transverse Doppler shift $\Delta E/E$ between emitter and absorber can then be calculated using Eq. (2.42) to be

$$\frac{\Delta E}{E} = \frac{\hbar\omega' - \hbar\omega}{\hbar\omega} \approx \frac{\beta^2}{2}. \quad (2.47)$$

The velocity v needed for a relative shift $\Delta E/E$ is

$$v = c \sqrt{\frac{2\Delta E}{E}}. \quad (2.48)$$

For an ^{57}Fe Mössbauer emitter and absorber the transverse velocity necessary to move the unshifted lines off each other by a linewidth Γ is then given by $v = c\sqrt{2\Gamma/E}$. Given that the value $\Gamma/E = 3.2 \times 10^{-13}$ for ^{57}Fe , the transverse velocity can be calculated to obtain a value of about 240 m/s. Comparing this velocity to that necessary for the longitudinal shift (at the end of Section 2.2.1) shows that the transverse velocity is greater than the longitudinal velocity by a factor of 10^6 .

2.2.3. Derivation of Doppler Shift in the Proposed Experiment

Armed with Eq. (2.47) the expected transverse Doppler shift for the experiment can now be obtained. In the proposed experiment the emitter is located in the lab frame while the absorber is the disc location receiving the incident gamma rays. As seen in Figure 15, a collimator will be used to allow only unidirectional gamma rays to enter the disc at one location on the disc. The collimator and disc are positioned such that the paths of the gamma rays are perpendicular to the velocity vector \vec{v} of the absorber point. The absorber point will therefore have no longitudinal component relative to the source and so emitted photons will only undergo a transverse Doppler shift.

Since the disc velocities in the experiment are much smaller than the speed of light the expected transverse Doppler shift is given by Eq. (2.47) to obtain

$$\frac{\Delta E}{E} \approx \frac{\beta^2}{2} = \frac{v^2}{2c^2} \quad (2.49)$$

where $|\vec{v}| = v = \beta c$ is the speed of the absorber location relative to the source. Since $v = R\Omega$, Eq. (2.49) can be rewritten as

$$\frac{\Delta E}{E} \approx \frac{R^2 \Omega^2}{2c^2} \quad (2.50)$$

which is the equation of fundamental importance for the proposed experiment.

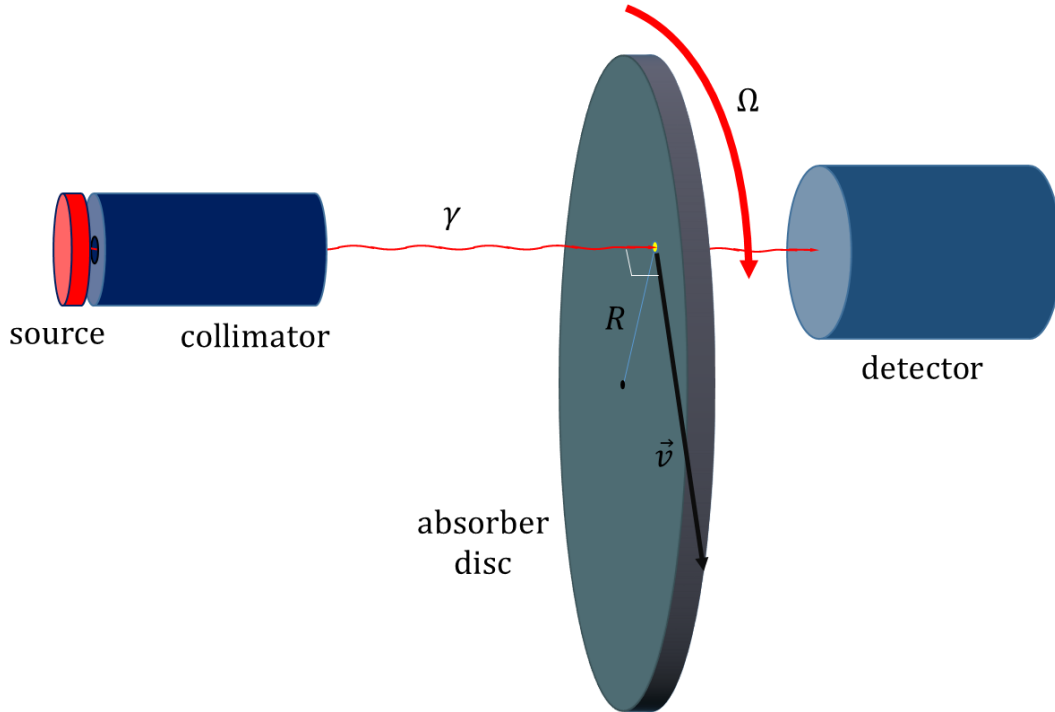


Figure 15. Diagram of the proposed experiment with transverse velocity. The collimator ensures that gamma rays emitted by the source travel unidirectionally to the disc which is rotating at angular velocity Ω . The rotating disc and collimator are positioned so that the gamma paths are perpendicular to the velocity \vec{v} of the absorber location and so the absorber moves only transversely relative to the emitter.

It should be noted that the application of Eq. (2.47) to the situation depicted in Figure 15 is only valid if the emitter and absorber point are in inertial reference frames. In actuality the absorber location is in an accelerating reference frame and is experiencing an acceleration directed toward the center of the disc. A derivation using special relativity would require the use of Doppler shifts in accelerating reference frames. However, for $\beta \ll 1$, the assumption of an inertial reference frame reasonably approximates the solution. As will be seen in Section 2.3 the result from the transverse Doppler shift analysis will differ from the result obtained from the equivalence principle by fourth order terms in powers of β and higher.

To calculate the velocity necessary to obtain a measurable shift Eq. (2.48) is used. Since the transverse velocity of the absorber disc at the location of absorption is given by $v = R\Omega$, substituting this into Eq. (2.48) gives

$$R\Omega = c \sqrt{\frac{2\Delta E}{E}}. \quad (2.51)$$

Eq. (2.51) can then be rearranged to find the angular speed necessary. For a radial distance of $R = 0.10$ m the angular speed needed for a natural linewidth shift is found by using $\Delta E/E = \Gamma/E = 3.22 \times 10^{-13}$. Substituting into a rearranged Eq. (2.51) yields

$$\begin{aligned} \Omega &= \frac{c}{R} \sqrt{\frac{2\Delta E}{E}} & (2.52) \\ &= \left(\frac{3.00 \times 10^8 \text{ ms}^{-1}}{0.1 \text{ m}} \right) \sqrt{2 \times 3.22 \times 10^{-13}} \\ &= 2400 \text{ rad s}^{-1} = 23,000 \text{ rev/min.} \end{aligned}$$

Therefore, an angular speed of over 20,000 rpm will be necessary to observe a relative shift of a natural linewidth.

Prior to the measuring the transverse Doppler shift a preliminary experiment measuring the longitudinal Doppler shift will be performed to both demonstrate that the Mössbauer effect can be measured and also to calibrate the proposed experiment. The setup is shown in Figure 16 and is very similar to the second Mössbauer transmission experiment shown in Figure 6. The disc is tilted from the vertical by an angle of θ and rotated at very low angular speed. At the absorber location the disc will have a velocity component longitudinal to the photon paths. This will result in a longitudinal Doppler shift that can then be measured by the change in transmission rate of 14.4 keV photons through the disc. Changing the rate of disc rotation allows the experimenter to adjust the longitudinal velocity component of absorber location on the disc and thereby scan over the entire resonance spectrum. It is noted that the absorber location still has a transverse velocity component to the photon path and so a transverse

Doppler shift will also be present. However, as will be examined in Section 2.4, the transverse Doppler shift is negligible relative to the longitudinal shift at low velocities for large angles.

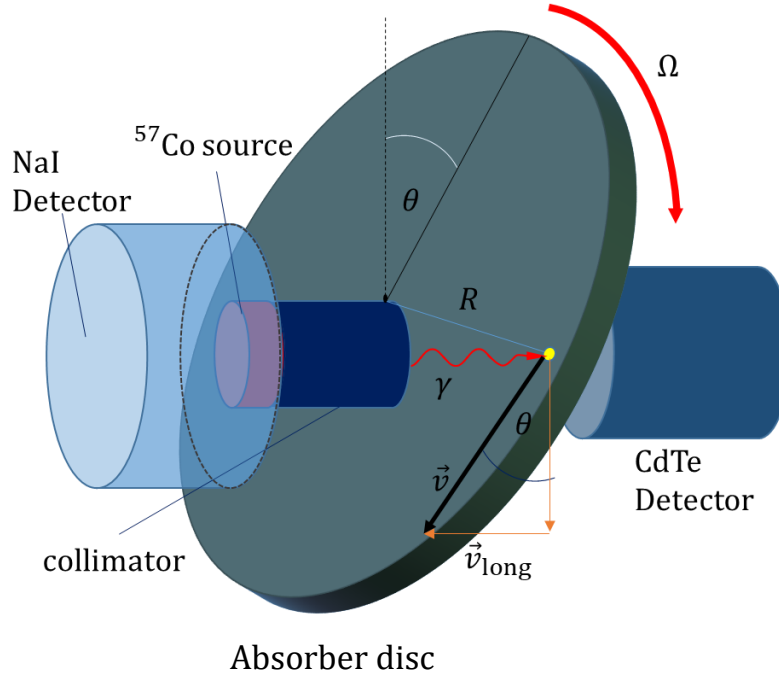


Figure 16. Diagram of the longitudinal Doppler shift experiment. The absorber disc is angled from the vertical by an angle of θ . It is rotated at angular speed Ω . A CdTe detector measures the rate of 14.4 keV gamma rays transmitted through the absorber disc in coincidence with 122.1 keV gamma rays from the ^{57}Co Mössbauer source that are measured by a NaI detector. At the location of absorption the disc has a velocity component longitudinal to the source resulting in a longitudinal Doppler shift between source and absorber.

Assuming that the absorber location is level with the disc center, the longitudinal velocity component of the absorber location toward the source is given by

$$v_{long} = v \sin(\theta) = R\Omega \sin(\theta) \quad (2.53)$$

where θ is the angle of inclination of the disc and $v = |\vec{v}|$ is the speed of the absorber location relative to the lab frame and is related to the angular speed by $v = R\Omega$. The longitudinal velocity needed to give the relative shift T/E of the natural linewidth is given by Eq. (2.44). Setting Eq. (2.44) and Eq. (2.53) equal to each and substituting $\Delta E/E = T/E$ gives

$$R\Omega \sin(\theta) = c \frac{\Gamma}{E}. \quad (2.54)$$

Using a tilt of 30° for the disc, a distance of 5 cm for the radial distance to the absorber location, and a value of 3.22×10^{-13} for Γ/E , the angular speed needed to give a relative shift of a linewidth is

$$\begin{aligned} \Omega &= \frac{\Gamma}{E} \frac{c}{R \sin(\theta)} = (3.22 \times 10^{-13}) \left(\frac{3.00 \times 10^8 \text{ms}^{-1}}{0.05 \text{ m} \times \sin\left(\frac{\pi}{6}\right)} \right) \quad (2.55) \\ &= 3.9 \times 10^{-3} \text{rad s}^{-1} = 0.037 \text{ rev/min}. \end{aligned}$$

To scan over the full spectrum the angular speed needed should range $-\nu_c < \Omega < \nu_c$ where ν_c is at least 3 times the linewidth of the resonance spectrum. Since the resonance spectrum linewidth will be twice the absorber/emitter linewidth [11], the angular frequency Ω needs to be able to range from about -0.22 rev/min to 0.22 rev/min. However, this is under the ideal condition that the resonance spectrum has a linewidth twice the natural linewidth of the ^{57}Fe 14.4 keV spectrum, which is about 0.1 mm/s. In actuality, additional effects [11] stretch the resonance spectrum out so that its linewidth is typically closer to 0.5 mm/s. The angular frequency therefore needs to range from -0.60 rev/min to 0.60 rev/min.

2.3. Derivation using Equivalence Principle

The second way to derive the photon energy shift is to apply Einstein's equivalence principle. The equivalence principle states that rather than considering the absorption as occurring in an accelerating reference frame, the absorption can equivalently be considered to occur in a gravitational field producing the same acceleration. The acceleration \vec{a} on any given fixed test particle on the disc is given by

$$\vec{a} = -r\Omega^2\hat{r} \quad (2.56)$$

when the angular velocity Ω of the disc is constant and the distance r is the radius from the center of the disc to the fixed particle. This acceleration is non-relativistic since the disc velocities used in the experiment are much smaller than c . When viewed in the inertial frame of the lab, the acceleration of the test particle is due to the centripetal force acting on the particle. Viewed in the non-inertial frame of the disc, however, the test particle acceleration

is zero since it is stationary within the disc frame. The centripetal force on the particle must therefore be counteracted by a field of equal strength. Therefore, by Einstein's equivalence principle, the particle acceleration observed in the lab frame (Eq. (2.56)) is replaced by an equivalent field when observed in the disc frame. The equivalent field in the disc frame is defined to be the force divided by the mass:

$$\vec{f} \equiv \frac{\vec{F}}{m} = r\Omega^2\hat{r} \quad (2.57)$$

where \vec{f} is the field at radius r , the mass of the test particle is m , and \vec{F} is the force exerted by the field on the test particle. By definition of potential $\vec{f} = -\vec{\nabla}\phi$, the potential function ϕ at radius r of the disc is given by

$$\phi = -\frac{1}{2}r^2\Omega^2. \quad (2.58)$$

Therefore, when the photon moves from emitter to absorber in the frame of the disc, it will experience a change in potential energy due to this potential which is equivalent to a gravitational field, causing it to be shifted up in energy as it falls in the potential. The absorber location is in the disc and so will be in the field. However, the emitter is in the lab frame and not in the disc frame. To evaluate the potential energy change between emitter and absorber the emitter must be assigned an equivalent location on the disc. Since the emitter is not accelerating in the lab frame, its potential is zero in the disc frame, the same as the disc center potential, and so can be considered as being at the disc center. The photon potential change as it travel from the disc center to the absorber location is given by

$$\begin{aligned} \Delta\phi &= \phi_{abs} - \phi_{emit} \\ &= \frac{1}{2}r_{emit}^2\Omega^2 - \frac{1}{2}r_{abs}^2\Omega^2 \end{aligned} \quad (2.59)$$

where r_{emit} and r_{abs} are the radial distances of emitter and absorber locations from the center of the disc. Since $R = r_{abs}$ as indicated in Figure 15 and $r_{emit} = 0$ for an emitter location at the disc center, Eq. (2.59) becomes

$$\Delta\phi = \frac{1}{2}(0^2 - r_{abs}^2)\Omega^2 = -\frac{1}{2}R^2\Omega^2. \quad (2.60)$$

However, to show the relative shift in energy of the photon by using the equivalence principle, there is the issue that a photon has no mass and so will undergo no change in potential energy. This problem is remedied by thinking of the photon as having an “apparent mass” m_a given by

$$m_a = \frac{E}{c^2} \quad (2.61)$$

where Einstein’s equation is used to calculate the mass of the photon if it were to have such a mass. The change in energy ΔE of the photon as it travels between emitter and absorber is the negative of its change in potential energy since the photon must gain energy ΔE as it loses potential energy ΔE . Then, using Eq. (2.58), $\Delta E/E_i$ will be given by

$$\frac{\Delta E}{E} = \frac{-m_a\Delta\phi}{m_a c^2} = \frac{\frac{R^2}{2}\Omega^2}{c^2} = \frac{R^2\Omega^2}{2c^2} \quad (2.62)$$

which is in fact equivalent to Eq. (2.50) demonstrating the two derivations are equivalent to second order in powers of β and R (since $\beta = R\Omega/c$).

To examine the deviation of the transverse Doppler shift derivation from the one just discussed, the expansion of γ in Eq. (2.40) must be done to higher powers of β . Doing so gives

$$\gamma = (1 - \beta^2)^{-\frac{1}{2}} = 1 + \frac{\beta^2}{2} + \frac{3\beta^4}{8} + \frac{5\beta^6}{16} + O(\beta^8) \quad (2.63)$$

for $|\beta| < 1$. Using a similar derivation to that used in Section 2.2.2 for the transverse Doppler shift gives the corrected relative Doppler shift as

$$\frac{\Delta E}{E} = \frac{\beta^2}{2} + \frac{3\beta^4}{8} + \frac{5\beta^6}{16} + O(\beta^8) \quad (2.64)$$

which can be modified to the specific experimental equation

$$\frac{\Delta E}{E} = \frac{R^2\Omega^2}{2c^2} + \frac{3R^4\Omega^4}{8c^4} + \frac{5R^6\Omega^6}{16c^6} + O\left(\left(\frac{R\Omega}{c}\right)^8\right) \quad (2.65)$$

by recalling that $\beta = v/c$ by definition and that $v = R\Omega$ for the experiment. The deviation of Eq. (2.65) from Eq. (2.62) is only apparent in powers of β or $R\Omega/c$ greater than three. Since $\beta \ll 1$ (in the case of the experiment about 10^{-6}), these are negligible. However, the derivation for the energy shift using the equivalence principle must still give the same result as the transverse Doppler shift if the experiment is to successfully test the equivalence principle. Critically, two important assumptions were made in the derivations of the energy shift of the photon that relax this condition so that the two results need only be approximately the same. First, the transverse Doppler shift derivation made use of inertial frames which was only a close approximation of the actual situation where the absorber is in an accelerating reference frame. Second, the derivation using the equivalence principle assumed non-relativistic mechanics, a close approximation given the non-relativistic speeds for the experiment. Therefore, since the two derivations are themselves approximations, the results will probably only be the same to low powers of β or $R\Omega/c$ which is clearly the case here. Taking this into account the two derivations appear consistent with each other.

2.4. Implication of Uncertainty due to Longitudinal Doppler Effect

In the design of any experiment the sources of uncertainty need to be considered. The greatest single source of experimental uncertainty is probably the introduction of uncontrolled longitudinal Doppler shift. This could arise in the form of disc vibration since the absorber location would therefore be moving toward or away from the source. It could also arise from a tilt in the disc relative to the source and collimator. To determine the significance of these sources of uncertainty the relative magnitudes of the longitudinal and transverse Doppler effects need to be examined.

The relative Doppler shifts resulting from longitudinal and transverse Doppler effects are given by Eqs. (2.43) and (2.47) respectively. To compare the Doppler shift magnitudes of the two effects Eq. (2.43) is divided by Eq. (2.47). This gives

$$\frac{\Delta E_L/E}{\Delta E_T/E} = \frac{\Delta E_L}{\Delta E_T} \approx \frac{\beta_L}{\frac{\beta_T^2}{2}} \approx \frac{\beta_L}{\beta_T^2} \quad (2.66)$$

where $v_L = \beta_L c$ is longitudinal velocity and $v_T = \beta_T c$ is the transverse velocity. Generally, $\beta_L, \beta_T \ll 1$ so the expression lends itself toward being quite large unless $\beta_T \gg \beta_L$. This is advantageous for the longitudinal Doppler Shift experiment where both β_L and β_T are on the order of 10^{-13} or 10^{-12} . Eq. (2.66) reduces to $\Delta E_L/\Delta E_T \approx 10^{12}$ meaning that the transverse Doppler effect is negligible for that experiment. However, this feature is a disadvantage for the transverse Doppler Shift experiment. For β_T in the range 10^{-6} , the approximate value of β_T necessary for the proposed experiment, Eq. (2.66) gives $\Delta E_L/\Delta E_T \approx \beta_L 10^{12}$. This means that for $\beta_L > 10^{-12}$ the longitudinal Doppler shift will dominate and if the uncertainty on β_L is much larger than 10^{-12} then the experiment will almost inevitably fail.

Unfortunately, an analysis of the proposed experiment reveals it will suffer from just such an issue and so will almost certainly fail. Figure 17 shows the scenario where the collimated photons from the source will not strike the disc perfectly perpendicular to the local disc velocity. The absorber location velocity is angled from the perpendicular to the photon path by an angle α . The lab frame containing the source will be denoted as the S frame. The inertial frame of reference containing the absorber location is denoted as the S' frame and it moves at velocity \vec{v} relative to frame S . The x -axes of both frames are chosen to be parallel to vector \vec{v} as shown in Figure 17. The Doppler shift experienced by photons when moving from frame S to frame S' is therefore given by Eq. (2.38).

For $v \ll c$ the factor γ is approximated by Eq. (2.40) allowing Eq. (2.38) to be approximated as

$$\begin{aligned}\omega' &\approx \omega \left(1 + \frac{\beta^2}{2}\right) (1 - \beta \cos(\theta)) \\ &\approx \omega \left(1 - \beta \cos(\theta) + \frac{\beta^2}{2}\right)\end{aligned}\tag{2.67}$$

where θ is angle between the photon wave vector and the x -axis of the S frame when viewed from the S frame.

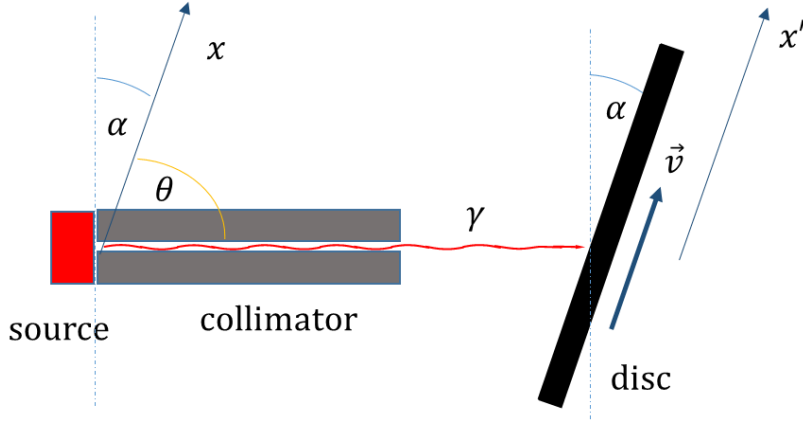


Figure 17. Side Diagram of collimated source and angled disc. The source is collimated so as to emit unidirectional gamma rays with very small spread. The rotating disc is viewed from the side with the absorber location moving at velocity \vec{v} relative to the source. The disc is slightly angled from the perpendicular to the gamma ray path by an angle α . The absorber location then has move a longitudinal and transverse component relative to the emitter.

From Figure 17 it can be seen that $\alpha + \theta = \pi/2$ so $\cos(\theta) = \sin(\alpha)$. Substituting this into Eq. (2.67) and making the small angle approximation $\sin(\alpha) \approx \alpha$ yields

$$\omega' \approx \omega \left(1 - \beta\alpha + \frac{\beta^2}{2} \right). \quad (2.68)$$

By using Eq. (2.42) and rearranging Eq. (2.68), the relative Doppler shift is found to be

$$\frac{\Delta E}{E} \approx -\beta\alpha + \frac{\beta^2}{2}. \quad (2.69)$$

Since β is on the order of 10^{-6} , the relative Doppler shift will therefore be dominated by the longitudinal Doppler shift unless the angle $\alpha \approx \beta$ or smaller. This would imply that the disc must be perpendicular to the gamma rays to within an angle of 10^{-6} radians. It seems doubtful that this can be achieved, especially when the possibility of vibration is present. Even if such precision is attainable, the photon spread from the source through the collimator is sufficient to destroy any meaningful results. Assuming the spread is symmetrical the result would be a smearing effect on the resonance spectrum due to the longitudinal Doppler shift, with some photons shifted up in energy while others are shifted

down in energy depending on the angle at which they strike the disc. As with the disc angle, the spread would need to be extremely small for the experiment-around 10^{-6} . For a collimator of length 1 m and tube width of 1 mm the angular spread is still about 10^{-3} radians. The longitudinal shift would be $\beta\alpha \approx 10^{-6}10^{-3} = 10^{-9}$, which is still 10^3 greater than the transverse shift. The resonance spectrum obtained would therefore be smeared out by about a factor of 1000. Since the experiment already necessitates the use of a small source, the presence of a large smearing effect and the use of a collimator with such small angular spread would by themselves probably make the experiment unfeasible.

The significance of the relative longitudinal shift is also seen when vibration is considered. From Section 2.2.1 the necessary longitudinal velocity to produce a relative shift of a natural linewidth Γ for an ^{57}Fe Mössbauer experiment is on the order of 0.1 mm/s. The equipment to be used for the proposed experiment would probably allow for significant vibration meaning that there would be a significant longitudinal shift. Since the vibration speed of the absorber is not uniform, varying between a maximum velocity as it moves toward the source and a maximum negative velocity as it moves away from the source, the resonance spectrum would again be subjected to a smearing effect.

As a result of disc tilt, angular spread of the photons, and vibration the proposed experiment is being redesigned. In the new design the absorber and source would be placed in a long tube which would then be rotated about an axis perpendicular to the tube. This is shown in Figure 18. Such a design would have the advantage that the source and absorber would both be rigidly fixed in the rotating frame. Angular spread of the photons and tilt would have no effect on the photon energy shift because there can be no longitudinal motion of the absorber relative to the source. The only way to introduce a longitudinal Doppler shift would be if the distance between source and absorber changed with time. This should not be possible when both are fixed in the accelerating frame, except for vibration of the source relative to the absorber. Should the tube vibrate from side to side the source and absorber could also begin to vibrate about their fixed positions in the tube out of phase to each other. This could act to somewhat spread out the spectrum but requiring that both source and absorber be placed

in the tube avoids the catastrophic smearing resulting from vibration of the whole absorber system relative to the lab frame (as in the case of the original design).

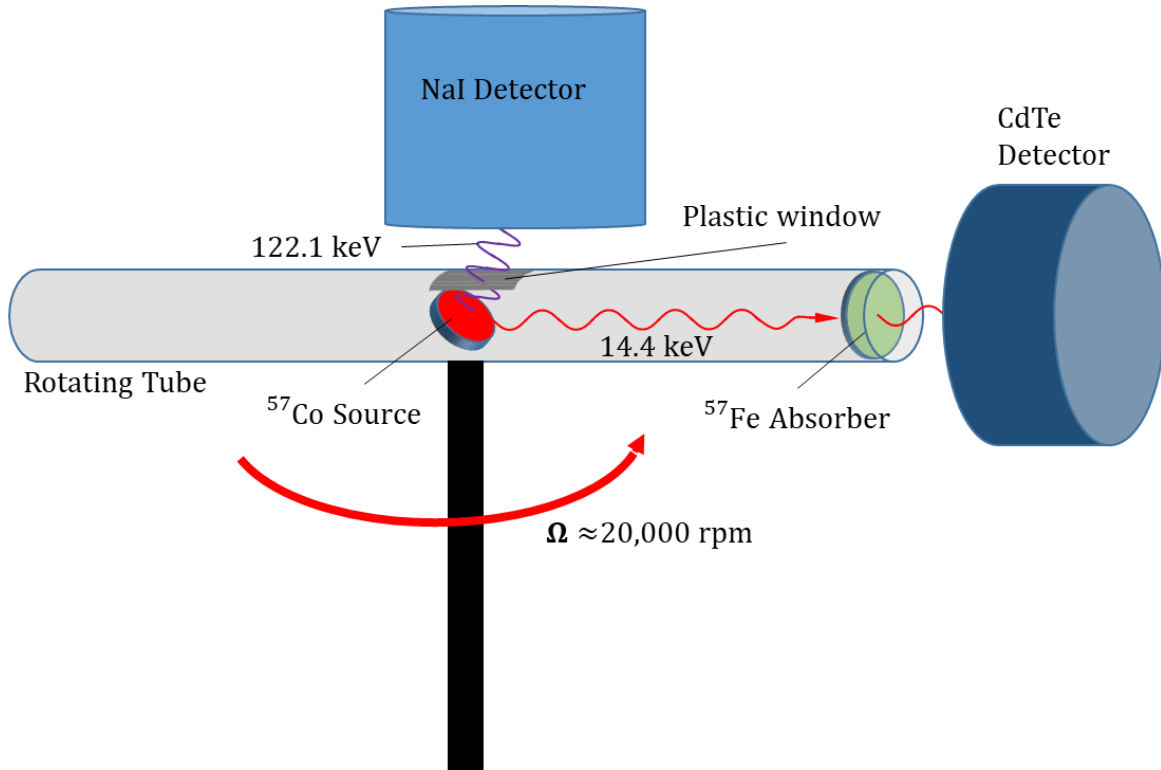


Figure 18. Diagram of Modified experiment for transverse Doppler shift. A tube is rotated perpendicularly about its center at angular speed up to 20,000 rpm. The ^{57}Co source is fixed in the radial middle of the tube while the absorber is fixed at the end of the tube. Gamma rays of energy 14.4 keV will experience a transverse Doppler shift as they travel from source to emitter. When the source, absorber and CdTe detector are aligned, the CdTe detector measures the transmission rate of 14.4 keV gamma rays through the absorber in coincidence with 122.1 keV gamma rays that are measured by the NaI detector.

In the redesigned experiment the absorber is placed at the end of the tube while the ^{57}Co Mössbauer source is placed at the radial center of the tube. The transmission rate of 14.4 keV gamma rays through the absorber is measured by a CdTe detector in coincidence with 122.1 keV gamma rays from the source detected by a NaI detector. The CdTe detector is placed just outside the radial arc swept out by the spinning tube so that once per revolution the source, absorber, and CdTe detector all lie on the same axis. The CdTe detector will be gated so as to only measure pulses when it is collinear with the source and absorber, thereby eliminating

the background noise during the periods of time the CdTe detector cannot be expected to measure transmission counts through the absorber. The NaI detector will be placed directly above the spinning tube so as to have as large a solid angle as possible. A thin plastic window will allow 122.1 keV gamma rays to pass from the source into the NaI detector.

2.5. Derivation of Energy shift for Modified Experimental Design

A new derivation of the energy shift for the modified experimental design is necessary because placing the source and absorber both in the reference frame of the tube introduces some additional factors in the experimental analysis. To consider these factors it is observed that the experiment could also be easily analyzed by imagining that source and absorber are fixed in a rotating disc. To reduce the disc scenario to that of the experiment, the source and absorber locations need only be restricted to a small range of locations that would lie in the tube. It would be faster to analyze the modified experimental design by imagining that the source and emitter lay on the central axis through the tube but while approximately true this analysis neglects the finite width of both absorber and source and does not account for the possibility that source or absorber could have some small deviation from the tube axis. Analyzing the situation by considering the emitter and absorber on a rotating disc allows such deviations to be accounted for. In addition it offers the chance to demonstrate more generally that analysis of the energy shift by using the Doppler shift agrees with an analysis using the equivalence principle.

The situation to be considered is shown in Figure 19. The absorber and emitter are both fixed in the disc frame which is rotated at angular speed Ω . The absorber and emitter locations do not generally lie on the same radial line or have the same radial distance from the center of the disc. In addition, it is not assumed that the emitter and absorber locations are in the same x, y -plane since they could be located at different depths within the disc. As such the emitter and absorber will generally have different z -coordinates as well.

The derivation for the energy shift of the photon between the emitter and absorber locations in the disc can again be performed by using special relativity to find the Doppler shift or by using the equivalence principle to arrive at the equivalent gravitational energy shift of the photon as it moves in the disc frame. As will be seen in Section 2.5.2, the derivation using

Einstein's equivalence principle is almost identical to that used in Section 2.3. However, the derivation of the energy shift as a Doppler shift for the modified experimental design is more involved and can no longer be treated as simply a transverse Doppler shift since the emitter and source do not generally move transversely to each other. Nevertheless, it can be shown that they behave as if they do as far as the Doppler shift is concerned.

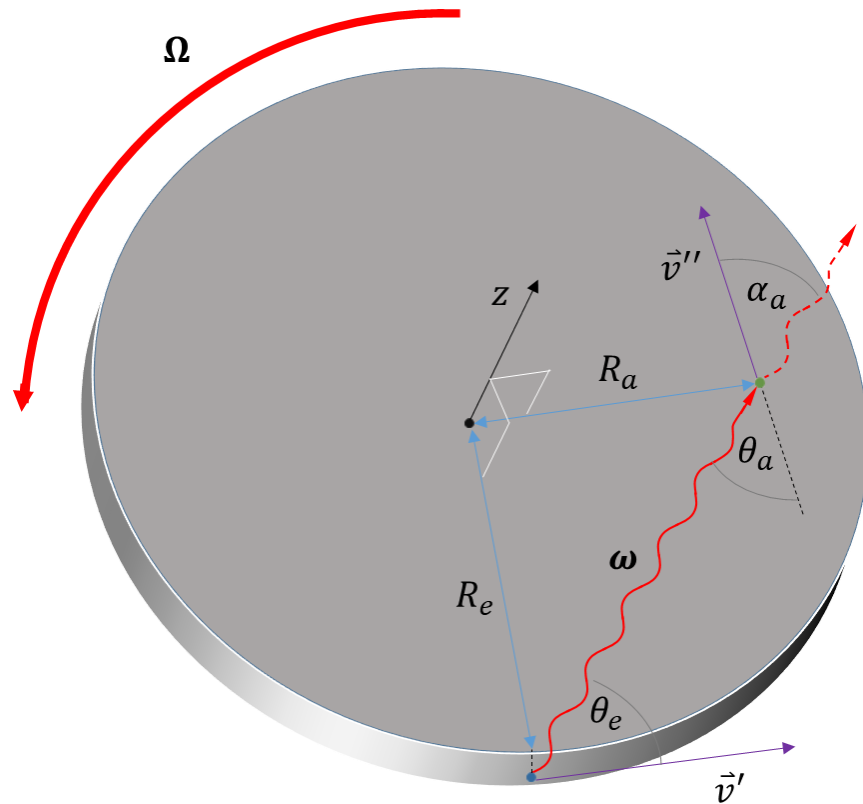


Figure 19. Diagram of photon traversing rotating disc. The disc axis is chosen as the z -axis. A photon with angular frequency ω in the lab frame travels from the emitter location (radius R_e from the z -axis) to the absorber location (radius R_a from the z -axis). The angles θ_e, θ_a correspond to the angles (in the lab frame) the photon path makes with the tangent to the disc at the emitter and absorber locations respectively. The disc rotates at constant angular speed Ω . The velocities \vec{v}' and \vec{v}'' correspond to the velocity of the disc at the emitter and absorber locations respectively.

2.5.1. Derivation using Special Relativity

For the derivation of the Doppler Shift of the photon shown in Figure 19, three reference frames are established. The L frame will denote the lab frame, the S' frame will denote the inertial frame of the first location (the emitter frame), and the S'' frame will denote the inertial frame of the second location (the absorber frame). Again, the assumption is that the

two locations can be treated by special relativity as if they were in inertial frames though in reality they are accelerating frames. For $\beta \ll 1$ the solution obtained by treating the frames as accelerating reference frames can be approximated by the solution obtained from treating them as inertial frames. In this scheme the velocity vectors \vec{v}' and \vec{v}'' of the emitter and absorber relative to the lab frame become the relative respective velocities of the S' and S'' frames to the L frame. The overarching process will be to use Lorentz transformations to transform the photon's 4-wave vector K^μ from the S' frame into the L frame and then from the L frame into the S'' frame.

The relevant transformation of the photon's angular frequency between a rest frame and a moving frame is given by Eq. (2.34). The vector \vec{v}' is the velocity that the S' frame moves relative to the L frame. The L and S' frames are chosen such that their x -axes lie parallel to \vec{v}' , as shown in Figure 20. Letting $\beta_1 = v'/c$, and $\gamma_1 = (1 - \beta_1^2)^{-1/2}$, Eq. (2.34) can be applied to the transformation of angular frequency between the S' and L frames to give

$$\frac{\omega'}{c} = \gamma_1 \left(\frac{\omega}{c} - \beta_1 k_x \right) \quad (2.70)$$

where ω' is the angular frequency of photon in the S' frame, ω is the angular frequency of the photon in the L frame, and k_x is the x -component of the photon wave vector \vec{k} in the L frame.

In Eq. (2.34) the photon angular frequency ω' in the moving frame was a function of the angular frequency component ω in the rest frame and the wave vector component k_x in the rest frame. The other two components in rest frame, k_y and k_z , were ignored. However, this is no longer possible in the scenario illustrated in Figure 19 since the k_z component will play an important role in the transformation from the S' to the S'' frame. Therefore, whereas before the only angle necessary for the transformation was the angle θ of the photon path from the x -axis in the L frame, two other angles must be introduced here in order to obtain k_x and k_z . As shown in Figure 21, the angle ψ is used to denote the angle the photon path makes with the z -axis. Then, the wave vector \vec{k} can be split into two orthogonal components.

The vertical component will then be k_z by definition. The component of \vec{k} that lies in the x, y -plane is denoted as \vec{k}_\perp and the angle it makes with the x -axis is denoted Θ .

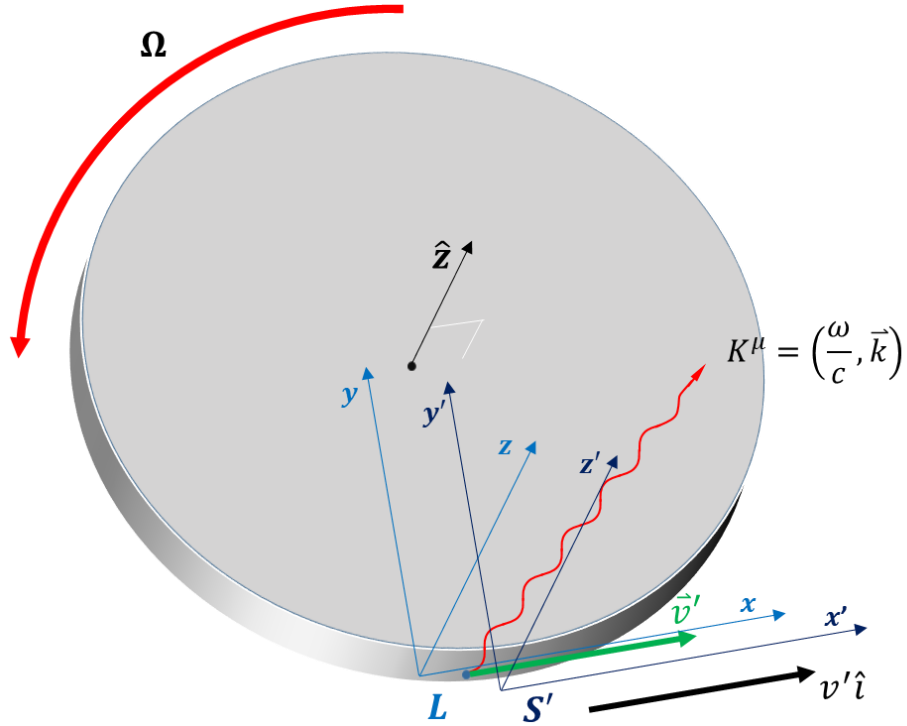


Figure 20. Diagram of L frame and S' frame aligned along emitter velocity \vec{v}' . The emitter has tangential velocity \vec{v}' relative to the laboratory. The L frame and S' frames are chosen so that their x -axes lie parallel to \vec{v}' . The L frame is at rest in the lab while the S' frame moves at velocity $v' \hat{i}$ relative to the L frame and therefore acts as the emitter inertial frame.

The components can then be found in terms of $k = |\vec{k}|$ and the angles ψ and Θ . The component k_z is found to be

$$k_z = k \cos(\psi) \quad (2.71)$$

and then, by using Eq. (2.71), component k_\perp is found to be

$$\begin{aligned} k_\perp &= \sqrt{k^2 - k_z^2} = \sqrt{k^2 - k^2 \cos^2(\psi)} = k\sqrt{1 - \cos^2(\psi)} \\ &= k \sin(\psi). \end{aligned} \quad (2.72)$$

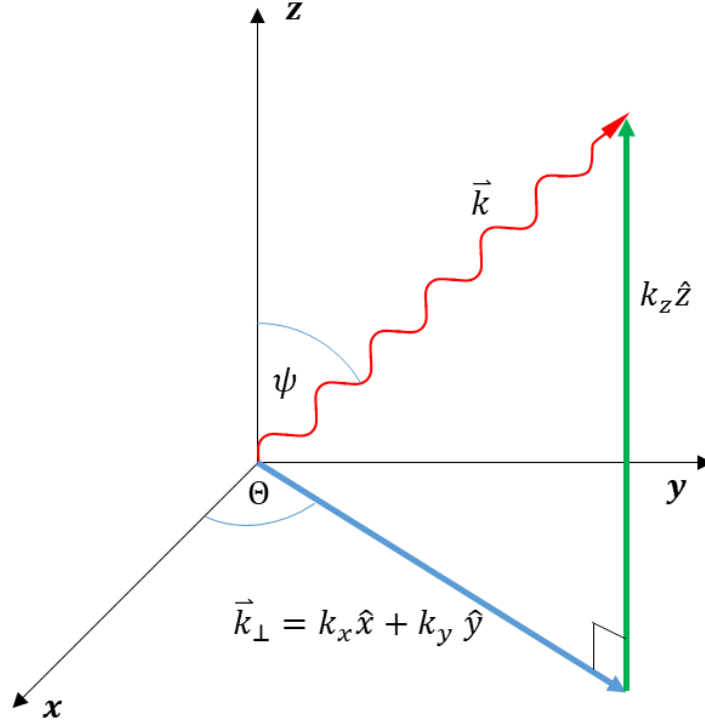


Figure 21. Diagram of k_z and k_{\perp} components of photon wave vector \vec{k} . The wave vector \vec{k} in the L frame can be split into the two orthogonal components $k_z \hat{z}$ and \vec{k}_{\perp} . The angle ψ is the angle the photon path makes with the z -axis. The angle θ is the angle \vec{k}_{\perp} (which lies in the x, y -plane) makes with the x -axis.

The k_x component is therefore given as

$$k_x = k_{\perp} \cos(\theta) = k \sin(\psi) \cos(\theta). \quad (2.73)$$

Substituting k_x into Eq. (2.70), the transformation of the angular frequency from the S' to the S frame in can be rewritten as

$$\frac{\omega'}{c} = \gamma' \left(\frac{\omega}{c} - \beta' k \sin(\psi) \cos(\theta) \right). \quad (2.74)$$

By recalling that $k = \omega/c$, Eq. (2.74) can be simplified and rearranged to give

$$\omega = \frac{\omega'}{\gamma'(1 - \beta' \sin(\psi) \cos(\theta))}. \quad (2.75)$$

For the transformation from the L frame to the S'' frame the L frame is first rotated about the z -axis such that its x -axis is parallel to the \vec{v}'' vector. The axes for S'' are also chosen such that its x -axis lies along the \vec{v}'' vector and its z -axis is parallel to the z -axis in the L frame. The arrangement is shown in Figure 22 and Figure 23.

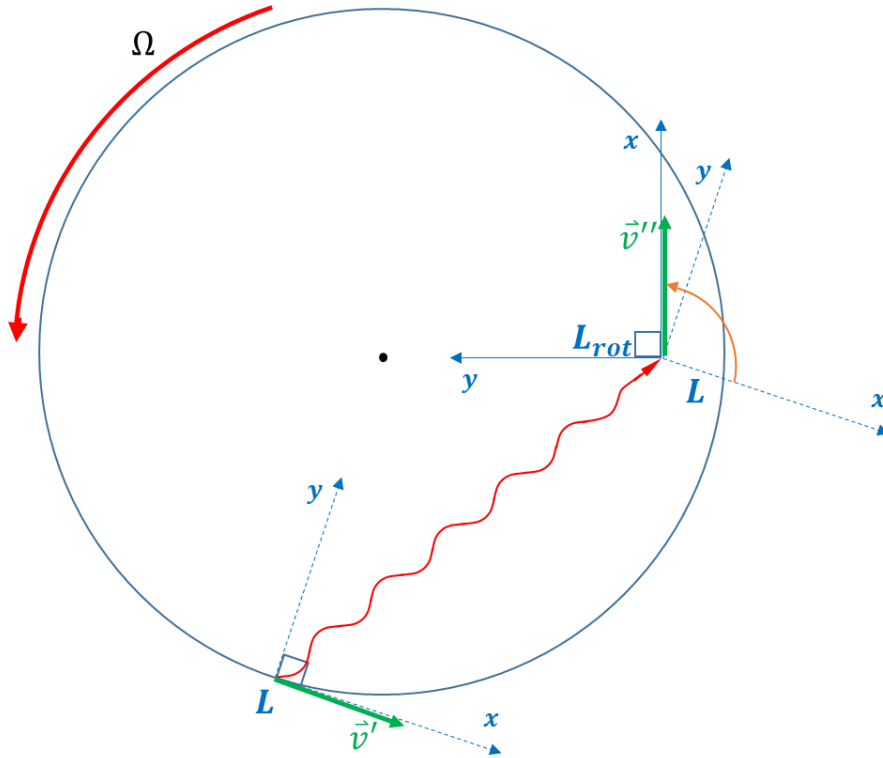


Figure 22. Rotating the L frame. The L frame (shown as the dashed axes) is rotated about its z -axis to form the L_{rot} frame (solid blue axes). The x -axis of the original L frame was parallel to the emitter velocity \vec{v}' while the x -axis of the L_{rot} frame is chosen to align with the absorber velocity \vec{v}'' . Both the original L frame and the rotated L frame are inertial lab frames.

This rotation of the L frame affects the \vec{k} for the photon (though not its length) but leaves unchanged the angular frequency ω and the k_z component of the. Denoting $\beta_2 = v''/c$ and $\gamma_2 = (1 - \beta_2^2)^{-\frac{1}{2}}$, Eq. (2.34) becomes

$$\frac{\omega''}{c} = \gamma_2 \left(\frac{\omega}{c} - \beta_2 \bar{k}_x \right) \quad (2.76)$$

where ω is both the angular frequency in the original and rotated L frame, ω'' corresponds to the angular frequency in the S'' frame, and \bar{k}_x is the k_x component of \vec{k} in the rotated L frame (denoted the L_{rot} frame).

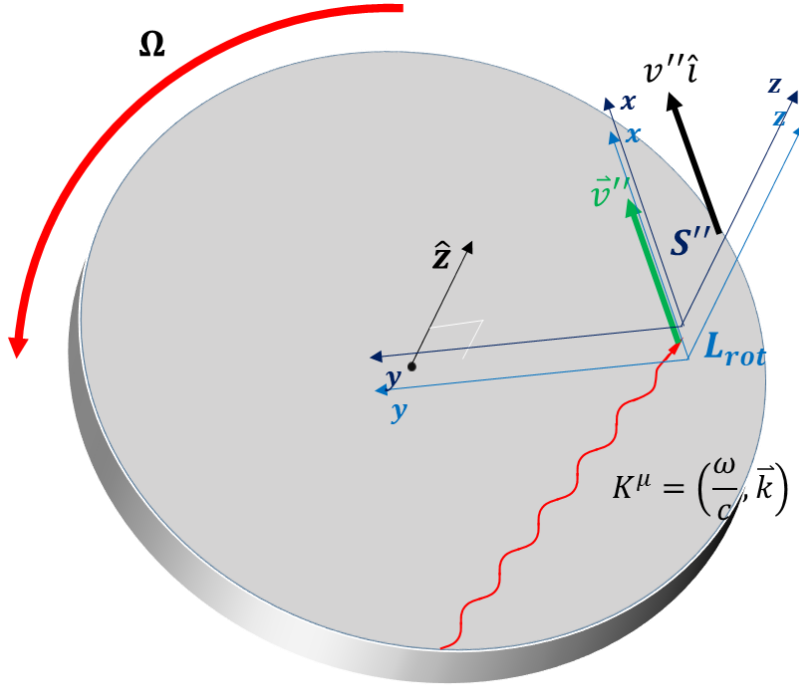


Figure 23. Diagram of L_{rot} frame and S'' frame aligned along absorber velocity \vec{v}' . The L_{rot} frame and the S'' frame have been chosen so that their x -axes align with \vec{v}' . The L_{rot} frame is at rest in the lab while the S'' frame moves with velocity $v''\hat{i}$ relative to it making the S'' frame the inertial reference frame of the absorber.

In order to rewrite \bar{k}_x in terms of ω and the two angles Θ and ψ it is necessary to realize that the rotation of L about the z -axis left ψ unchanged but did effect Θ . Since k and k_z are unchanged by a rotation about the z -axis, the angle ψ that \vec{k} makes with \hat{z} remains constant. On the other hand, while the magnitude k_\perp remains constant under the rotation, the angle that \vec{k}_\perp makes with the new x -axis is changed and so is denoted as $\bar{\Theta}$ in the rotated L frame. Using the same reasoning that was applied to Eq. (2.74), Eq. (2.76) is then rewritten as

$$\frac{\omega''}{c} = \gamma_2 \left(\frac{\omega}{c} - \beta_2 k \sin(\psi) \cos(\bar{\Theta}) \right). \quad (2.77)$$

By recalling again that $k = \omega/c$, Eq. (2.77) can be simplified to

$$\omega'' = \gamma_2 \omega (1 - \beta_2 \sin(\psi) \cos(\bar{\Theta})) \quad (2.78)$$

Eq. (2.75) and (2.78) taken together represent the angular frequency in all three inertial frames only expressed in terms of each other and the angles Θ , $\bar{\Theta}$ and ψ .

Substituting Eq. (2.75) into Eq. (2.78) yields

$$\omega'' = \frac{\gamma_2 (1 - \sin(\psi) \beta_2 \cos(\bar{\Theta}))}{\gamma_1 (1 - \sin(\psi) \beta_1 \cos(\Theta))} \omega'. \quad (2.79)$$

However, it can be demonstrated that $\beta_1 \cos(\Theta) = \beta_2 \cos(\bar{\Theta})$, greatly simplifying this expression. Figure 24 displays a simplified view of the disc and the geometry formed by the tangent lines, radial lines, and the photon path in the x, y -plane.

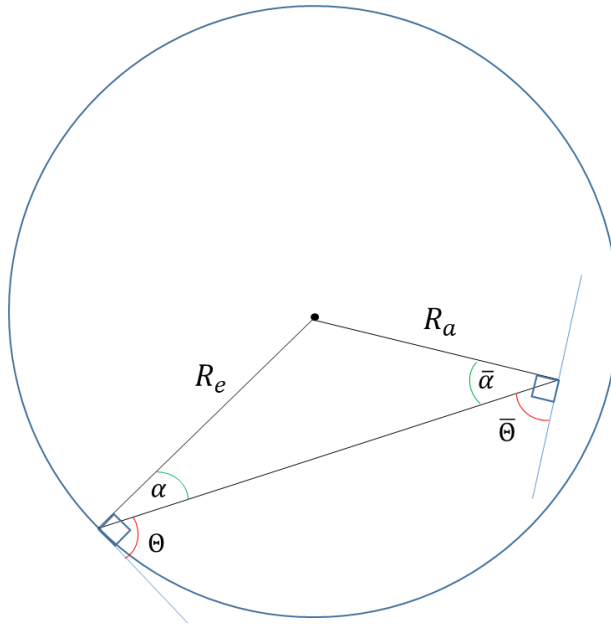


Figure 24. Diagram of the photon path geometry. Angles α and $\bar{\alpha}$ are the angles formed by the line between the photon path (projected onto the x, y -plane) and the radial lines to the center of the disc at emitter and absorber points respectively. Lengths R_e and R_a are respectively the distances of the emitter and absorber from the center of the disc. Angles Θ and $\bar{\Theta}$ are the angles the projection of the photon path onto the x, y -plane makes with the tangent to the emitter and absorber locations on the disc respectively.

By the law of sines,

$$R_e \sin(\alpha) = R_a \sin(\bar{\alpha}). \quad (2.80)$$

Since $\frac{\pi}{2} - \bar{\alpha} = \bar{\theta}$ and $\frac{\pi}{2} - \alpha = \theta$ Eq. (2.80) becomes

$$R_e \sin\left(\frac{\pi}{2} - \Theta\right) = R_a \sin\left(\frac{\pi}{2} - \bar{\Theta}\right) \quad (2.81)$$

which then reduces to

$$R_e \cos(\Theta) = R_a \cos(\bar{\Theta}). \quad (2.82)$$

Since $v' = R_e \Omega$ and $v'' = R_a \Omega$, it is seen that by substituting Eq. (2.82)

$$\beta_1 \cos(\Theta) = \frac{R_e \Omega}{c} \cos(\Theta) = \frac{R_a \Omega}{c} \cos(\bar{\Theta}) = \beta_2 \cos(\bar{\Theta}). \quad (2.83)$$

Eq. (2.79) therefore reduces to

$$\omega'' = \frac{\gamma_2}{\gamma_1} \omega'. \quad (2.84)$$

This expression is very similar to the expression obtained for a transverse Doppler shift in Eq. (2.45) despite the fact that the absorber is not generally moving transversely to the emitter. Eq. (2.84) suggests that the shift between emitter and absorber on the disc can be considered a combination of two transverse Doppler shifts. One interesting result that is obtained from this expression is that $\omega'' = \omega'$ if absorber and emitter are moving at the same relative speeds to the lab frame since $\gamma_1 = \gamma_2$ in this scenario. This corresponds to no Doppler shift if the emitter and absorber have the same radius from the center of the disc, a conclusion that is supported by the experimental results of Champeney and Moon's experiment [17]. For low spin velocities of the disc (non-relativistic) Eq. (2.84) can be reasonably approximated to second order by the binomial expansion. Noting that

$$\gamma_2 = (1 - \beta_2^2)^{-\frac{1}{2}} \approx 1 + \frac{\beta_2^2}{2} \quad (2.85)$$

for $\beta_2 \ll 1$ and that

$$\frac{1}{\gamma_1} = (1 - \beta_1^2)^{\frac{1}{2}} \approx 1 - \frac{\beta_1^2}{2} \quad (2.86)$$

for $\beta_1 \ll 1$, Eq. (2.84) can be approximated to second order in powers of β_1 and β_2 as

$$\omega'' \approx \left(1 + \frac{\beta_2^2}{2} - \frac{\beta_1^2}{2}\right) \omega'. \quad (2.87)$$

Substituting in the expression for β at a given spot on the disc gives

$$\omega'' \approx \left(1 + \frac{R_a^2 \Omega^2}{2c^2} - \frac{R_e^2 \Omega^2}{2c^2}\right) \omega' \quad (2.88)$$

which is the equation of interest in considering the Doppler shift of the photon as it move from an emitter to absorber when both are fixed in a disc. This is easily reduced to the relative Doppler shift by using Eq. (2.42) to obtain

$$\frac{\Delta E}{E} = \frac{\hbar\omega'' - \hbar\omega'}{\hbar\omega'} \approx \frac{R_a^2 \Omega^2}{2c^2} - \frac{R_e^2 \Omega^2}{2c^2}. \quad (2.89)$$

Unsurprisingly this is essentially the same result found in Eq. (2.50) and Eq. (2.62) for the energy shift in the original experiment except that there is the additional term involving the emitter location. In the original experimental design the emitter location was in the lab frame (or equivalently had the same potential as the disc center) and so the emitter contributed nothing to the energy shift. In the modified experimental design the emitter location can only be considered to be at the disc center if it is physically located at that location.

2.5.2. Derivation using Equivalence Principle

The derivation of the energy shift for the modified experimental design using the equivalence principle is almost trivial by comparison to the one for the Doppler shift. The derivation in Section 2.3 for the equivalent gravitational potential difference between an absorber and emitter in the disc frame holds true for the current scenario. Therefore, the potential difference $\Delta\phi$ between the source and absorber is given by Eq. (2.59). In Section 2.3 an argument was necessary to place the emitter at the disc center since it was physically located outside the disc. In the modified experimental design no such argument is necessary since the emitter is physically fixed in the disc frame. Assuming the argument in Section 2.3 for the photon having an “apparent” mass $m_a = E/c^2$, Eq. (2.59) can be used to obtain the relative energy shift of the photon between emitter and absorber as

$$\frac{\Delta E}{E} = -\frac{m_a \Delta \phi}{E} = -\frac{\frac{E}{c^2} \left(\frac{1}{2} r_{emit}^2 \Omega^2 - \frac{1}{2} r_{abs}^2 \Omega^2 \right)}{E} \quad (2.90)$$

which reduces to the final result

$$\frac{\Delta E}{E} = \frac{R_a^2 \Omega^2}{2c^2} - \frac{R_e^2 \Omega^2}{2c^2} \quad (2.91)$$

since $R_e = r_{emit}$ and $R_a = r_{abs}$. This is of course the same as Eq. (2.89) to second order in powers of β . Again, the deviation (higher powers β) is expected to be a result of the non-relativistic assumption when deriving the shift predicted by the equivalence principle and the assumption made that in the Doppler derivation the accelerating reference frames could be treated as inertial reference frames. As with the original proposed experiment the two derivations appear to be consistent with each other. This is particularly notable since the more generalized scenario examined here required multiple transformations between source and absorber when analyzed using the Doppler shift. That the results from the two methods are still consistent with each in a much more generalized scenario is strong evidence that the two approaches are equivalent in general.

Another intent of this analysis was to determine what effect the additional factors in the modified design had on the relative shift. An examination of Eq. (2.91) indicates that the energy shift between emitter and source will only be dependent on their radii from the central axis of rotation for the disc (or of the tube as in the actual experimental design). This makes it stable to tilt of the apparatus, photon angular spread, and deviations of the emitter or absorber from the central tube axis since these do not change the radial distance of emitter or absorber from the axis of rotation. The modified design would also be moderately stable to vibration since source and absorber are fixed into the same structure. Some vibrational broadening of the spectrum would still be expected as was the case in Kundig's experiment [18], which also used had source and absorber fixed into a rotating structure, but. is not expected to be catastrophic.

Chapter 3

EXPERIMENT

Although there exist a few undergraduate experiments using special relativity [21,22] there are no published undergraduate experiments using general relativity. The experiment described here would seek to change this by offering an experimental method that could be repeated in any modestly equipped undergraduate department. In addition it would offer a significant contribution to the ongoing discussion about the transverse Doppler effect since experiments testing the consistency of the transverse Doppler shift and Einstein's equivalence principle have not been entirely satisfactory. In this chapter the proposed experimental design is discussed.

The proposed experiment requires three major steps. The first is to develop a methodology for consistently preparing a ^{57}Co Mössbauer source. The main difficulty is heating a foil electroplated with ^{57}Co to consistently produce a ^{57}Co Mössbauer source. This procedure is discussed in Section 3.1 with recent progress examined in Section 4.1. The second step is to set up an apparatus that will measure the longitudinal Doppler shift. This will be an effective test of the Mössbauer source. In addition, it will also provide the means to calibrate the final experiment. The third step is to perform the final experiment to measure the transverse Doppler shift. The method for measuring the longitudinal Doppler shift can be used to calibrate the results of the transverse Doppler shift experiment.

3.1. *Preparing the ^{57}Co Source*

Preparing the ^{57}Co source has been the most challenging aspect of the experiment so far. For a source to be prepared a small amount of ^{57}Co must be electroplated onto a thin steel foil that has been thoroughly cleaned. The foil must then be heated at high temperatures to ensure that some ^{57}Co diffuses into the lattice structure of the steel foil. This ensures that the ^{57}Co atoms become part of the iron lattice so their emission recoil energy can be absorbed. It is only after this that the steel foil with the embedded ^{57}Co can be considered a Mössbauer

source. The series of steps given below are an outline for the source preparation procedure discussed in Sections 3.1.1 to 3.1.4.

1. The steel foil to be used as the source was carefully cut to specific dimensions to prepare it for the heating treatment. It was then thoroughly cleaned to remove surface impurities on the foil surface. Surface impurities interfered with effective electroplating as well as diffusion of ^{57}Co into the foil lattice structure during the heating process so it was imperative that the foil surface be extremely clean
2. The ^{57}Co was mixed with a solution of ^{59}Co to form a solution that was primarily composed of the inactive ^{59}Co with trace amounts of radioactive ^{57}Co . This was a necessary step before electroplating the ^{57}Co onto the foil could begin because a dilute solution of cobalt ions would not preferentially electroplate onto the foil. The cobalt ion concentration therefore had to be increased by adding ^{59}Co to the solution.
3. The solution of ^{57}Co and ^{59}Co was electroplated onto the steel foil. Measurements of the integrated current and then later the mass as well as the radioactivity of the foil were taken. These three measurements were used to calculate the efficiency of the electroplating process, which was particularly important in evaluating the efficiency of the electroplating process.
4. The foil was placed in a vacuum chamber and heated to about 1000 °C for two hours to ensure that ^{57}Co diffused into the iron lattice of the foil. The use of a vacuum chamber was necessary because at high temperatures the foil would react with oxygen. After the foil was heated, its radioactivity was again measured to determine the ^{57}Co loss from the foil since the foil would sputter when being heated.

The procedure discussed in the next several sections is intended to be a somewhat condensed version of the full procedure for preparing a source. For full details of the procedure refer to August Gula's thesis, especially his Appendix [24].

3.1.1. Step 1-Foil Preparation

The first step in preparing a ^{57}Co source was to prepare the foil onto which the ^{57}Co could be electroplated. The foil used was type 302 stainless steel foil with thickness 0.0254 mm (0.001 inches). The rectangular piece of foil was cut out with dimensions of 13.5 mm by 26 mm. It was particularly important that the sides of the foil were parallel since the heating method passed a high current along the length of the foil and any asymmetry in the width resulted in the foil melting where foil width was smallest. In addition, the foil was cut avoiding any wrinkles. Foils with wrinkles or creases tended to melt along these lines.

Once the foil was cut, it was washed using distilled water, then with isopropanol to remove organic materials on the foil, and then finally with distilled water. The foil was then placed in a solution of 6 M hydrochloric acid to remove inorganic compounds. Once cleaned it was rinsed again with distilled water and dried in an oven for 5 to 10 minutes at 150 °C. The foil's mass was then taken as a baseline measurement before cobalt was electroplated onto it.

Gloves were used for in all 4 steps of the source preparation process to avoid contamination of the foil surface. After electroplating, the now radioactive foil was not touched with bare hands.

3.1.2. Step 2-Preparing the ^{57}Co electroplating solution

For this step a solution of ^{59}Co in the form of $^{59}\text{CoCl}_2 \cdot 6\text{H}_2\text{O}$ was mixed with the ^{57}Co in order to obtain a solution with a high concentration of Cobalt ions. This was necessary prior to the step of electroplating since a highly dilute solution of ^{57}Co (the total amount of ^{57}Co used being 37 kBq or 2.1×10^{-12} Mol) would not preferentially electroplate to the surface of the foil in the presence of the other solutes. A mass of 1.8021 g of 0.1 M HCl was used to dissolve the ^{57}Co and then a mass of 0.1353 g of $^{59}\text{CoCl}_2 \cdot 6\text{H}_2\text{O}$ was added to the mixture to form a cobalt solution of 0.316 M with a ^{57}Co concentration of 1.16×10^{-9} M. Afterwards, a radioactivity measurement of the solution was performed, the geometry of the setup being carefully noted, in order to establish a baseline count for the mixture activity.

3.1.3. Step 3-Electroplating the $^{57}\text{Co}/^{59}\text{Co}$ solution onto the foil

A glass T, a hollow glass tube with a bifurcation, was clamped onto the surface of the foil as shown in Figure 25 and the $^{57}\text{Co}/^{59}\text{Co}$ solution was pipetted into the glass T. Using the foil as the negative electrode and a platinum wire with an enlarged tip as the positive electrode, a current was passed through the solution, electroplating the positive ^{57}Co and ^{59}Co ions onto the foil surface. The voltage across the solution was supplied by a Mastech HY3003-3 DC Variable Power Supply. A range of 3.5 to 4 V were usable for the electroplating process so long as the distance of the positive electrode from the foil surface was held constant at 10 mm. Voltages above this range produced atypical current fits meaning they were not modeled well by Eq. (3.1). For voltages below this range the iron on the foil surface reacted with the HCl in the solution to form black particulates in the solution and a black deposit on both the platinum electrode and the inside of the glass T. This was particularly undesirable because the iron loss from the foil surface was unknown and therefore made calculations for the cobalt deposition on the foil difficult.

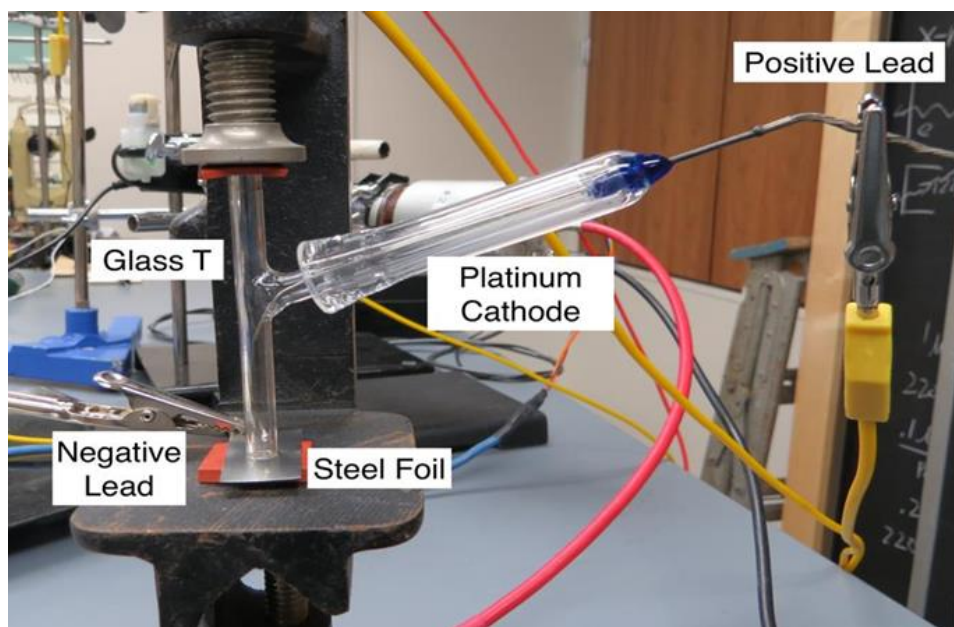


Figure 25. Electroplating setup. A glass T was clamped onto the steel foil and the cobalt solution pipetted into the glass T. The negative lead was connected to the steel foil while the positive lead was connected to a platinum cathode. The tip of the platinum cathode was held at a distance of 10 mm above the foil surface. Image taken from Ref. [24].

The electroplating current was measured by a Mastech MS8050 Digital Multimeter and then integrated with respect to time to obtain the total cobalt electroplated onto the foil surface. The fit

$$I(t) = Ae^{-Bt} - Ct + D \quad (3.1)$$

for the current I as a function of time t was used to model the exponentially decaying cobalt current as cobalt ions were removed from the solution plus an additional first order current due to the other ions present in the solution. The fit was found to be a good approximation of the current flow. The Ae^{-Bt} term, the cobalt ion current during the electroplating process, was integrated over the time period of the process to obtain the total charge of the cobalt ions electroplated, which was then converted to find the mass of the electroplated cobalt. Comparing the electroplated cobalt mass to the total mass of cobalt pipetted into the glass T, which was calculated from the cobalt ion concentration of the mixture and volume pipetted, gave the efficiency yield of the electroplating process.

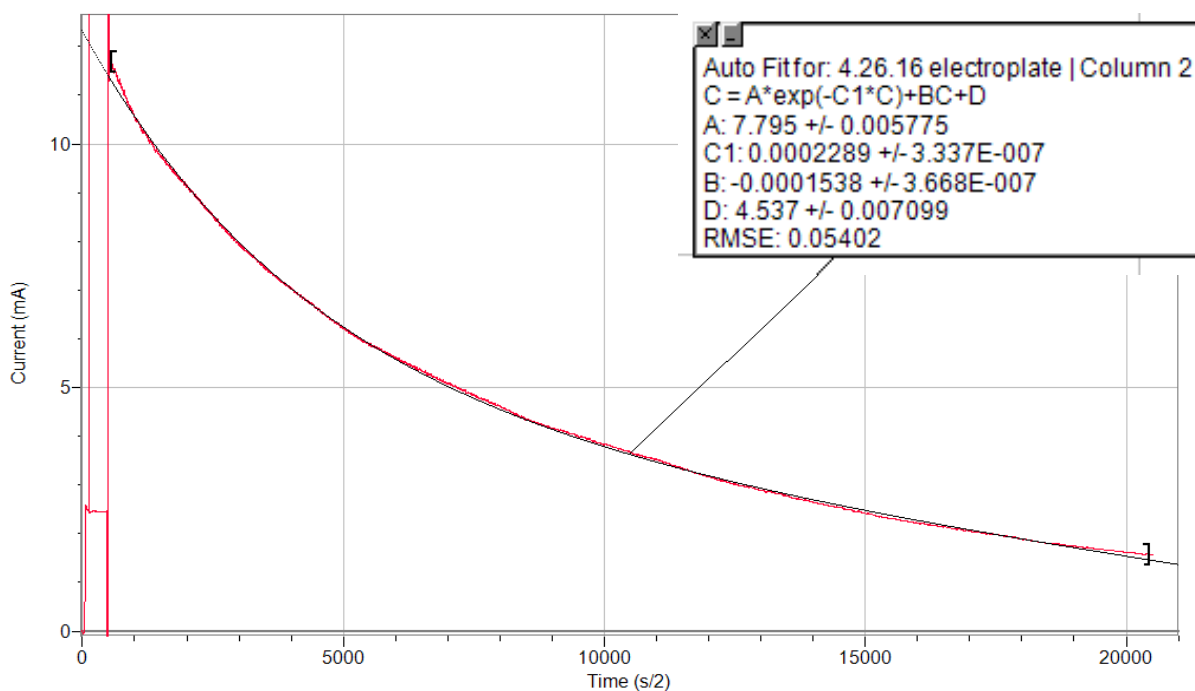


Figure 26. Exponential fit to an electroplating run. The current in mA through the electroplating solution is measured as a function of time. The time scale is denoted in half seconds. The current through the solution went from 12 mC per half second to 2 mC per half second by the end of the run, which was about 2 h and 50 min long. Run performed on April 26, 2016.

The efficiency of the electroplating process was measured two other ways to improve the accuracy. First, the change in mass of the iron foil due to the electroplating process was measured and then compared to the total mass of cobalt present in the electroplating solution. The assumption used was that the change in foil mass would be entirely due to electroplated cobalt. This assumption was reasonable as long as iron appeared not to have left the foil surface and into the solution. Any hydrogen gas that might have formed on the foil surface would have dissipated long before the foil's mass could be recorded.

The second method by which efficiency was calculated was by measuring the radioactivity of the mixture after the electroplating process. The solution left in the glass T was removed and placed back into the original vial containing the rest of the original mixture. Enough HCl was added to ensure that the geometry of the mixture was identical to that of the original radioactivity measurement in Step 2 of the source making process. The activity of the mixture was then recorded under identical conditions to the first radioactivity measurement. Assuming the difference in time between these two measurements was at most a day or two, the difference in measured activity of the mixture would be primarily due to the loss of ^{57}Co atoms by electroplating with the reduction in activity due to decay at most only 0.5 %. Since the ratio of ^{57}Co to ^{59}Co in the original mixture was known, the total cobalt electroplated to the foil could be found from the loss of ^{57}Co in the mixture due to electroplating. A comparison of this value to the cobalt present in the electroplating solution would yield another efficiency measurement.

3.1.4. Step 4-Heating the foil

Once electroplating was completed the activity of the foil was measured, the geometry of the measurement being carefully noted prior to heating. The heating process was necessary to diffuse the ^{57}Co atoms into the crystal lattice of the foil. A temperature of about 1000 °C for a period of 2 hours was sufficient [25] to allow a significant number of the ^{57}Co atoms to embed into the steel matrix. Since the steel foil would react with oxygen in the air and ignite if heated to such high temperatures in the lab, the foil had to be placed in a vacuum chamber with sufficiently low pressure that oxidation due to residual oxygen would be minimal. It was heated by passing an electric current through it parallel to its length.

To achieve this the foil was placed into a vacuum chamber with the 13.5 mm sides bolted to two copper rods of a vacuum feedthrough as shown in Figure 28. These rods were connected to a Mastech HY1550EX DC Power Supply power supply capable of delivering 50 A. The air was evacuated from the chamber using a Welch Duo-Seal fore pump with the pressure being monitored by a KJL275806 Kurt J. Lesker Pirani Pressure Gauge. Once the pressure was on the order of 10 mTorr an air cooled Varian 0159 diffusion pump was activated in order to achieve pressures less than a μ Torr. A Lesker TNR6XA150QF liquid nitrogen cold trap situated above the diffusion pump could also be used to decrease pressure further. Since the Pirani Pressure Gauge could not accurately read pressures less than a mTorr a Duniway Stockroom Corporation I-100-K Ion Gauge read out by a Stanford Research Systems Model IGC100 Ion Gauge Controller was used to measure pressures on the order of 10^{-5} Torr or less. The chamber is shown in Figure 29.

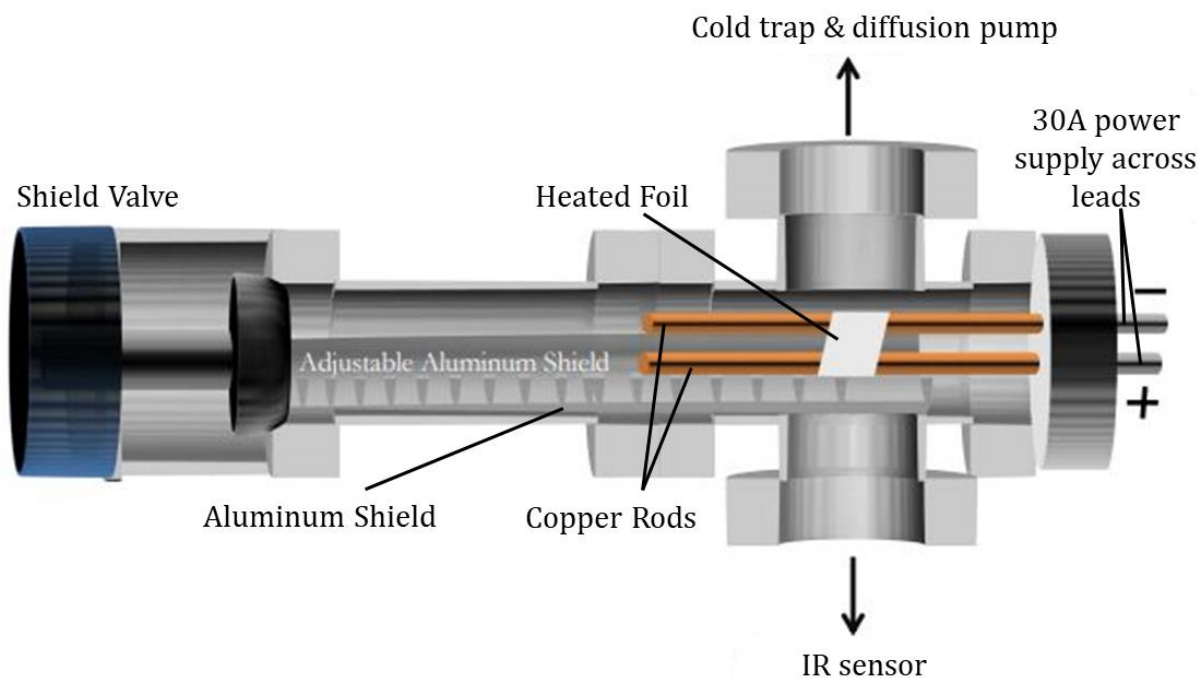


Figure 27. Diagram of chamber apparatus to heat foil. The foil was bolted to two copper rods through which a 30A current was passed to heat the foil. An aluminum shield was retracted to take temperature readings using the IR sensor and then re-extended to protect the IR sensor from foil sputter. Image taken from Ref. [24] with some added annotation.

Once pressure was on the order of 10^{-6} Torr the power supply was turned on at a baseline current of 1.5 A. The current was slowly increased to about 28 A in order to heat the foil to a temperature of about 1000 °C. To measure the foil temperature a dismantled IR gun was positioned so as to observe the foil face. A retractable aluminum shield protected the IR sensor from sputtering when it was not in use. The shield was only retracted for measurements and was moved back over the sensor the rest of the time.

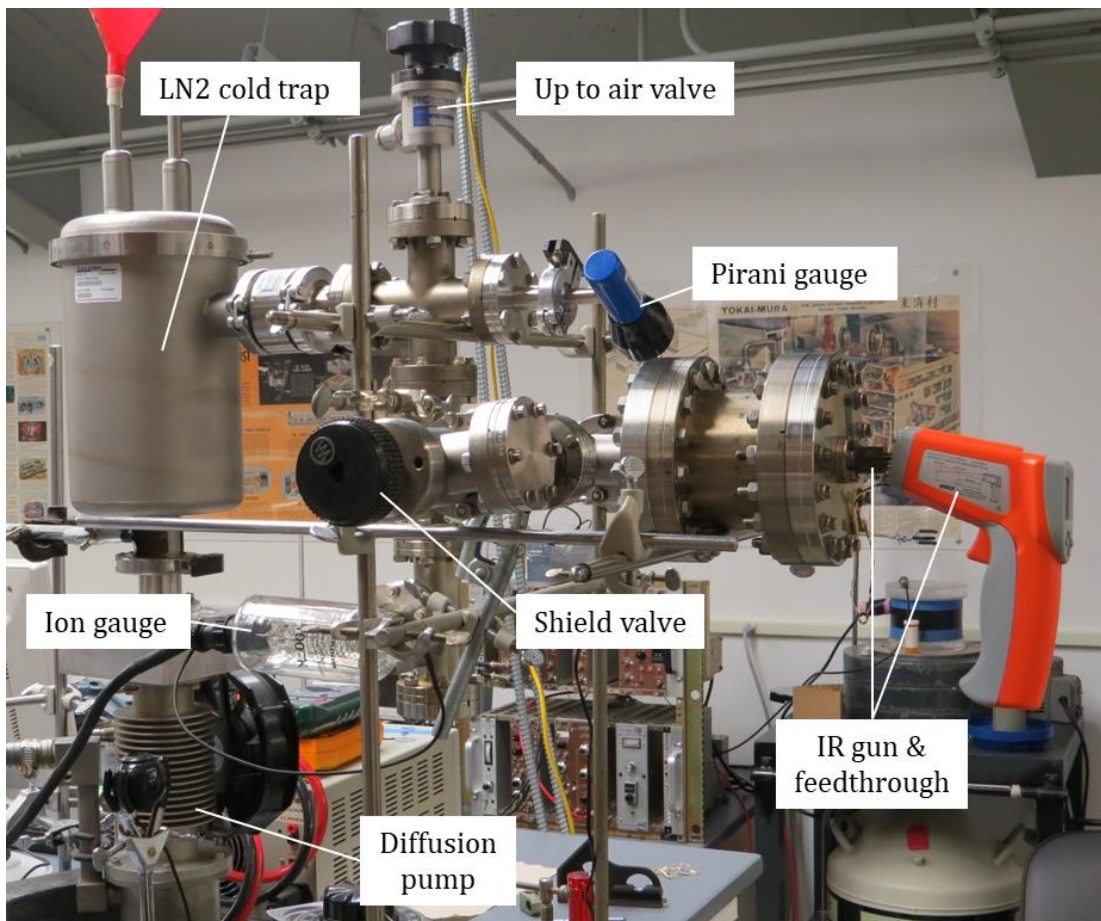


Figure 28. Vacuum chamber setup. The fore pump vacuum hose line (not shown) was connected to the diffusion pump. A LN2 cold trap was used to reduce pressure. Once pressure was reduced to 10^{-6} Torr, as measured by the ion gauge, foil heating could begin. The IR gun and shield were used in conjunction to take temperature readings of the heated foil while protecting the IR sensor from foil sputtering when not in use.

Once the foil was heated to 1000 °C it was allowed to bake for 2 hours before the current was turned off. Air was reintroduced into the chamber only once the foil had cooled completely.

When it was finally removed from the chamber the foil activity was measured using an identical geometry to that prior to heating. The final activity measurement was compared to the first measurement to determine the amount of ^{57}Co that had been lost during heating. The mass of the foil after heating was also recorded though the mass loss during heating had little value for determining how much ^{57}Co was retained on the foil since it was unknown what fraction of mass loss was iron loss instead of cobalt loss. Once the last activity measurement had been taken the foil was ready to be used as a ^{57}Co Mössbauer source.

3.2. Experiment Description

The designs for the second and third experimental steps, the measurement of the longitudinal Doppler shift and the transverse Doppler shift, are examined here. Both steps make use of a rotating absorber disc. While this is expected to successfully measure the longitudinal Doppler shift the analysis from Section 2.4 indicates that the use of a rotating absorber disc for the transverse Doppler shift is not feasible due to the enormous expected uncertainty. As such the experiment has been redesigned as described in Section 3.2.3.

3.2.1. Longitudinal Doppler Shift Experiment

Prior to measuring the transverse Doppler shift the longitudinal Doppler shift will be measured. This is important because it is an effective means of testing the ^{57}Co Mössbauer source and can be used as a calibration technique for the transverse Doppler shift, as was done in Kundig's experiment [18]. The design for the longitudinal shift experiment is shown in Figure 29.

A standard 120 mm diameter polycarbonate CD disc was used as the absorber disc. A 0.025 mm (0.001 in) thick SAF 304 stainless steel foil was epoxied to the face of the disc. To make the disc uniformly absorbent the foil surface had to be smooth; otherwise wrinkles could make an absorber region thicker and thereby increase the natural absorption of that region of the disc. SAF 304 stainless steel contains natural iron of which only 2.5% is ^{57}Fe . Only the ^{57}Fe isotope can absorb 14.4 keV gamma rays resonantly but obtaining sufficient foil enriched in ^{57}Fe to cover the CD disc would be too expensive despite the advantages of greater resonance absorption.

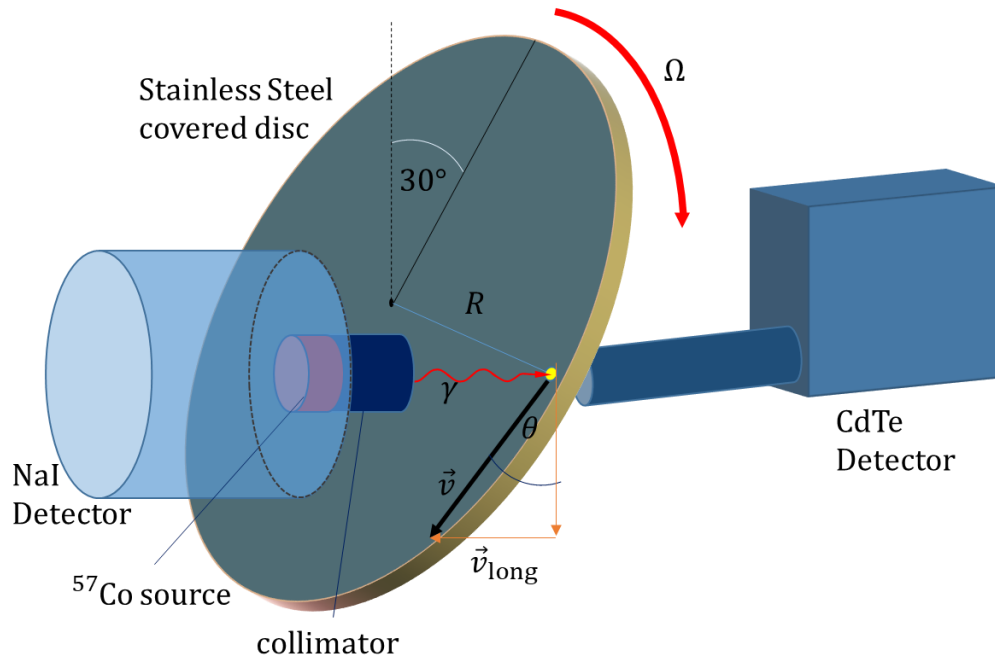


Figure 29. Diagram of experiment for longitudinal Doppler shift. A CdTe detector measures the rate of 14.4 keV gamma rays transmitted through the absorber disc in coincidence with 122.1 keV gamma rays from the ^{57}Co Mössbauer source that are measured by a NaI detector. The disc, which is polycarbonate covered by a 0.025 mm thick stainless steel sheet, is angled from the vertical by an angle of 30° . It is rotated at an angular speed Ω that is varied between -0.6 rev/min and 0.6 rev/min. At the location of absorption the disc has a longitudinal velocity component relative to the path of the collimated 14.4 keV gamma rays.

The absorber disc was initially positioned vertically so that its face was perpendicular to the collimated 14.4 keV gamma rays. The absorber location on the disc receiving the gamma rays was 5 cm from the disc center and at the same height. The disc was then angled from the vertical by 30° introducing a longitudinal velocity component when the disc was rotated. To measure the longitudinal Doppler shift longitudinal velocities on the order of 0.5 mm/s were needed. As was shown in Section 2.2.3, this corresponded to angular frequencies speeds ranging between -0.6 rev/min and 0.6 rev/min in order to scan over the whole resonance spectrum. To achieve these low angular speeds an Actobatics gear motor, part number 638142, was used to rotate the disc. A HY3003-3 DC Power Supply was used to adjust the voltage to the gear motor to control its angular speed. The angular speed was measured using a Vernier rotation probe.

Once a viable ^{57}Co Mössbauer source is produced a 3 mm by 3 mm crystal Amptek XR-100T-CdTe X-ray detector will measure the transmission rate of 14.4 keV gamma rays through the tilted disc in coincidence with the 122.1 keV gamma rays striking a 2.5 cm thick by 5.1 cm diameter crystal 2M1/2 NaI Bicron detector. To increase the counting statistics the ^{57}Co Mössbauer source will be placed as close to the disc surface as possible without the collimator touching it. Since only 14.4 keV gamma rays detected in coincidence with 122.1 keV gamma rays are measured, the NaI solid angle also affected count rate. Placing the ^{57}Co source directly onto the surface of the NaI detector increases the solid angle of the NaI detector to about 2π steradians which corresponds to about half of the 14.4 keV gamma transmissions through the absorber disc being counted. Figure 30 shows the rough setup.

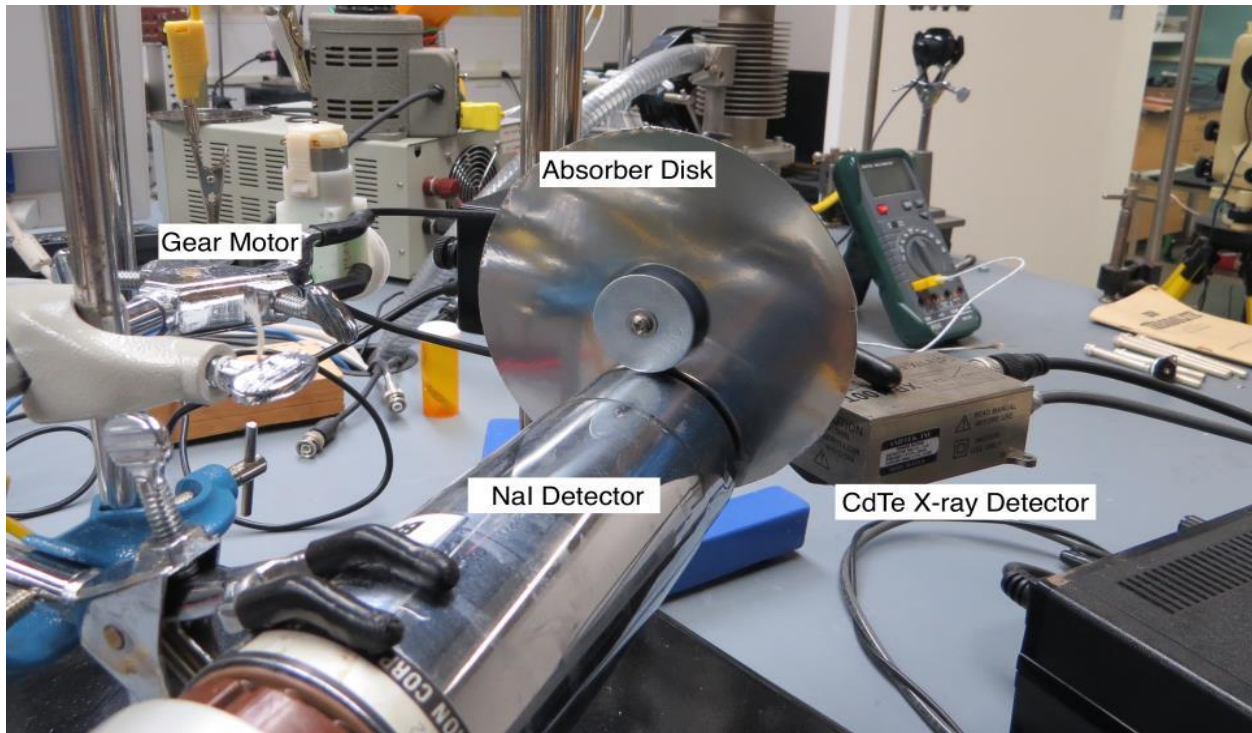


Figure 30. Apparatus for longitudinal Doppler shift experiment. The ^{57}Co source is taped directly to the front of the NaI detector to increase count rate. A gear motor is used to achieve the low rotation rate necessary to scan over the resonance spectrum using the longitudinal Doppler shift. Image taken from Ref. [24].

The circuit diagram for the longitudinal Doppler shift experiment is shown in Figure 31. Pulses from the CdTe detector were amplified and then a timing single channel analyzer

(TSCA) produced a logic pulse whenever the input was a 14.4 keV gamma ray. Pulses from the NaI detector were similarly amplified and a logic pulse produced for 122 keV gamma rays. A delay adjusted for the different processing times of the two circuits which were used to start and stop a time-to-amplitude converter (TAC). The NaI signal started the TAC and the CdTe signal stopped it. A TSCA then selected the TAC output signals corresponding to a coincidence-like time difference between the NaI and CdTe signals. The TSCA output opened the gate of a Linear Gate while a delayed CdTe amplifier signal was input. The Linear Gate output, which was the transmitted gamma ray pulse height for events in coincidence with the 122 keV gamma ray, was recorded by a MCA. The circuit therefore eliminated the majority of background events except for the accidental coincidences.

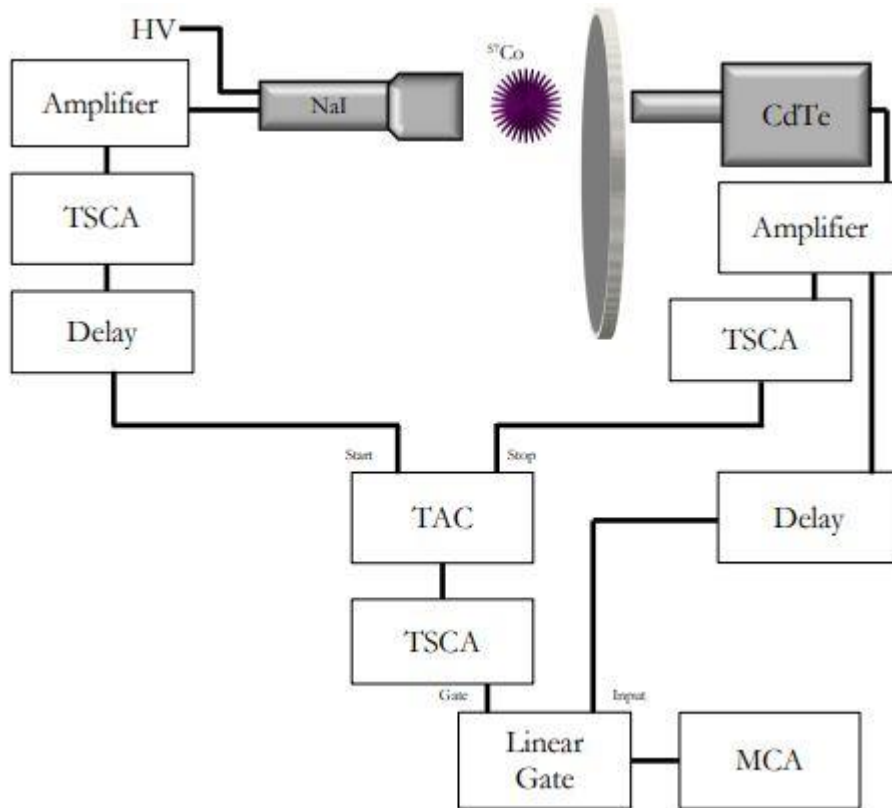


Figure 31. Circuit diagram of Longitudinal Doppler shift experiment. The CdTe detector detected the 14.4 keV gamma rays while the NaI detector detected the coincident 122 keV gamma. Diagram taken from Ref. [24].

The apparatus for the longitudinal Doppler shift experiment can also be used for calibration. In the originally proposed transverse Doppler shift experiment the disc cannot be tilted. This

cannot be used to scan over the spectrum of the resonance spectrum. However, the introduction of a second longitudinal velocity drive, shown in Figure 32, would allow scanning to be performed not only by adjusting the disc speed for the longitudinal Doppler shift experiment but also by using a screw to drive the NaI detector and ^{57}Co source at low speeds towards and away from the disc. Using this setup would also provide important data about the operation of the screw such as its acceleration and response time to voltage input changes, necessary information in calibrating for the transverse Doppler shift experiment. However, until a ^{57}Co Mössbauer source can be successfully prepared, building the secondary velocity drive remains to be done.

3.2.2. Transverse Doppler Shift Experiment

Once the longitudinal Doppler shift experiment is successfully performed the next step is the transverse Doppler shift experiment, which in its original form uses the same setup as the longitudinal Doppler shift experiment with two key differences. The disc angle would be adjusted such that the disc velocity at the absorber location would be totally perpendicular to the path of the 14.4 keV gamma rays being emitted by the ^{57}Co source. In addition, the disc would be rotated at angular speeds about 1,000,000 times greater than those needed for the longitudinal Doppler shift. This is shown in Figure 32. As was shown in Section 2.4 and will be further discussed in Section 3.2.3 this experimental setup is no longer believed to be viable.

As with the longitudinal Doppler shift, the ^{57}Co source would be placed as close as possible to the NaI detector face to increase the solid angle of the detector when measuring the 122.1 keV gamma rays emitted by the source. It would be important to collimate the gamma rays since any longitudinal velocity component of the absorber would result in an unwanted longitudinal Doppler shift. As such the collimator aperture width to length ratio would have been very small to ensure that the gamma paths were perpendicular to the absorber velocity. At rotational speeds up to 20,000 rpm the resonance spectrum would be measurably shifted down in energy due to the transverse Doppler shift. To scan over the spectrum the NaI detector, ^{57}Co source, and collimator would have been moved longitudinally toward the disc at velocities in the range of $-1.5 \text{ mm/s} < v < 1.5 \text{ mm/s}$. However, this velocity range may

have needed to be increased since it is believed that the resonance spectrum would be broadened due to vibration as was seen in Kundig's experiment [18]. A protective structure around the disc would be needed since the CD disc might disintegrate at 20,000 rpm. The radius of the disc would have been about 10 cm instead of 6 cm since increased radius means a decreased angular speed to achieve the same transverse Doppler shift.

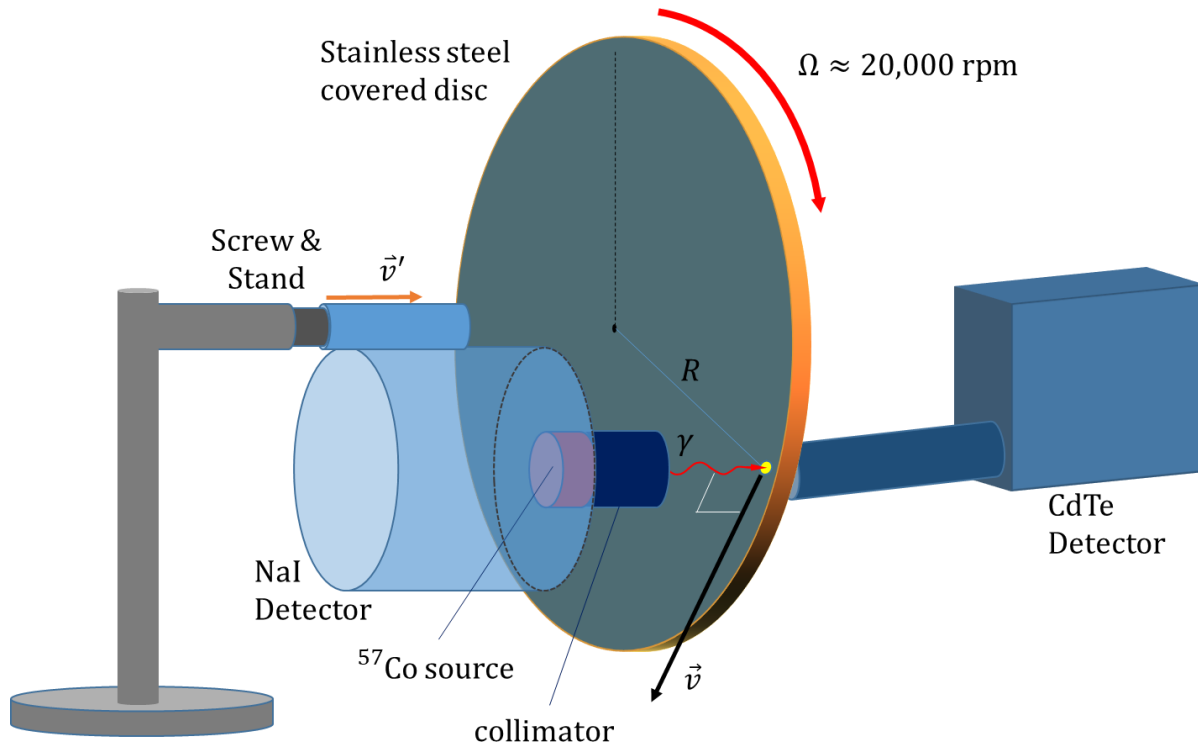


Figure 32. Diagram of originally proposed transverse Doppler shift experiment. The stainless steel covered disc is placed vertically and rotated at angular velocities up to 20,000 rpm. A CdTe detector measures the transmission rate of 14.4 keV gamma rays from a ^{57}Co Mössbauer source through the absorber disc in coincidence with 122.1 keV gamma rays that are measured by a NaI detector. A collimator ensures that the 14.4 keV gamma rays strike the absorber disc at a location where the local disc velocity is transverse to the gamma ray path in the lab frame. A velocity drive using a screw moves the ^{57}Co toward and from the disc at adjustable velocity \vec{v}' to scan the resonance spectrum.

3.2.3. Modified Experiment to Measure Transverse Doppler Shift

Unfortunately, as discussed in Section 2.4, the proposed experiment for the transverse Doppler shift is not workable. The large uncertainty due to the longitudinal Doppler shift will almost certainly overwhelm the transverse Doppler shift. Three major sources of a longitudinal velocity will be present in the proposed design given in Section 3.2.2.

First, if the velocity of the absorber location on the disc is not perfectly perpendicular to the incoming gamma rays then a small but very significant longitudinal velocity component is introduced between the gamma rays and the absorber location. As discussed in Section 2.4 the angle of the disc necessary to produce a longitudinal Doppler shift on the same order of magnitude as the expected transverse Doppler shift is 10^{-6} radians. This level of precision is probably not attainable for the proposed experimental apparatus.

A second source of longitudinal velocity component is introduced by the angular spread of the gamma rays exiting the collimator. A photon exiting the collimator at a slight angle will have the same effect as if the disc was tilted by the same angle. Therefore, the angular spread of the gamma rays would again have to be 10^{-6} radians or less. While a tilted disc will result in a similar longitudinal Doppler shift for all the incident gamma rays, an angular spread will result in a range of the magnitudes of the longitudinal shift since not all the photons exiting the collimator will have the same deviation from the perpendicular. The overall result will be that the spectrum will be smeared out. As noted in Section 2.4, a collimator that was 1 m long with an aperture of 1 mm would still result in a spectrum smeared out by a factor of 1000. Since the source is small, good statistics are particularly important for the proposed experiment. A very small angular spread also means a drastic reduction in count rate so an angular spread on the order of 10^{-6} would render the experiment ineffective. In fact, an angular spread of 10^{-6} radians with a 37 kBq source would imply that the experimenter would need to wait about 400 days for a single 14.4 keV photon to reach the disc-and that is without taking into account the half-life of the source.

Finally, the existence of vibration introduces longitudinal velocity between source and absorber. A disc rotating at 20,000 rpm will undoubtedly vibrate from side to side and this vibration alone would probably destroy the resonance spectrum since it only need be about 0.1 mm/s to produce a longitudinal shift on the same order as the transverse Doppler shift. The result would be a smearing out of the resonance spectrum due to the vibration that would make effective measurement of the spectrum shift near impossible.

Therefore, as explained in Section 2.4 and 2.5, a new experimental design is needed where the relative longitudinal velocity between source and absorber is kept small. This will be

achieved by using an experimental design similar to that used by Kholmetski et. al [20]. The source and absorber will be placed at different locations along a tube that is rotated perpendicularly about its center as seen in Figure 33.

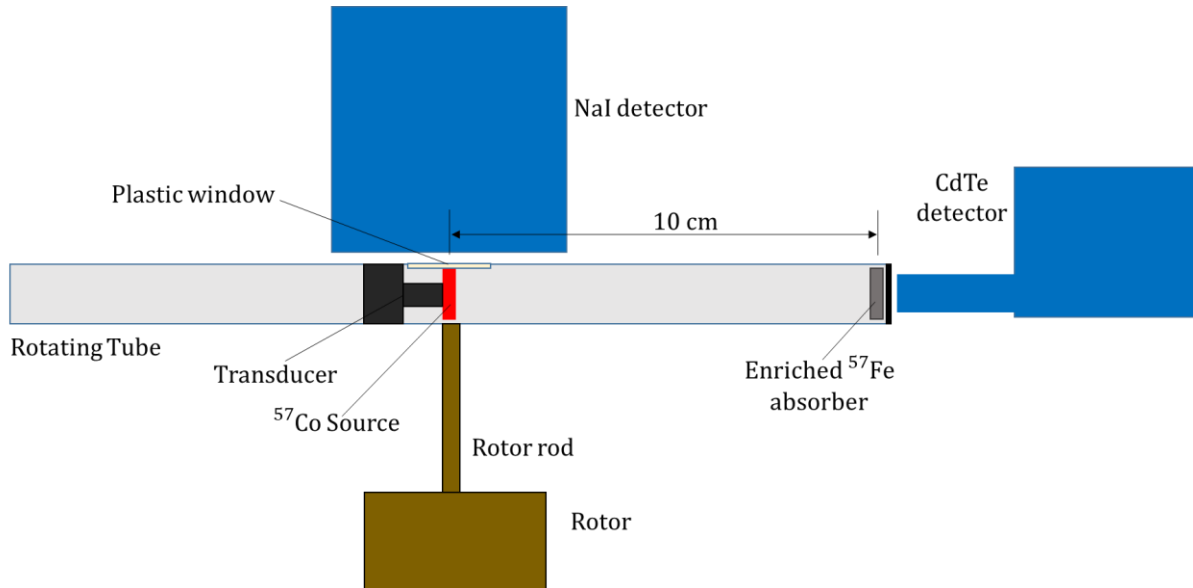


Figure 33. Schematic of Modified experiment for transverse Doppler shift. A tube is rotated perpendicularly about its center at angular speed up to 20,000 rpm. The ^{57}Co source is mounted on a transducer in the radial middle of the tube while the absorber is fixed at the end of the tube. Gamma rays of energy 14.4 keV will experience a transverse Doppler blueshift as they travel from source to emitter. When the source, absorber and CdTe detector are aligned, the CdTe detector measures the transmission rate of 14.4 keV gamma rays through the absorber in coincidence with the NaI detector measuring the 122.1 keV gamma rays from the source.

In this modified experimental design the absorber will be placed at the end of the tube while the ^{57}Co Mössbauer source would be mounted on a transducer at the radial center of the tube. The transmission rate of 14.4 keV gamma rays through the absorber will be measured by a CdTe detector in coincidence with 122.1 keV gamma rays detected by a NaI detector. The CdTe detector will be placed just outside the radial arc swept out by the spinning tube so that once per revolution the source, absorber, and CdTe detector all lie on the same axis. The NaI detector will be placed directly above the spinning tube so as to have as large a solid angle as possible. A thin plastic window will allow 122.1 keV gamma rays to pass from the source into the NaI detector. A transducer will be used as a longitudinal velocity drive by moving the ^{57}Co Mössbauer source toward and away from the absorber. This will allow

scanning of the resonance spectrum, which is expected to broaden by an unknown amount at high rotational velocities due to vibration.

The modified design will avoid the large uncertainty due to the longitudinal Doppler shift present in the original proposed experiment. The longitudinal velocity of the source relative to the absorber will be entirely due to the velocity drive and the vibration of the source and absorber about their positions in the tube. The velocity drive is carefully controlled while the broadening of the vibrations is not expected to be overwhelming as was demonstrated in both Kundig's and Kholmetski's experiment [18,20]. Longitudinal Doppler shift from angular spread and disc tilt will be eliminated completely in the modified design. Vibration will still be present but the absorber and source are relatively well fixed within the same rigid structure so the vibration should be dramatically reduced.

Unfortunately, the drawback of the new design is that it severely decreases the count statistics for the experiment since the CdTe detector can only measure the transmission rate of 14.4 keV gamma rays through the absorber when it is collinear with the absorber and source. This would happen about 3% of the time for a tube of width 2 cm. One idea to increase the count statistics would be to use a detector array around the outside of the tube arc to increase the percentage of the time that transmitted gamma rays can be measured. This might require the use of a different detector type. Another idea is to make the tube wider and place a longer absorber strip inside the tube, thereby increasing the percentage of time that CdTe detector is collinear with the absorber and source. If the tube were changed from a cylinder to a rectangle with the width of the tube made about 6 cm the CdTe detector could measure 9% of the time. The longitudinal velocity drive for the source limits how much wider the tube can be made. The transducer only acts along a line so any absorber location offset from this line will experience a slightly reduced longitudinal Doppler shift component. This is negligible for small offsets but as the angle of deviation becomes larger the longitudinal velocity component quickly decreases. A combination of tube widening and multiple detectors may be necessary to increase the counting statistics.

Chapter 4

RESULTS

Most progress to date has been in preparation of a ^{57}Co Mössbauer source. Recent progress has been in two main areas: calibrating the infrared detector used in measuring the foil temperature during the heating process, and calibrating the radioactivity measurements of electroplated foils.

4.1. Calibrating the Infrared Gun

At the moment, the most significant impediment to further progress in the experiment is being able to consistently make a usable source. The source making process typically fails at the heating stage where the foil melts at high temperature. It is believed that this is primarily caused by inaccurate IR gun calibration, resulting in foil heating beyond the necessary 1000 °C. The IR gun was calibrated earlier, but either the calibration has drifted or was inaccurate. Foil temperature data had been sparse for high temperatures and uncertainty in these data points was large. In addition, the entire vacuum chamber was disassembled the fall of 2017 because of oil backstreaming into the chamber during a power failure. It seemed very likely that after the reassembly process the IR calibration would have drifted further. Consequently, the IR gun was recalibrated during the spring of 2018.

The infrared gun used to measure the temperature of the foil being heated in the vacuum chamber was a Cheerman DT8011 Infrared Thermometer. It was partially disassembled in order to house the IR sensor inside the vacuum chamber. A feedthrough sent the electrical output from the detector into the electronics located outside the vacuum chamber. A photograph of this setup is shown in Figure 34. To calibrate the IR gun, the sensor (with the feedthrough still attached) was taken out of the vacuum chamber and pointed down at a foil having the same dimensions and thickness as the Mössbauer foil. This foil was heated using a large soldering iron to temperatures in excess of 700 °C. The distance between foil and sensor was 59.4 mm which, to within 0.1 mm, was the same distance between foil and sensor in the vacuum chamber. The voltage supplied to the soldering iron was controlled in 10 V

increments from 0 V to 140 V using a variac. At each voltage the temperature from the IR gun was recorded. The temperature varied across the surface of the foil since not all locations were in contact with the soldering iron so two K-type thermocouples measured the temperature of the foil and were averaged. The setup for this is shown in Figure 35. The first thermocouple was intentionally placed near a darker, less heated location of the foil and the second thermocouple was placed on a location that consistently glowed brightest during the heating process.

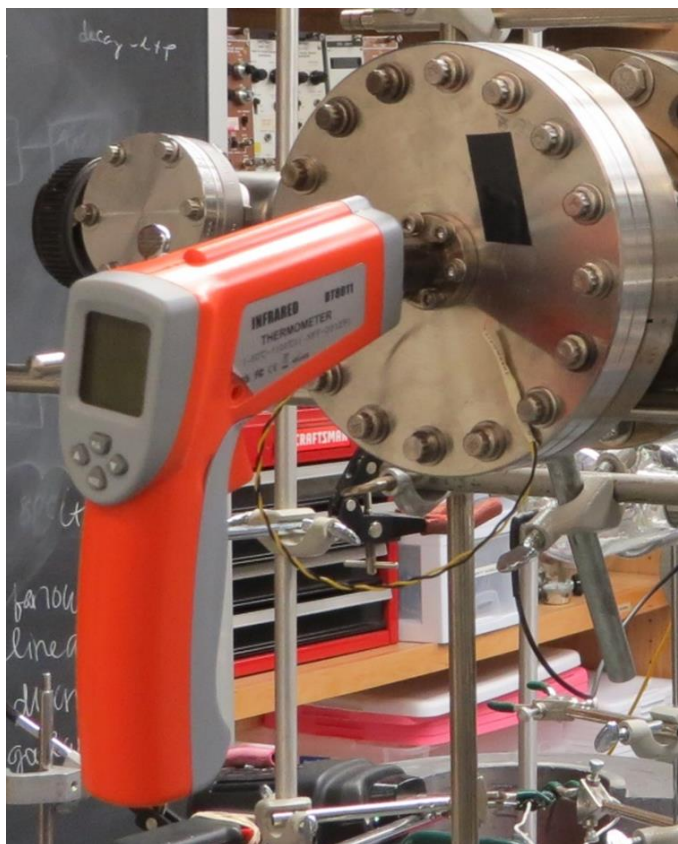


Figure 34. External view of the IR gun used to measure foil temperature. The sensor is removed from the main unit and placed inside the vacuum chamber. A feedthrough connects the sensor to the main unit, allowing the sensor to view the foil while keeping the electronics and display outside the chamber.

The calibration data are shown in Figure 37. For these measurements the emissivity setting of IR gun was left at the default 0.95. The fit to the calibration data was a significant improvement over previous calibrations, shown in Figure 36, where the emissivity setting

was 0.3. The emissivity setting of 0.3 had been chosen because it was approximately the emissivity of the steel foil.

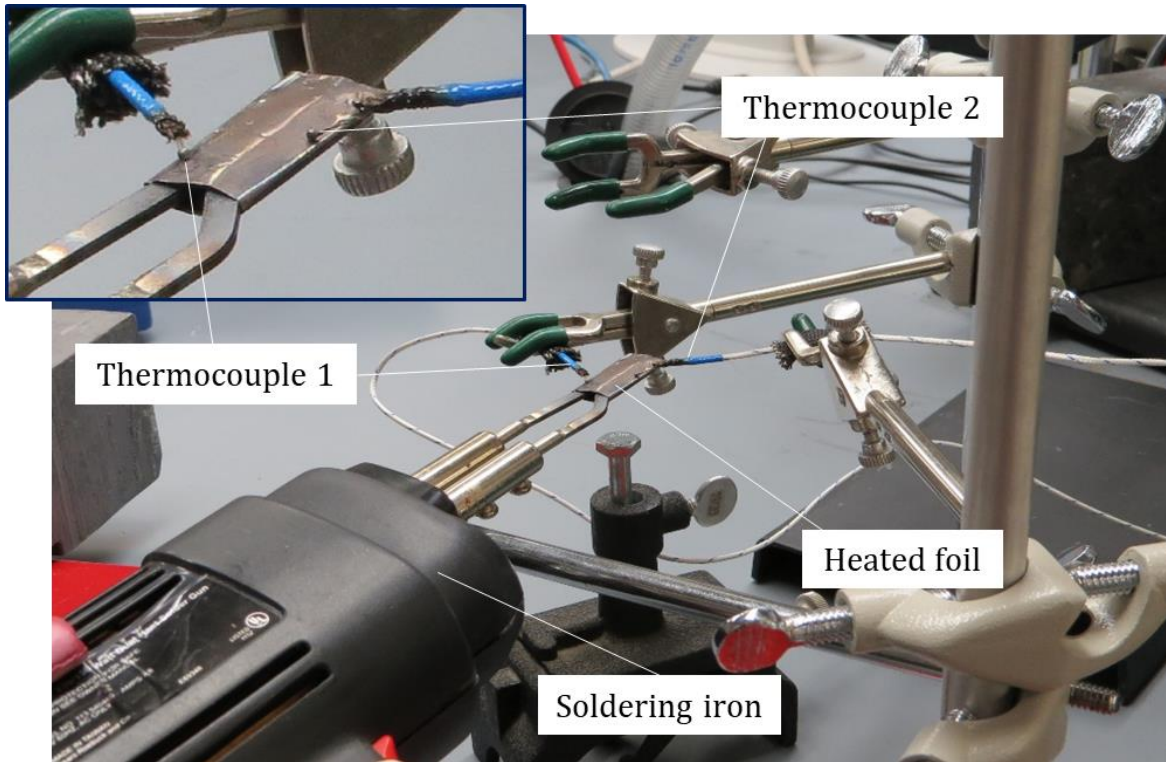


Figure 35. Calibration setup to heat and record foil temperature. The soldering iron supply voltage was controlled by a voltage variac and was ranged between 0 V and 140 V. The heated foil was of the same dimensions and placed the same distance from the IR sensor (not shown) as a Mössbauer foil would be in the chamber. The foil was heated to temperatures in excess of 700 °C. A close-up of the foil and thermocouples is shown in the top left corner.

However, for these previous calibrations a “jump” or discontinuity was observed in the sensor readings. When using a hot plate and an emissivity setting of 0.3 the discontinuity occurred around 250 °C. The IR gun readout would increase suddenly and then follow a new linear fit. When using a heated foil, this jump occurred around 600 °C as seen in Figure 36. Since there did not exist a means by which to heat the foil to temperatures between 750 °C and 1000 °C, this meant there was a lack of data over perhaps the most crucial part of the temperature range, particularly because the few data points obtained above temperatures in excess of 600 °C were not even sufficient to extrapolate with.

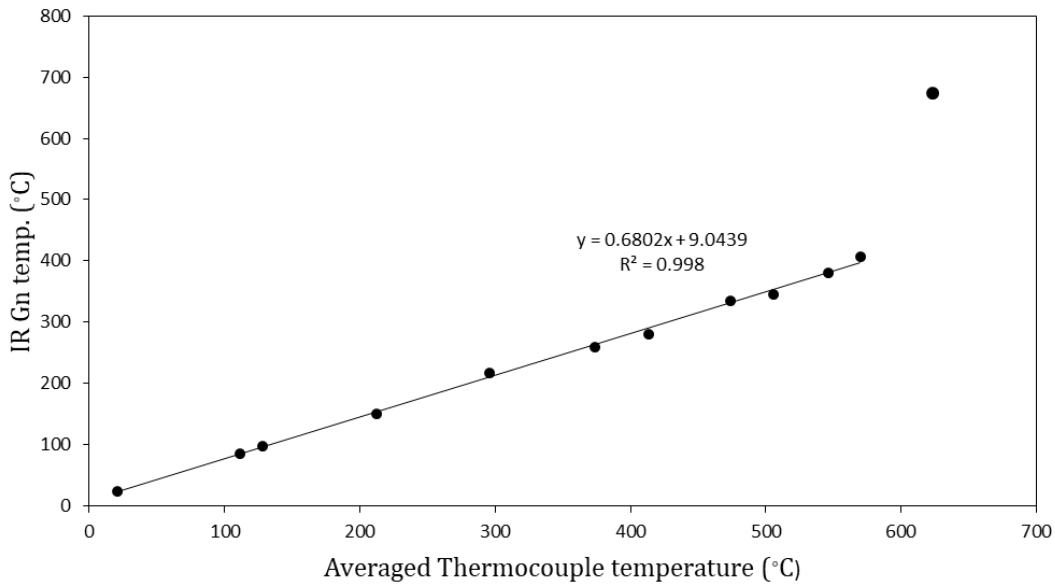
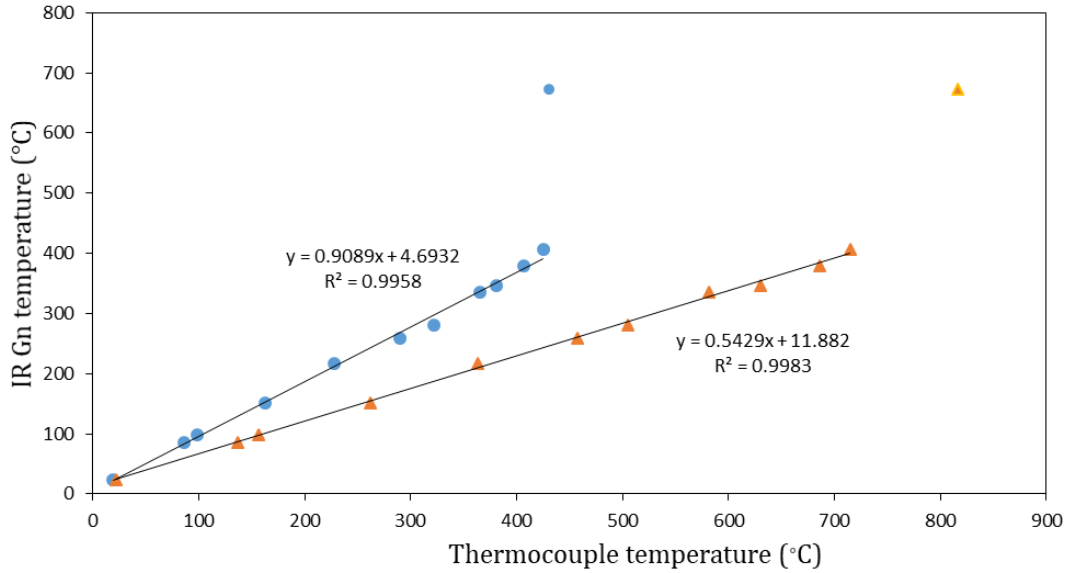


Figure 36. Plot of IR calibration of foil at emissivity setting 0.3. The IR gun temperature reading as a function of the thermocouple temperature (top) (thermocouple 1=blue, thermocouple 2=orange), and as a function of the thermocouple average (bottom). The observed discontinuity was typical at this emissivity setting. Data taken May 3, 2017.

It was discovered that the temperature at which this jump occurred seemed to increase with the emissivity setting. For the recalibration the emissivity setting was set at 0.95 with the hopes that the discontinuity temperature would be shifted to such high a high value that a single linear fit would apply to all data points in the desired range of 0 °C to 1000 °C. From

the data gathered so far this appears to be working, as seen in Figure 37, though it could not be confirmed without data points at higher temperatures.

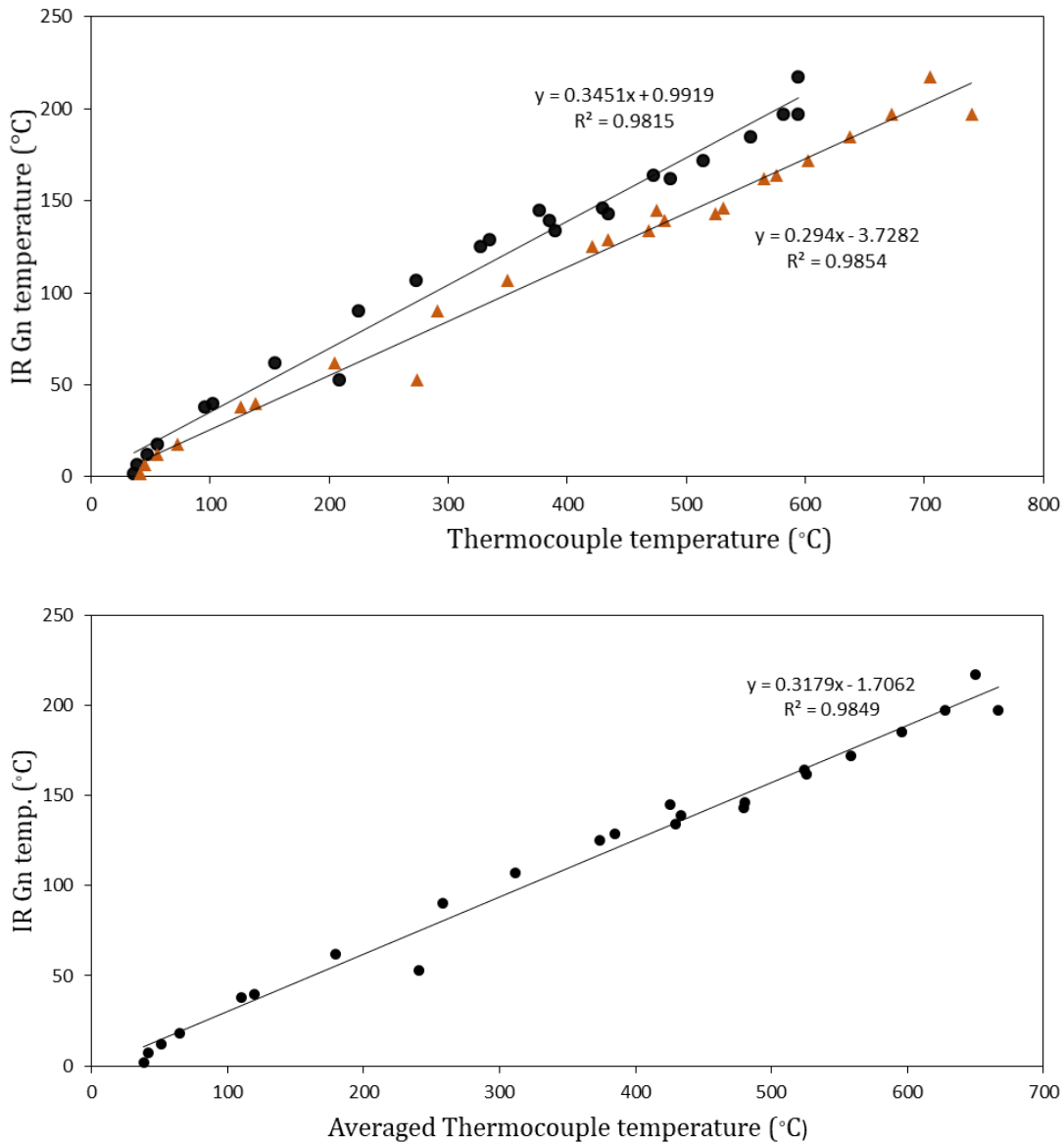


Figure 37. Plots of IR calibration curve at emissivity setting 0.95. The IR gun temperature reading as a function of the thermocouple temperature (top) (thermocouple 1=black, thermocouple 2=orange), and as a function of the thermocouple average (bottom). Data taken February 22, 2018.

Unfortunately, it was discovered several months later that the calibration changed when the sensor and foil were placed inside the vacuum chamber. The calibration had been performed outside the chamber because it was considerably easier, the assumption being that inside

the chamber the environment would have minimal effect on the IR gun readings. When the foil was placed in the air-filled vacuum chamber, still being heated by the soldering iron controlled by the variac, it was discovered that the variac voltage and IR gun readings no longer fell on the calibration curve obtained when the calibration was done outside. In fact, the temperature reading of the IR gun was much higher than previously. The test had originally been performed to determine if iron sputtered onto the IR sensor had increased after a foil had violently melted in the chamber while the shield was out of position. If this had been the case it was believed the IR readings would be lowered due to decreased transmission of radiation to the sensor. Instead, it was discovered that more radiation appeared to be reaching the sensor, possibly due to reflection of the IR radiation off of the chamber walls. A comparison of the two curves, the first done outside and the second done inside the chamber, is shown in Figure 38.

The calibration with two thermocouples therefore needs to be performed again but in situ so that calibration takes into account the reflection of the IR radiation. The same heating mechanism for creating Mössbauer foils could be used to heat the calibration foil. Doing so would enable both IR and thermocouple data to be taken at high temperatures, one of the major challenges for all the calibration attempts to date. In addition, by placing the foil inside the chamber the calibration can be done in vacuum. This is important because it was observed that the foil discolored in the open air at higher temperatures, potentially due to oxidation, which changed the emissivity. Therefore, it is possible that the spring 2018 calibration would have been unusable anyway simply because the foil emissivity in air at high temperatures might greatly differ from the foil emissivity in vacuum where the foil surface did not oxidize. The challenge of the in situ calibration is placing the thermocouples in direct contact with the heated foil in the confined space of the vacuum chamber. To remedy this the thermocouple outputs will be fed through a feedthrough while the thermocouples are pressed against the back of the foil so as not to impede the IR sensor's view of the foil. The thermocouples will also have to be modified to not outgas when the chamber is evacuated.

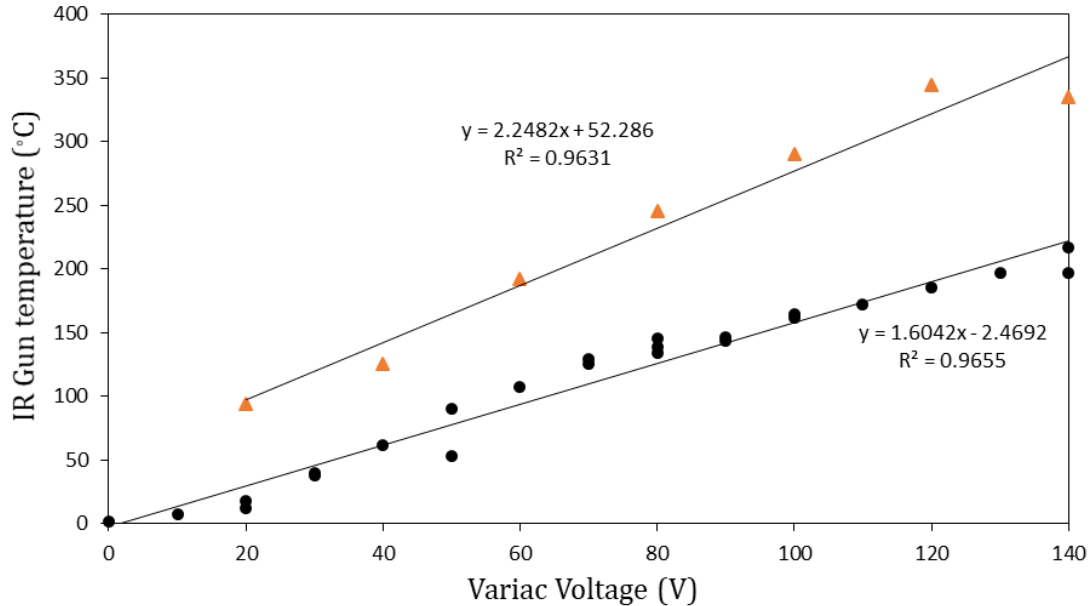


Figure 38. Comparison of calibration curves taken outside and inside the chamber. The IR gun readings taken outside (black circles) and inside the chamber (orange triangles) are plotted as a function of the variac voltage supplied to the soldering iron that heated the foil. The curve for inside the chamber suggested that the sensor was receiving more radiation from the foil while in the chamber compared to outside the chamber for the same power to the soldering iron. Data taken April 28, 2018.

4.2. *Calibrating the NaI detector*

The most straightforward measurement technique for determining the amount of ^{57}Co on a foil is to measure the activity of the foil. Unlike measuring the mass of the foil or the electroplating current this technique is direct since it does not require the ^{57}Co to ^{59}Co ratio to find the amount of ^{57}Co present. For this reason it is the only measurement technique that can be used after the foil is heated since the uncertainty in iron emissions from the foil render indirect techniques useless. However, to determine the amount of ^{57}Co present on the foil requires a reliable measurement of either the 122 keV or 14.4 keV.

To identify the 122 keV peak, an energy calibration was done for the 2.5 cm thick by 5.1 cm diameter crystal 2M1/2 NaI Bicron detector. The 122 keV peak was chosen since it is both much larger than the 14.4 keV peak and the NaI detector is more sensitive to gamma detections of higher energy. Two calibration sources were used: ^{22}Na and ^{133}Ba . The ^{22}Na source emits positrons that annihilate with electrons to form two back-to-back gamma rays of energy 511 keV. The ^{133}Ba source has three main peaks at energies 31 keV, 81 keV, and

356 keV. When the foil activity was measured after electroplating and before heating a strong peak (the presumed 122 keV peak) was observed with a much smaller peak at around 85 keV which has yet to be identified. Figure 39 shows peak energy as a function of channel number.

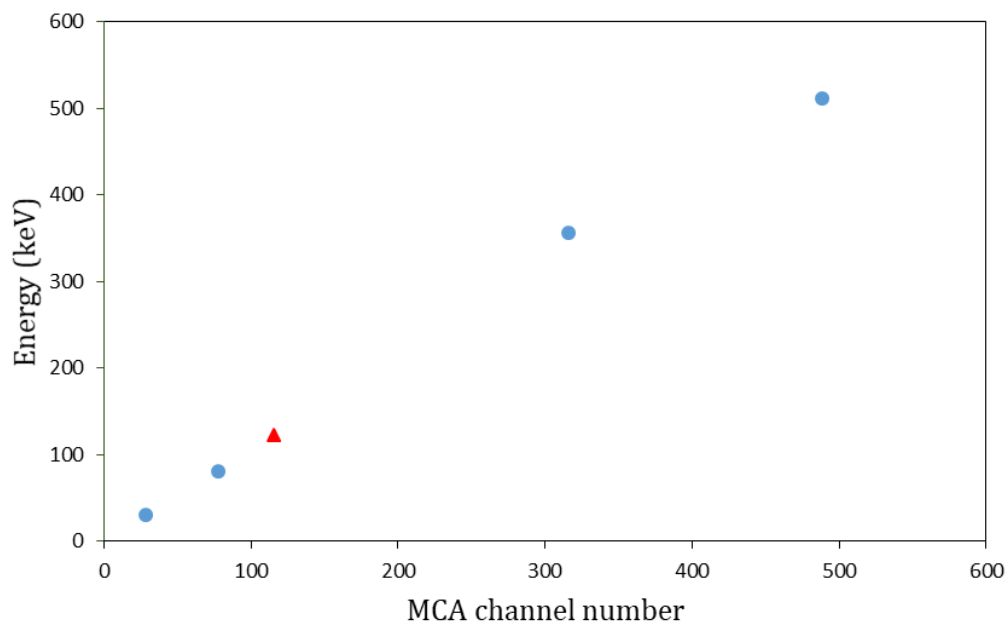


Figure 39. Plot of NaI detector calibration peaks. The known peak energy is plotted as a function of Multichannel Analyzer channel number. The foil data point is shown as the red triangle and is plotted as if its peak energy is the 122.1 keV peak of ^{57}Co .

To identify if the ^{57}Co foil peak was the 122.1 keV peak of ^{57}Co several fits were applied to the other four data points. Using a quadratic fit for all four data points gave the energy of the foil peak as 134 keV. However, this included the ^{22}Na 511 keV peak which, along with ^{133}Ba 356 keV peak, are not near the foil peak. Applying a quadratic fit on only the ^{133}Ba data points, extrapolating from the two nearest data points, and using linear regression respectively gave the foil peak energy as 122 keV, 120 keV, and 126 keV. Applying fits that give greater weight to the nearby peaks suggests that the foil peak is in fact the 122.1 keV peak. This calibration therefore appears to confirm that the foil has ^{57}Co electroplated to it.

Identifying the 122.1 keV peak of the ^{57}Co is the first step to using the activity measurement as a means to determine the ^{57}Co on the foil. In order to calculate the ^{57}Co on the foil the

absolute efficiency of the detector still needs to be determined. A background measurement also needs to be performed and then subtracted from the ^{57}Co measurement. In conjunction with the absolute efficiency the ^{57}Co on the foil will then be calculated to obtain the efficiency of the heating process, important data for assessing the ^{57}Co Mössbauer source preparation process.

Chapter 5

CONCLUSION

An experiment to measure the transverse Doppler shift in an accelerating frame using the Mössbauer effect is underway at Houghton College. The experiment would test Einstein's equivalence principle since the theoretical shift in energy of photons moving in the accelerating reference frame can also be derived using the equivalence principle. The experiment has been subdivided into three steps. The first step is developing a methodology for consistently preparing a weak ^{57}Co Mössbauer source. A steel foil was electroplated with a mixture of ^{57}Co and ^{59}Co atoms with the efficiency of the process monitored by using three independent measurements of the amount of ^{57}Co electroplated. The foil was then heated in a vacuum chamber to make a ^{57}Co Mössbauer source. Since the process typically fails at the heating stage due to the foil melting most recent progress has been in calibrating the IR gun used to measure the temperature of the foil during the heat treatment. The next step is to calibrate the IR gun by measuring the temperature of the foil in situ while the chamber is evacuated. The heating progress can then hopefully be monitored so as to reliably produce a usable ^{57}Co Mössbauer source.

Future plans are to perform steps two and three of the experiment once a source has been created. Measuring the longitudinal Doppler shift, the second step, will demonstrate that a usable ^{57}Co Mössbauer source has been made. The apparatus, which makes use of a coincidence technique to measure the transmission rate of 14.4 keV gamma rays from the source through a rotating absorber, has been set up and awaits a usable source to be tested. The experimental setup for measuring the transverse Doppler shift, the third step, has been redesigned to minimize anticipated problems with vibration and disc tilt. The source and absorber will be fixed in a tube that will be rotated at angular velocities in excess of 20,000 rpm. Using the coincidence technique from the longitudinal Doppler shift experiment the rate of 14.4 keV gamma rays through the absorber will be measured as a function of angular velocity to determine the transverse Doppler shift. To enhance statistics a wider tube and a detector array might be used to capture more 14.4 keV gamma rays.

References

-
- [1] R.W. Wood, Proc. Phys. Soc. London, 19, 764 (1903).
- [2] V. Weisskopf, Ann. Physik, 9, 23 (1931).
- [3] P. B. Moon, Proc. Phys. Soc. 64, 76, (1951).
- [4] R. L. Mössbauer, Z. Physik 151, 124 (1958).
- [5] R. L. Mössbauer, Z. Naturwissenschaften, 45, 538 (1958).
- [6] H. Frauenfelder, The Mössbauer Effect, (W. A. Benjamin, New York, 1962), pg. 12-13, 37-39, 50.
- [7] National Nuclear Data Center, information extracted from Nuclear Data Sheets, <https://www.nndc.bnl.gov/nudat2/decaysearchdirect.jsp?nuc=57CO>
- [8] National Nuclear Data Center, information extracted from Nuclear Data Sheets, <https://www.nndc.bnl.gov/nudat2/decaysearchdirect.jsp?nuc=191OS>
- [9] H. Frauenfelder, The Mössbauer Effect, (W. A. Benjamin, New York, 1962), pg. 36.
- [10] B. Fultz, in Characterization of Materials, edited by Elton N. Kaufmann, (Wiley, New York, 2011).
- [11] A. J. Bearden, P. L. Mattern, and P. S. Nobel, Am. J. Phys. 32, 109 (1964).
- [12] R. V. Pound and G. A. Rebka, Phys. Rev. Lett. 3, 439 (1959).
- [13] R. V. Pound and G. A. Rebka, Phys. Rev. Lett. 4, 337 (1960).
- [14] R. V. Pound and J. L. Snider, Phys. Rev. Lett. 13, 539 (1964).
- [15] A. Einstein, "What is The Theory of Relativity", London Times (November 28, 1919).
- [16] H. J. Hay, J. P. Schiffer, T. E. Cranshaw, and P. A. Egelstaff, Phys. Rev. Lett. 4, 165 (1960).
- [17] D. C. Champeney and P. B. Moon, Proc. Phys. Soc. 77, 350 (1961).
- [18] W. Kundig, Phys. Rev. 129, 2371 (1963).
- [19] A. L. Kholmetski, T. Yarman, and O. V. Missevitch, Physica Scripta, 77, 035302 (2008).
- [20] A. L. Kholmetski, T. Yarman, O. V. Missevitch, and B. I. Rogozev, Physica Scripta, 79, 065007 (2009).
- [21] M. Lund and U. I. Uggerhøj, Am. J. Phys. 77, 757 (2009).
- [22] P. A. Egelstaff et. al., Am. J. Phys. 49, 43 (1981).
- [23] National Institute of Standards and Technology, information extracted from Atomic Spectra Database, https://physics.nist.gov/PhysRefData/ASD/lines_form.html
- [24] A. Gula, BS Thesis, Houghton College, 2016.
- [25] K. W. Mann, BS Thesis, Houghton College, 2013.